

FORCE-INDUCED MECHANOCHEMICAL REACTIONS IN POLYMERIC SYSTEMS

BY
CORISSA LEE

DISSERTATION

Submitted in partial fulfillment of the requirements
for the degree of Doctor of Philosophy in Materials Science and Engineering
in the Graduate College of the
University of Illinois at Urbana-Champaign, 2013

Urbana, Illinois

Doctoral Committee:

Professor Paul V. Braun, Chair and Director of Research
Professor Nancy R. Sottos
Assistant Professor Kristopher A. Kilian
Professor Jeffrey S. Moore

ABSTRACT

Chemical reactions traditionally rely on energy from stimuli such as heat, light, or electric fields to overcome activation barriers separating desired products from starting materials. In the field of mechanochemistry, the energy from mechanical force is harnessed to induce and direct chemical reactions. One focus of the research presented investigates the spiropyran (SP) mechanophore (force-sensitive molecule) incorporated into different polymer systems. The SP mechanophore converts to a colored and fluorescent merocyanine (MC) form upon the application of heat, UV light, or mechanical force, when linked into a polymer backbone. The SP to MC (activation) reaction is also reversible, and can be driven back to the colorless SP form by visible light. The SP mechanophore incorporated into polyurethane (PU) was demonstrated to be mechanochromic, and the conversion to the colored MC form was characterized by changes in absorption and fluorescence. PU's optimized balance of mechanical toughness and elasticity also allowed for the change in SP-MC equilibrium to be studied.

Segmented polyurethane (SPU) is a phase separated copolymer of a soft and hard segment PU. The incorporation of the SP mechanophore into PU by step growth polymerization allows for controlled placement of SP in either the soft or hard domain. Upon either tensile stretching or irradiation with UV light the SP-linked segmented polyurethanes (SP-SPU) adopts a deep purple coloration and is fluorescent, demonstrating the force and UV-induced activation to the open MC form of the mechanophore, respectively. Order parameters calculated from the anisotropy of the fluorescence polarization of MC were used to characterize the orientation of the mechanophore in each phase. Exploiting the ability of SP to be force activated, the SP-SPUs were also

mechanically activated to track the force and orientation in each domain of segmented polyurethane during uniaxial tensile loading.

The SP mechanophore was also used to investigate mechanical forces in crosslinked poly(methyl methacrylate) during swelling with common organic solvents. The SP was incorporated as a crosslinker and a correlation was observed between polymer swelling and fluorescence intensity; suggesting that the forces during swelling were sufficient to drive the electrocyclic ring-opening reaction of SP to its colored and fluorescent MC form. Control experiments and solvatochromic studies validated that activation was indeed due to swelling-induced mechanical forces, and not to solvent effects. Systematic studies varying solvents and crosslinking densities also provided insight on how these parameters influence mechanical forces at the molecular level during polymer swelling.

The second research focus explores the use of phase separated polymers as new mechanochemical systems. Utilizing the nature of different polymers to segregate into microdomains, polymers with complimentary reactive functionalities, isolated in phase separated domains, could be brought in contact with each other by means of mechanical force. When brought in contact, the complimentary phases can react, changing the innate properties of the starting combination of copolymers or polymers. The investigation of the contact mechanochemistry concept will be discussed for a poly(acid) and poly(amine) block copolymer system and a poly(thiol) (initially masked as a disulfide) and poly(glycidyl methacrylates), a polymer with an epoxy side chain. Success in the demonstration of the epoxide ring-opening chemistry by the unmasked thiol side chained polymer, lays down a foundation for future research steps, involving the development of this chemistry into a solid state mechanochemical system.

For My Family

Yi, thank you for being my best friend.

To Mom, Dad, and Amanda, for your endless support.

I would not be where I am today without each of you.

ACKNOWLEDGMENTS

I would first like to acknowledge the many professors, co-workers, and friends, who have taught me, encouraged me, and supported me throughout graduate school. Professor Paul Braun, I would like to express sincere appreciation for your years of guidance and mentoring. I thank you for the many research discussions, thoughtful insight, and for feeding me chocolate at most of our meetings. I would like to acknowledge my thesis committee, Professor Jeffrey Moore, Professor Nancy Sottos, and Professor Kristopher Kilian for all their helpful suggestions and discussions. I would also like to acknowledge Dr. Meredith Silberstein and Dr. Charles Diesendruck as honorary thesis advisors. Large portions of this dissertation would not have been possible without your guidance.

Thank you to the many AMS group members who have helped me with my research. I am indebted to Dr. Douglas Davis and Preston May for the synthesis of spiropyran all these years. I also truly appreciate all the practical chemistry lessons I received from the many Moore group members. I want to thank Dr. Brett Beiermann and Dr. Cassandra Kingsbury for the many helpful research discussions. To Braun group members past and present for their help, support and friendship throughout my time in the group. To Dr. Margaret Shyr, Dr. Abby Juhl, Dr. Amit Patel, Dr. Jericho Moll, Dr. Aaron Jackson, Dr. Matthew Kryger, Austin Pickett, Ariane Vartanian, Neil Krueger, Amanda Jones, Meg Grady, Windy Santa Cruz, and Kevin Hart, in addition to those I have already acknowledged, thank you for making lab a fun place to be, and for letting me sing and dance in the lab. A special thanks to Erica Malloch and Ashley Trimmell for all that you two do.

Outside of my life in Beckman, I have been blessed with so many friends who have made my time in Champaign-Urbana truly memorable. I would not have completed this doctorate without the prayers and support of many CFC members. Dr. Kyuri Kim and Dr. Eunice Chung, thank you for being good “unni’s”, you two always helped me put my research in perspective. To Crystal Ahn, Yaeinn Park, and Becky Yoon, I am grateful for the HM’s providing me with laughter when I most needed it. I would also like to give special thanks to the Illini Women’s Water Polo team for keeping me young all these years.

I am appreciative of the many facilities utilized for this work; The Beckman Institute for Advanced Science and Technology, the Imaging Technology Group at Beckman, the Aerospace Department machine shop, and the MatSE Staff. I want to express much gratitude for Cindy Brya and Michelle Malloch, who provided me with so much emotional support, whether I had good news or bad news, you two were always there for me to share it with. Furthermore, I gratefully acknowledge the Army Research Office for supporting this research.

Finally, I want to thank my parents, who have always stood by my side with unwavering support. Knowing how proud of me they are has driven me to work harder and has helped me achieve more than I believed I could alone. To my sister Amanda, I deeply appreciate your constant encouragement; I only hope I can return the favor. And to my always reassuring yet realistic cousin Brandan, thanks for meticulously reading over this document, your hours of time are greatly appreciated. Lastly, I would like to thank my husband, Yi, who has endured a roller-coaster of emotions these past five years. His patience and willingness to listen to my scientific rambling, daily frustrations, and emotional breakdowns will always be appreciated. Your love and understanding, even when we could only talk for a few minutes, has been incredible, thank you.

TABLE OF CONTENTS

LIST OF ABBREVIATIONS.....	ix
CHAPTER 1: INTRODUCTION AND BACKGROUND	1
1.1 Mechanochemistry	1
1.2 Background Information	15
1.3 Thesis Overview	19
CHAPTER 2: FORCE-INDUCED REDISTRIBUTION OF A CHEMICAL EQUILIBRIUM...	25
2.1 Introduction	25
2.2 Experimental Methods	27
2.3 Mechanical Activation and Controls	29
2.4 Activation with Increasing Stretch.....	30
2.5 Kinetic Studies	32
2.6 Mechanically Biased Equilibrium.....	34
2.7 Conclusions.....	36
CHAPTER 3: EXPLOITING FORCE SENSITIVE SPIROPYRANS AS MOLECULAR LEVEL PROBES.....	38
3.1 Introduction.....	38
3.2 Experimental Methods	41
3.3 Spiropyran-linked Segmented Polyurethane Characterization	46
3.4 UV-Activated Spiropyran-linked Segmented Polyurethane	49
3.5 Mechanically Activated Spiropyran-linked Segmented Polyurethane	51
3.6 Conclusions.....	57
CHAPTER 4: SOLVENT SWELLING ACTIVATION OF MECHANOPHORE CROSSLINKED POLYMERS.....	61
4.1 Introduction.....	61
4.2 Experimental Methods	63
4.3 Polymer Swelling and Spiropyran Activation	67
4.4 Solvent Interaction Studies	71
4.5 Crosslink Density vs. Activation	74
4.6 Conclusions	78
CHAPTER 5: CONTACT MECHANOCHEMISTRY: POLYACIDS AND POLYAMINES	81
5.1 Introduction	81
5.2 Poly(<i>tert</i> -butyl acrylate) and Poly(2-(dimethylamino)ethyl methacrylate) Copolymers	82

5.3	Poly(1-ethoxyethyl methacrylate) and Poly(2-(dimethylamino)ethyl methacrylate) Copolymers	93
5.4	Conclusions.....	105
CHAPTER 6: CONTACT MECHANOCHEMISTRY: POLY(DISULFIDES) AND POLY(GLYCIDYL METHACRYLATE)		110
6.1	Introduction.....	110
6.2	Experimental Methods	113
6.3	Poly(2-(pyridine-2-yl)disulfanyl) ethyl methacrylate) (PPDSEMA)	119
6.4	Poly(4-(pyridine-2-yl)disulfanyl) phenyl methacrylate) (PPDSPMA)	123
6.5	Phase Separation of PPDSPMA and PGMA Polymer Blends.....	132
6.6	Future Work	133
6.7	Conclusions.....	135
CHAPTER 7: CONCLUSIONS AND FUTURE DIRECTIONS		139
7.1	Summary of Thesis Research	139
7.2	Future Directions	141
APPENDIX A.....		143

LIST OF ABBREVIATIONS

AIBN	azobis(isobutyronitrile)
ATRP	atom transfer radical polymerization
BCP	block copolymer
BPO	benzoyl peroxide
CPDB	2-cyano-2-propyl benzodithioate
DCM	dichloromethane
DMA	dimethylaniline
DMAEMA	2-(dimethylamino)ethyl methacrylate
DSC	Differential Scanning Calorimetry
EBIB	ethyl 2-bromoisobutyrate
EEMA	1-ethoxyethyl methacrylate
ERO	electrocyclic ring opening
FTIR	Fourier Transform Infrared Spectroscopy
<i>g</i> DCCs	<i>gem</i> -dichlorocyclopropane
GPC	Gel Permeation Chromatography
HMTETA	1,1,4,7,10,10-Hexamethyltriethylenetetramine
HS	hard segment
LAOS	large amplitude oscillatory shear
MA	methyl acrylate
MC	merocyanine
PAA	poly(acrylic acid)
PMAA	poly(methacrylic acid)
PDMAEMA	poly(dimethylamino-ethyl methacrylate)
PEEA	poly(1-ethoxyethyl acrylate)

PEEMA	poly(1-ethoxyethyl methacrylate)
PEG	poly(ethylene glycol)
PMA	poly(methyl acrylate)
PTBA	poly(<i>tert</i> -butyl acrylate)
PTBMA	poly(<i>tert</i> -butyl methacrylate)
PTP	poly(thiophenol)
PMDETA	<i>N,N,N',N'',N'''</i> -pentamethyldiethylenetriamine
PU	polyurethane
RAFT	reversible addition fragmentation chain transfer
SP	spiropyran
SP-SPU	spiropyran linked into segmented polyurethane
SPSS	spiropyran in the soft segment
SPHS	spiropyran in the hard segment
SPU	segmented polyurethane
tBA	<i>tert</i> -butylacrylate
TGA	Thermal Gravimetric Analysis
THF	tetrahydrofuran

CHAPTER 1

INTRODUCTION AND BACKGROUND

1.1 Mechanochemistry

1.1.1 Introduction

Chemical reactions traditionally rely on energy from stimuli such as heat, light, or electric fields to overcome activation barriers separating desired products from starting materials. In the field of mechanochemistry, the energy from mechanical force is harnessed to induce and direct chemical reactions. Historically, early studies in mechanochemistry focused on the polymer degradation and breaking of bonds by mechanical force [1]. One of the earliest demonstrations of mechanochemistry was reported by Staudinger [2–5] in the 1930s. He demonstrated that masticating a polymeric material caused not only the expected conformation and positional changes in the polymer chains, but it also cleaved covalent chemical bonds, causing the molecular weight of the polymer to decrease. Later, Kauzmann and Eyring [6] refined the idea, suggesting that shortening of the polymer chain was due to homolytic cleavage of the C-C bonds along the polymer backbone under mechanical force. While mastication and degradation of polymers were concepts which developed the early ideas of mechanochemistry, more recently, the nascent field has been geared towards harnessing mechanical energy to do productive chemistry.

Researchers are continually finding ways to activate chemical pathways that favorably alter or enhance the properties of materials. The incorporation of these mechanically reactive chemistries into synthetic materials, such as polymers, has resulted in the development of “smart” polymers

capable of autonomically responding to external stimulus in ways which greatly increase the functionality of the polymer.

1.1.2 Mechanophores

Many different methods exist for designing polymer systems with mechanochemical functionalities; these methods include the use of photoluminescent dyes [7–11], cis-trans isomerizations [12], distortion of polymerized crystalline colloidal arrays [13], deformation-induced ion-pair dissociation in polymer brushes [14,15], and force-sensitive molecules [16–22]. The method adopted for much of this dissertation focuses on the use of force-sensitive molecules, known as mechanophores. Mechanical force is most commonly transferred to force sensitive molecules through the use of polymer chains covalently tethered to the mechanophore (Figure 1.1). A mechanophore can be defined as a chemical moiety which possesses a mechanically sensitive bond or functional group that changes under the influence of exogenous forces. While the nature of force to break chemical bonds can appear obvious, an underlying key to the broad definition presented is in the mechanophore design. Molecules or moieties are typically selected as mechanophores because they possess a structural element that responds to force in a predictable manner, or because they were purposefully designed and synthesized to contain a mechanically labile element. Therefore, chemical entities that simply decompose into indistinguishable products or exhibit random activation under mechanical stress are not considered mechanophores.

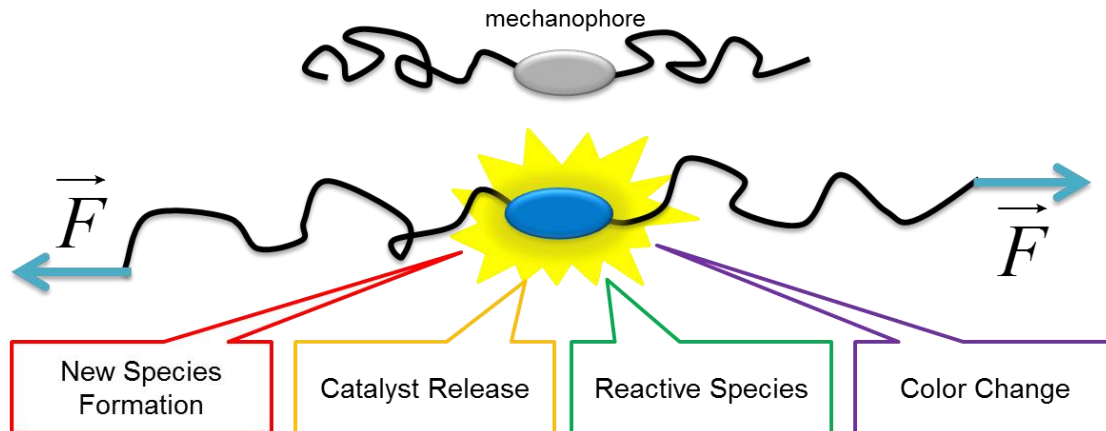


Figure 1.1 – Schematic of a mechanophore linked into a polymer chain. The application of force on the mechanophore induces a productive chemical change.

Over the past several years, researchers have developed a diverse range of mechanophores. While the use of ultrasound to mechanically activate polymers was first reported in the 1930s in the degradation of natural polymers such as starch and agar [23], the use of force from ultrasound was not directed nor selective. In 2005, Moore and co-workers [20] demonstrated that weak covalent bonds could be selectively targeted using ultrasound. A poly(ethylene glycol) (PEG) polymer containing a single diazo moiety located at the center of the polymer chain was subjected to ultrasonication, and the observed molecular weight reduction was consistent with cleavage of the polymer chain near the midpoint. This seminal work inspired the development of many other mechanophores. While the diversity of mechanophores can be categorized in a number of ways, this introduction will organize them by the functionality of the products formed or released by mechanical force. Current mechanophores, including those developed before the term “mechanophore” was defined, are here organized into four areas of mechanophore research: new species formation, catalyst release, formation of reactive species, and color change. In addition to the mechanophores mentioned below, a more complete description and summary of current mechanophores have been discussed in a number of recent reviews [22,24–27].

1.1.3 New Species Formation

Following the work with diazo-linked polymers, Hickenboth *et al.* [16] explored benzocyclobutene mechanophores. This work reported that mechanical forces imparted to the polymers in solution during sonication resulted in unconventional ring-opening reactions. *Trans* and *cis* isomers of 1,2-disubstituted benzocyclobutene were incorporated into PEG polymer chains and after sonication, mechanically biased pathways were evidenced by identical electrocyclic ring opening (EROs) products attained through a formally conrotatory and formally disrotatory ring-opening process (Figure 1.2). Exposure of the mechanophore to heat or light produced different products by mutually exclusive pathways. The violation of the Woodward-Hoffmann rules demonstrated that mechanical force is capable of altering energy pathways, which implied that mechanochemistry could be used to induce chemical reactions inaccessible through other stimuli (i.e. heat or light).

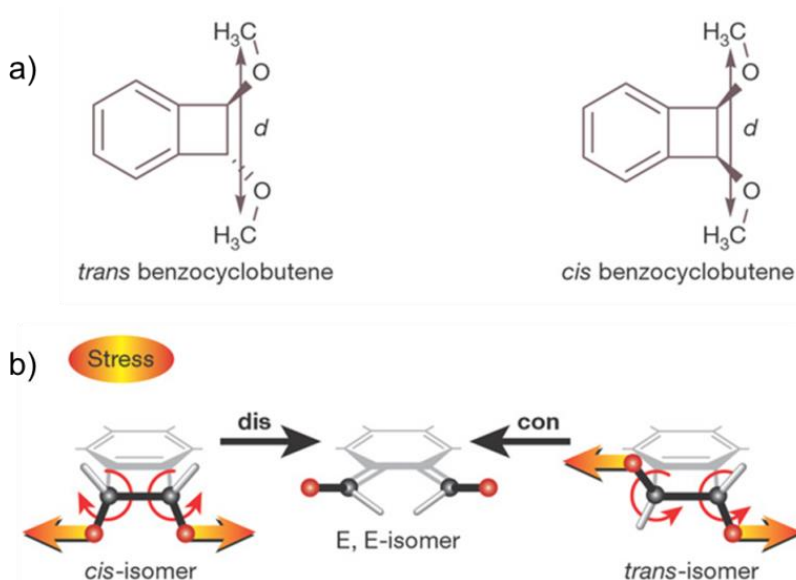


Figure 1.2 – a) Chemical structure of *trans* and *cis* benzocyclobutene mechanophore b) Activation by mechanical force producing E, E – isomer from both *trans* and *cis* mechanophores, violating the Woodward-Hoffmann rules. Adopted from Hickenboth *et al.* [16].

In 2009, Craig and co-workers reported on *gem*-dichlorocyclopropane (gDCCs) mechanophores [19]. The gDCCs mechanophore was incorporated into a polymer backbone of poly(1,4-butadiene) by treatment with dichlorocarbene resulting in gDCCs randomly dispersed through the polymer chain. Sonication of the gDCC-poly(1,4-butadiene) copolymer resulted in the ERO of some mechanophores into 2,3-dichloroalkenes; demonstrating activation of multiple mechanophores on a single chain, as well as new opportunities for post-polymerization modifications. For example, following this work, the Craig group also demonstrated that *gem*-dibromocyclopropanes could undergo force-induced ERO to 2,3-dibromoalkenes, which were susceptible to nucleophilic substitution chemistry [28]. Other similar mechanophores recently introduced include ring opening of *gem*-difluorocyclopropane (gDFC) moieties [31] into thermodynamically disfavored EROs, and also ring opening epoxide mechanophores [30], which result in transient carbonyl ylide intermediates.

1.1.4 Catalyst Release

An active area in the field of mechanophores has been the development of mechanocatalyst. Mechanocatalyst are mechanophores which consist of a latent catalyst that becomes activated through the application of mechanical forces. Sijbesma and co-workers [31] demonstrated that a polymer-functionalized silver bis(N-heterocyclic carbene) complex, when subjected to ultrasound, is able to liberate an active N-heterocyclic carbene organocatalyst (Figure 1.3a). The organocatalyst released was able to facilitate transesterification reactions. Also in this report, a mechanically activated latent olefin metathesis catalyst was also demonstrated. A polymer was functionalized with a ruthenium alkylidene complex (Figure 1.3b). When subjected to ultrasound irradiation, force induced ligand dissociation generated an active catalyst used to facilitate a ring-

closing metathesis of diethyl diallylmalonate as well as a ring-opening metathesis polymerization of cyclooctene.

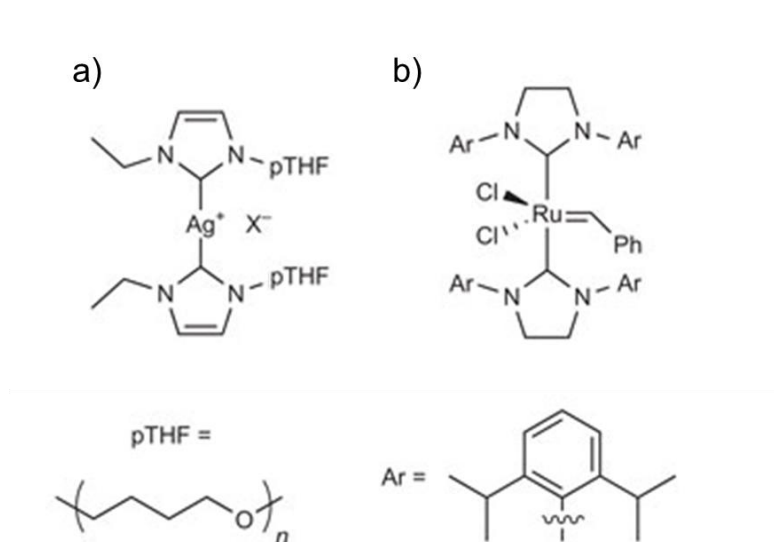


Figure 1.3 – a) Polymeric silver-N-heterocyclic (NHC) carbene complex and b) polymeric ruthenium-NHC complex [31].

Bielawski and co-workers have also developed a series of mechanocatalyst, which focused on pincer-type palladium pyridyl complexes [32]. When the mechanocatalyst was subjected to ultrasound two different latent catalysts were released. First, the putative mechanocatalyst which facilitated the cross-coupling of benzylic nitriles and N-tosylimines, and second a pyridine ligand moiety, which facilitated the polymerization of α -trifluoromethyl-2,2,2-trifluoroethyl acrylate (Figure 1.4). The researchers were able to design a mechanically responsive catalyst with the ability to mechanically activate two latent catalysts with different reactivities. More recently, the Bielawski group has also reported on the activation of a boron-based mechanocatalyst with pyridine capped PMA ligands [33]. Collectively these mechanocatalyst are examples of new opportunities in the growing field of latent catalysis and have revealed alternative routes to facilitating bond-forming reactions.

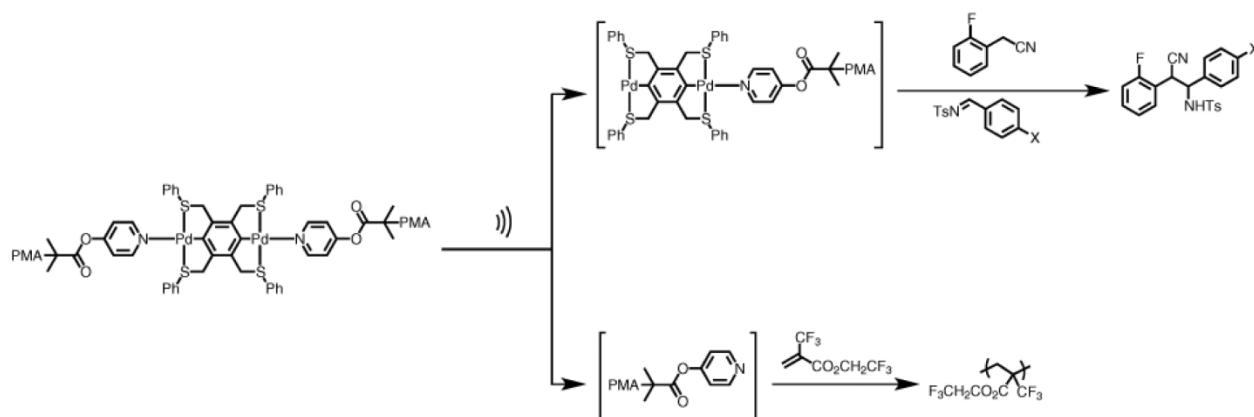


Figure 1.4 – Simultaneous mechanical activation of a pyridine organocatalyst and an organometallic palladium catalyst from the same mechanophore. Adopted from Brantley *et al.*[22].

Finally, Diesendruck *et al.* [21] reported on an acid-releasing mechanophore, which could be used as a simple catalyst for chemical changes in materials. The mechanophore was based on a *gem*-dichlorocyclopropanated indene (Figure 1.5), and was linked into poly(methyl acrylate) (PMA) as a crosslinker. Upon the application of compressive forces in the solid state, the mechanophore underwent rearrangement and aromatization elimination, generating HCl. The acid produced is not part of the polymer chain, but released as a small molecule, giving the acid the mobility in the solid state to catalyze different reactions, including polymerizations.

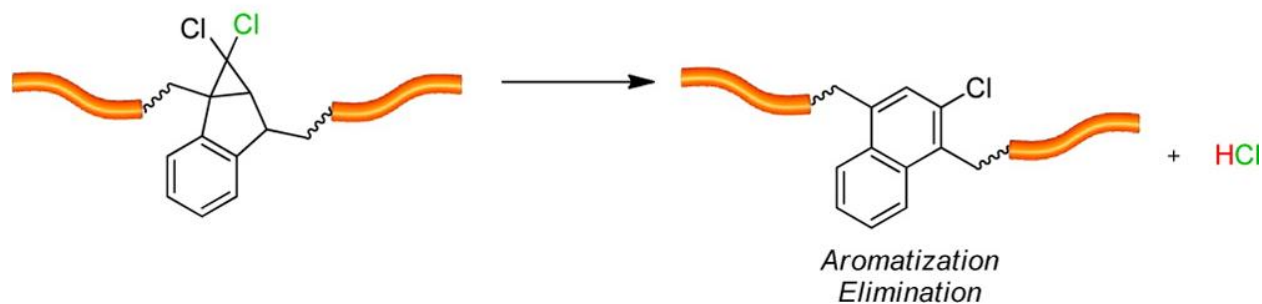


Figure 1.5 – Mechanical activation of *gem*-dichlorocyclopropanated indene mechanophore in the solid state by compression, resulting in the release of a small molecule acid capable of catalyzing chemical reactions. Adopted from Diesendruck *et al.*[21].

1.1.5 Formation of Reactive Species

Mechanical damage of polymers is often a destructive and irreversible process. However, mechanophores that can generate reactive moieties when subjected to mechanical force hold much potential in the engineering of polymer systems with self-healing or self-strengthening capabilities. In 2010, Kryger *et al.* [18] demonstrated a mechanically induced ring opening of a dicyano-substituted cyclobutane mechanophore. Under sonication, the mechanophore linked into the center of a PMA polymer mechanically activated through cycloreversion, generating a highly reactive cyanoacrylate. Since cyanoacrylates are known to autopolymerize, the formation of such a species could, upon mechanical, damage facilitate a self-healing process.

Wiggins *et al.* [34] demonstrated a retro [4+2] cycloaddition of an oxanorbornene-based mechanophore. When the mechanophore was subjected to ultrasonication, chain scission near the center of the polymer chain was observed, and the generation of maleimide-terminated and furan-terminated polymer fragments was confirmed by chemical labeling. These products, which were mechanically induced, is a well-known healing chemistry [35]. In addition to this mechanophore, Bielawski and co-workers have also developed a number of other mechanophores which can be mechanically triggered to undergo cycloreversion reactions [29,34,36,37].

One particularly interesting system developed by the Bielawski group is the 1,2,3-triazole moieties which can be “unclicked” into their azide and alkyne precursors [36]. PMA polymer chains were grown from the mechanophore, and under ultrasonication, there is a reduction of molecular and consistent cleavage of the polymer near the centrally located triazole mechanophore (Figure 1.6). The resulting azide and alkynes are commonly used for click chemistry, which is popular because of its rapid kinetics and mild conditions, and therefore hold much potential for self-healing or self-strengthening type chemical reactions after mechanical

activation (via mechanical damage). It was also demonstrated that the polymer fragments could be recoupled using copper-catalyzed reaction of the two products.

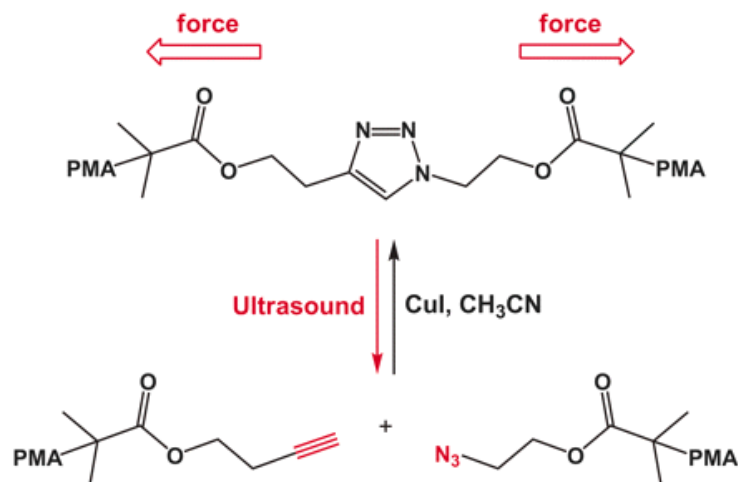


Figure 1.6 – 1,2,3-triazole mechanophore embedded within a PMA chain undergoes retro [3+2] cycloaddition under ultrasound. The liberated azide and alkyne reactive moieties can be “clicked” back together to the starting triazole mechanophore. Adopted from Brantley *et al.* [36].

1.1.6 Color Change

The activation of traditionally thermo-chromic and photo-chromic molecules by mechanical stress has been investigated by a number of research groups. Force triggered color changing molecules (including fluorescence and photoluminescence) are of particular interest for self-sensing materials, as they can be used as strain sensors or for damage detection.

Rubner [38,39] first studied the color changing optical properties of polydiacetylene in a segmented polyurethane and reported on its thermochromic and mechanochromic properties. Since then, other reports[40–43] have described the use of mechanochromic polydiacetylenes to study the organization and role of the hard segment domains in segmented polyurethane during tensile deformation. Kim *et al.* [12] used the trans-to-cis isomerization of diaminoazobenzenes as a “strain recording material.” The chemically inserted azobenzene was first transformed to the

cis-form by ultraviolet irradiation, then when the material was strained, a change in absorbance at $\lambda=380$ nm indicated the force-induced transformation back to the *trans* form.

Weder and co-workers blended and covalently incorporated cyano-substituted oligo(*p*-phenylene vinylene) (cyano-OPV) into a number of different polymers [7,8,44]. Mechanical deformation of these systems led to irreversible diassociation of dye aggregates exhibiting corresponding photoluminescent color change (Figure 1.7).

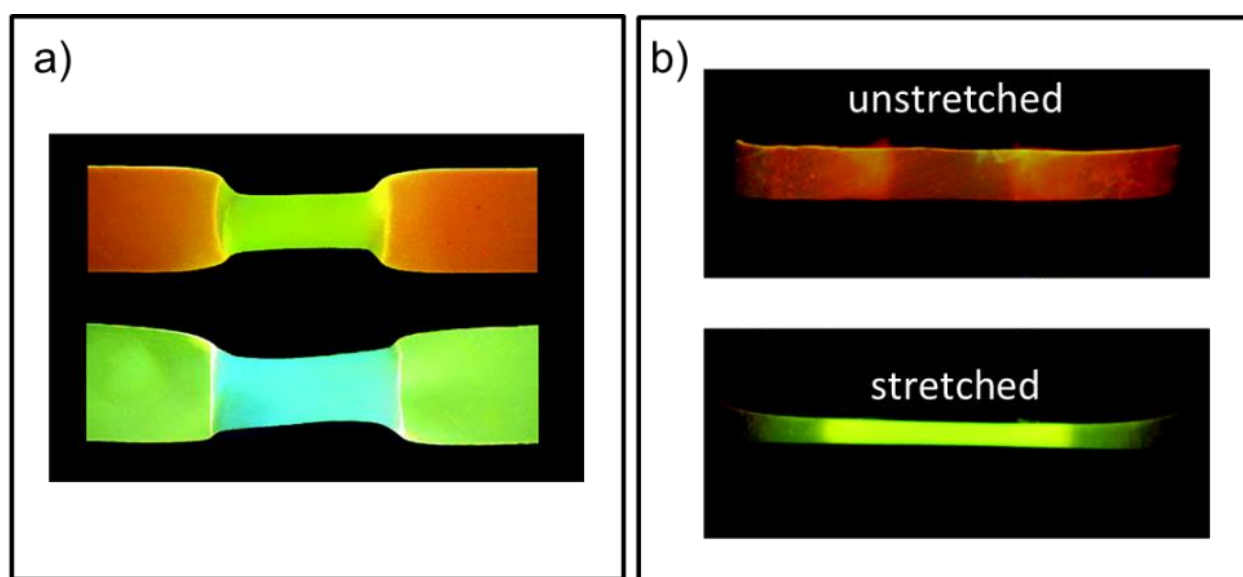


Figure 1.7 – a) Picture of blend films of LLDPE two different concentrations of cyano-OPV mechanophore (0.18% w/w, top; and 0.20% w/w bottom) stretched to a draw ratio of 500% [8]. b) Pictures taken of cyano-OPVs covalently incorporated into thermoplastic polyurethane films [44]. Both images were taken under UV light excitation ($\lambda=365$ nm).

Most recently, Chen *et al.*[45] demonstrated that bis(adamantly)-1,2-dioxetane incorporated into a polymer chain or network is a luminescent mechanophore that emits visible light upon mechanical activation (Figure 1.8). The luminescent mechanophore was imported into both linear PMA and also a crosslinked PMA, and demonstrated mechanical activation by opening of the 1,2-dioxetane four member ring in sonicated solutions (linear PMA) as well as in bulk

samples (crosslinked PMA). Real-time monitoring of light emission during the deformation of the polymers highlights the potential of luminescent mechanophores for the study of polymer failure in exceptional detail. In addition, the mechanically activated chemiluminescence could be recorded directly from the singlet state of the product adamantanone, or it could also be harvested by energy transfer to suitable acceptors, which enables tuning of the emission color and also increases the sensitivity of this autoluminescent system.

The spiropyran mechanophore, also known to be mechanochromic, is investigated and discussed extensively in this dissertation and will be discussed in more detail in the next sections.

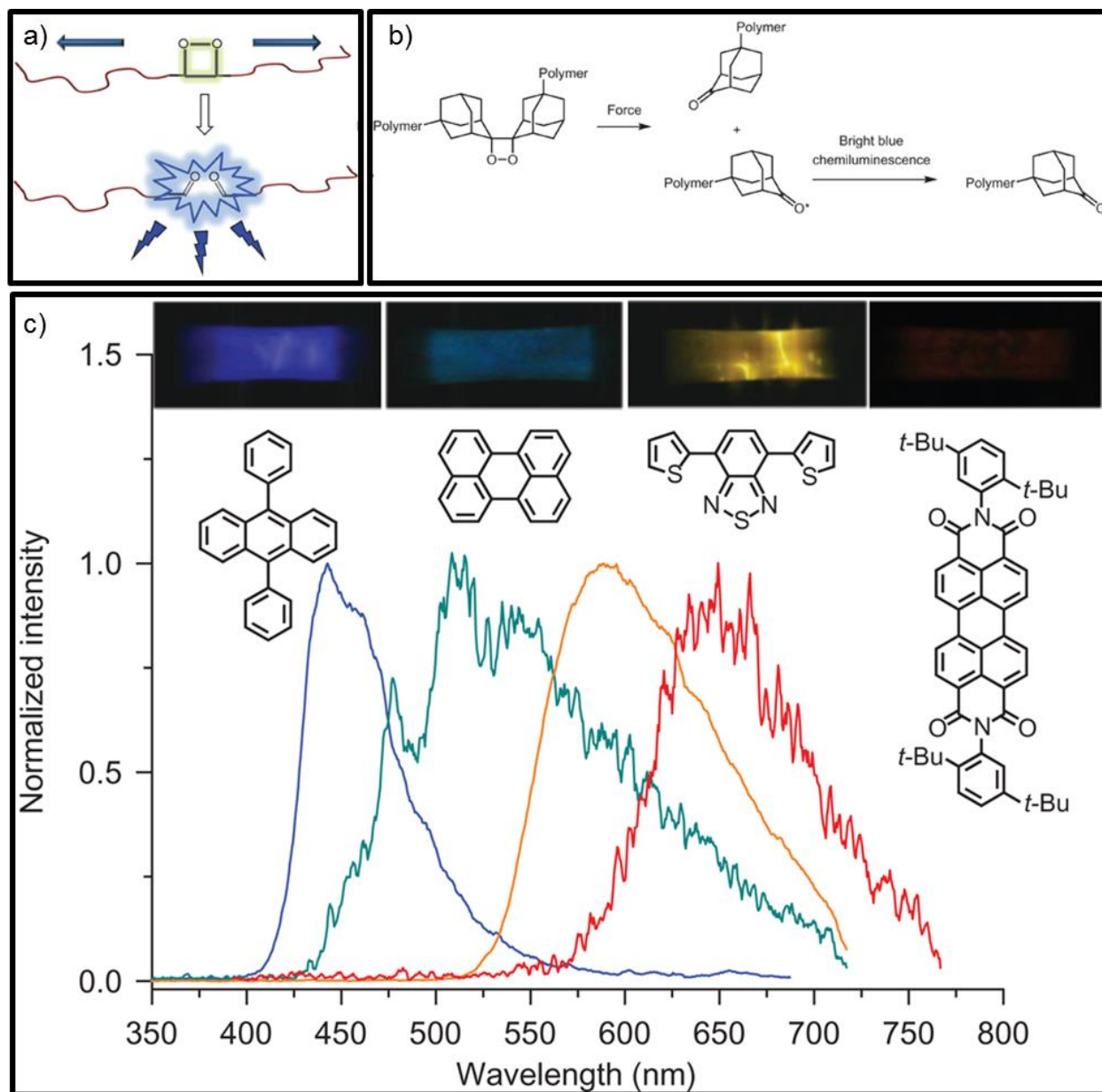


Figure 1.8 – a) Schematic representation of the mechanically induced decomposition of a polymeric bis(adamantyl) dioxetane that results in chemiluminescence when the ketone product relaxes from its excited state to the ground state. b) Chemical structure of mechanophore and its mechanically induced chemiluminescence product. c) Optical images of films and absorption during deformation with the chemical structures of corresponding acceptors, which tune the emission color. Adopted from Chen *et al.*[45].

1.1.7 Spiropyran Mechanophore

The mechanophore investigated in this dissertation is the molecule spiropyran, which has been extensively studied since the 1950s [46,47]. This molecule is traditionally known to be thermo and photo-chromic [48], as it undergoes an electrocyclic ring-opening reaction of a weak carbon-oxygen spiro bond transforming it from a colorless spiropyran (SP) conformation to a highly colored and fluorescent merocyanine (MC) conformation under thermo and photo (UV light) stimuli (Figure 1.9). Under visible light, the MC conformation reverses back to the SP conformation. In 2001, Tipkin [49] demonstrated that SP molecules could be mechanochemically converted to the MC form by grinding the small molecule with a mortar and pestle. Later, Potisek *et al.*[50] developed a procedure to covalently link the SP molecule into a polymer backbone and demonstrated that mechanical force by means of sonication could also provide pathway for the ring-opening to occur. The SP mechanophore was covalently linked into PMA, and after sonication showed visible color change indicating mechanically triggered conversion of the colorless SP to colored MC (Figure 1.10).

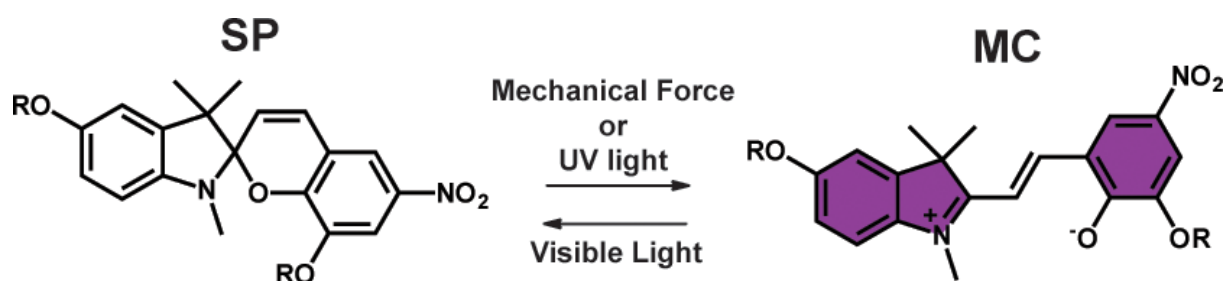


Figure 1.9 – Electrocyclic ring-opening reaction of spiropyran to colored and fluorescent merocyanine.

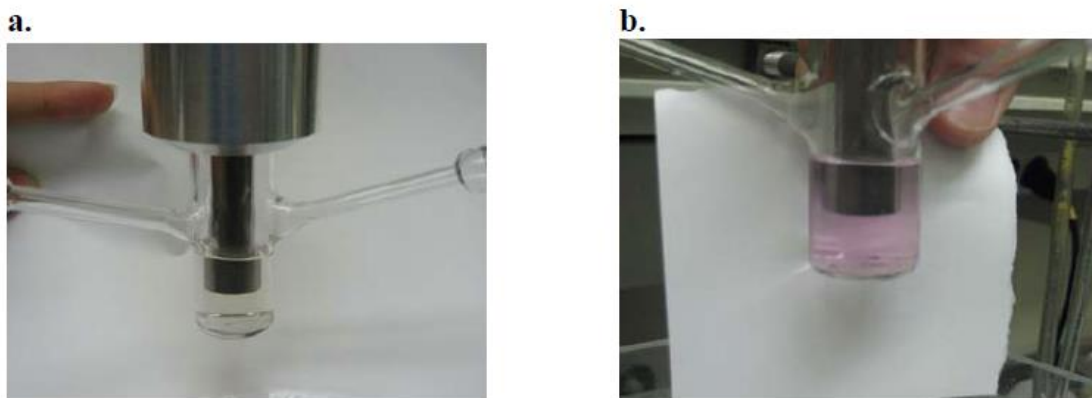


Figure 1.10 – Images illustrating the visible color change of SP-linked PMA in CH_3CN a) before sonication and b) after sonication displaying color change of the SP mechanophore to the MC form [50].

Following the work of Potisek *et al.*, Davis *et al.* [17] successfully demonstrated the solid state activation of the SP mechanophore in linear PMA and crosslinked poly(methylmethacrylate) (PMMA) during tension and during diametric compression, respectively. More recently, mechanochemical reactivity of SP has been demonstrated in a number of different polymer systems [17,51–54]. The research conducted on these polymer systems has added to the understanding of how force interacts with mechanophores at the molecular level. The work of Beiermann *et al.*[51,55] determined a critical temperature window over which SP could be activated in glassy linear PMMA as well as the role of orientation in mechanical activation of SP in PMA and PMMA. Kingsbury *et al.*[53] investigated and characterized SP-linked polymers under shear loading, and reported on the strain rate dependence, polymer architecture dependence, and time-dependence of mechanically activated SP-linked polymers. The work presented in this dissertation will add to this growing knowledge of how macroscopic stress on polymer systems translates to the force-induced activation of the SP mechanophore at the molecular level.

1.2 Background Information

1.2.1 Polyurethanes

Polyurethanes are a broad class of polymers containing the urethane group (-NHCO-O-). The urethane group is generally formed by a reaction between isocyanate and hydroxyl group. Isocyanate groups are very reactive and allow easy, quantitative conversion into urethane groups without by-products. Since polyurethanes were first discovered by Otto Bayer and co-workers in 1937 [56], they have become ubiquitous throughout industry. The abundant use of polyurethanes in industry stems from the versatile chemistry and many different processing techniques, which can turn polyurethane into fibers, films, thermoplastics, foams, thermosets, and elastomers.

Polyurethane elastomers are a very important class of materials because of their many useful properties in materials engineering. They have high abrasion and chemical resistance, excellent mechanical and elastic properties, and are blood and tissue compatible [57]. The typical polyurethane elastomer is a linear block copolymer containing three primary components: a polyol, a diisocyanate, and a chain extender. Depending on the nature and the amount of these components, the polyurethane can have many different physical properties. The polyols used for polyurethane elastomers usually consist of two classes: polyethers or polyesters, with molecular weights ranging from 1000 to 4000 g/mol. The diisocyanate is commonly 4,4'-diphenylmethane diisocyanate (MDI) or 1,6 hexamethylene diisocyanate (HDI), and the chain extenders are short-chain aliphatic diamines or diols such as butanediol (BD) [58].

On the basis of the above compositions, the polyurethane formed would have chains comprised of alternating hard (isocyanate and chain extender) and soft segments (long chain polyols). The two segments are generally incompatible; they tend to phase separate into so-called microphase domains (Figure 1.11). As with all phase separated polymer systems (i.e. block copolymers and polymer blends), the degree of separation depends on the thermodynamic driving forces and the

kinetic pathways during processing. With polyurethanes the morphology usually consists of hard segment rich domains, on the order of 10s to 100s of angstroms dispersed in a matrix of soft segments [59–61]. Use of soft segments that do not hydrogen bond can better facilitate microphase separation [62], as well as the increase in the segmental length and concentration of the hard segment [63].

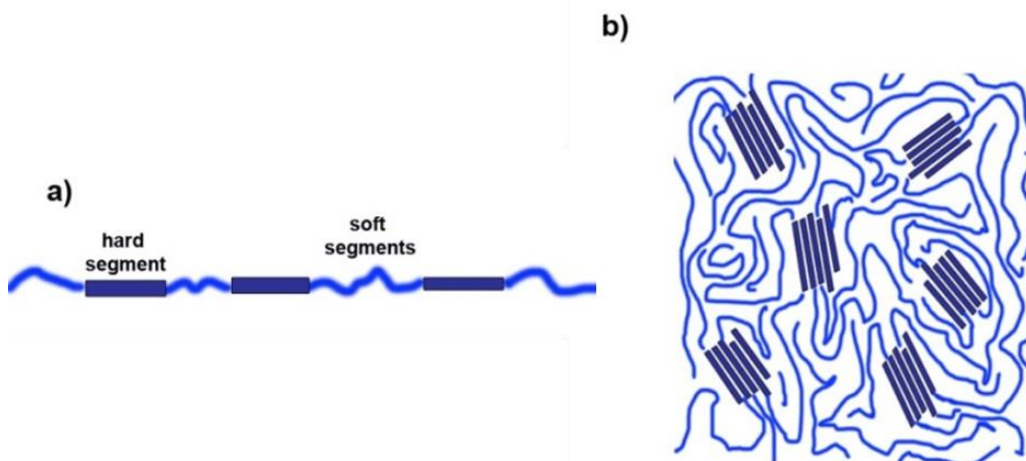


Figure 1.11 – a) Schematic representation of the structure of SPU, and b) two-phase structure of bulk SPU polymers.

1.2.2 Swelling of Crosslinked Polymers

When a three-dimensional polymer network is placed in a solvent, it absorbs large quantities of the solvent rather than dissolving. The absorption of the solvent causes the solid polymer to swell through imbibition to a degree depending on the solvent and the structure of the polymer. When the network structure is permanent (i.e. covalent or chemical crosslinks) a state of equilibrium swelling can be attained. As more solvent is absorbed (dissolved) the polymer network progressively expands (Figure 1.12). The polymer chains between crosslinks are forced to take on more elongated, less probable, and therefore higher energy configurations. While increase in the entropy of mixing causes elongation of the polymer there is an opposing retractive force from

the polymer due to the decrease in chain configurational entropy [64]. The balance between these two opposing entropies results in the equilibrium state of swelling.

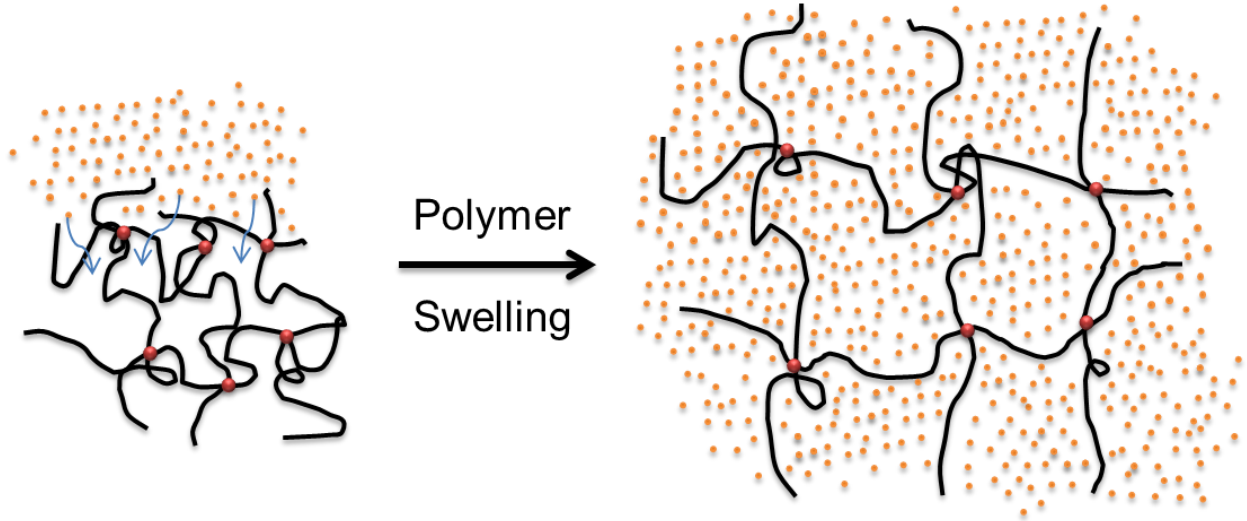


Figure 1.12 – Schematic of crosslinked polymer swollen by the imbibition of solvent molecules (orange dots)

1.2.3 Block Copolymers

Block copolymers consist of chemically distinct polymer chains (i.e blocks) covalently joined together forming a single macromolecule. Rarely are the two constituent polymers miscible, and therefore phase separation is induced [65,66]. The phase separation is driven by thermodynamics of the block copolymer system, which follows the thermodynamics of mixing:

$$\frac{\Delta G^{mix}}{RT} = \frac{\varphi_a}{x_a} \ln(\varphi_a) + \frac{\varphi_b}{x_b} \ln(\varphi_b) + \chi \varphi_a \varphi_b \quad (1)$$

where ϕ is the mole fraction, x is the degree of polymerization, and χ is the chi-parameter. χ , also known as the “Flory-Huggins interaction parameter” describes the free energy cost for polymer A and polymer B to be in contact with each other as described by eq (2):

$$\chi_{ab} = \frac{z}{k_b T} \left[\varepsilon_{ab} - \frac{1}{2} (\varepsilon_{aa} + \varepsilon_{bb}) \right] \quad (2)$$

z is the number of nearest-neighbors, and ε_{ab} is the interaction energy between polymer A and polymer B. If χ_{ab} is positive then there is a net repulsion between polymer A and B, but if the value is negative the free-energy drives the system towards mixing. For two different polymers χ is generally positive and there is a net repulsion between the two polymers, but because they are covalently bonded they cannot macroscopically phase separate and instead phases separate to mesoscopic length scales resulting in microdomains [67]. As a result, with varying volume fractions of the two blocks, different morphologies form, to minimize the surface energy between the two thermodynamically incompatible blocks. The morphologies are generally spheres and cylinders because curved surfaces minimize the repulsive interfacial contact between the two blocks and also minimize the free energy. Based on a self-consistent mean-field theory, there are four equilibrium morphologies: spherical(S), cylindrical(C), gyroid(G), and lamellar(L) (Figure 1.13). The different morphologies depend on the volume fraction of polymers A and B and the Flory-Huggins interaction parameter χ . A more detailed description of the exploration of block copolymers for mechanochemistry can be found in Chapter 5.

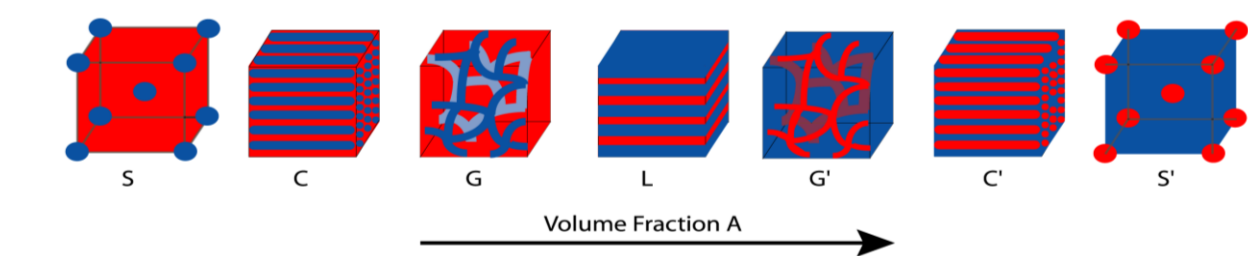


Figure 1.13 – Typical equilibrium microdomain morphologies for an diblock copolymer where the polymer A is blue and Polymer B is red. The four theoretical morphologies are Spheres (S), cylinders (C), gyroids (G), and lamellar (L), and their inverse morphologies (G', C', and S') [65,68].

1.3 Thesis Overview

In this dissertation, the mechanical activation of the SP mechanophore is investigated in a number of different polymer systems. In **Chapter 2**, the incorporation of the SP mechanophore into step-growth synthesized polyurethane, and bulk solid state activation of the SP mechanophore is reported. In addition, polyurethane's unique combination of elasticity and mechanical toughness provided an optimized polymer environment to study the opening and closing kinetics of the SP to MC conversion. Utilizing the polyurethane synthesis developed, **Chapter 3** describes the incorporation of the SP mechanophore into segmented polyurethane (SPU). The polymerization of SPU's by step growth polymerization allowed for the incorporation of the SP into either the “soft” or “hard” segment of the phase separated materials, and for the study of these force sensitive molecules as molecular level probes.

In **Chapter 4**, the SP mechanophore is incorporated as a crosslinker in crosslinked PMMA. When the SP-linked crosslinked PMMA is swollen in different organic solvent, swelling of the polymer is accompanied by color change, suggesting that the forces during swelling are sufficient to drive the electrocyclic ring-opening reaction of SP to its colored and fluorescent MC

form. Systematic studies varying solvents and crosslinking densities provides insight on how these parameters influence mechanical forces at the molecular level during polymer swelling.

A new concept in mechanochemistry utilizing the ideas of phase separation will be explored. In Chapter 5, a block copolymer consisting of a protected poly(acid) and a poly(amine) will be investigated as possible chemistry for contact mechanochemistry, where the mechanical mixing of phase separated block copolymer phases with complementary reactivity's will be discussed. Major challenges and future design considerations for block copolymer mechanochemistry will be presented. In Chapter 6, a new chemistry for contact mechanochemistry is described. Preliminary results, demonstrating the feasibility of a disulfide polymer and poly(glycidyl methacrylate) chemical system for contact mechanochemistry, will be presented. Finally, a summary of the completed work is provided in Chapter 7, along with suggestions for future work.

REFERENCES

- [1] M.K. Beyer, H. Clausen-Schaumann, Mechanochemistry: The Mechanical Activation of Covalent Bonds, *Chem Rev.* 105 (2005) 2921–2948.
- [2] H. Staudinger, Über Isopren und Kautschuk, 20. Mitteil.: Über die Kolloidnatur von Kautschuk, Guttapercha und Balata, *Berichte Dtsch. Chem. Ges. B Ser.* 63 (1930) 921–934.
- [3] H. Staudinger, H.F. Bondy, Über Isopren und Kautschuk, 19. Mitteil.: Über die Molekülgröße des Kautschuks und der Balata, *Berichte Dtsch. Chem. Ges. B Ser.* 63 (1930) 734–736.
- [4] H. Staudinger, W. Heuer, Über hochpolymere Verbindungen, 93. Mitteil.: Über das Zerreißen der Faden-Moleküle des Poly-styrols, *Berichte Dtsch. Chem. Ges. B Ser.* 67 (1934) 1159–1164.
- [5] H. Staudinger, E.O. Leupold, Über Isopren und Kautschuk, 18. Mitteil.: Viscositäts-Untersuchungen an Balata, *Berichte Dtsch. Chem. Ges. B Ser.* 63 (1930) 730–733.
- [6] W. Kauzmann, H. Eyring, The Viscous Flow of Large Molecules, *J Am Chem Soc.* 62 (1940) 3113–3125.

- [7] B.R. Crenshaw, M. Burnworth, D. Khariwala, A. Hiltner, P.T. Mather, R. Simha, *et al.*, Deformation-Induced Color Changes in Mechanochromic Polyethylene Blends, *Macromolecules*. 40 (2007) 2400–2408.
- [8] B.R. Crenshaw, C. Weder, Deformation-Induced Color Changes in Melt-Processed Photoluminescent Polymer Blends, *Chem. Mater.* 15 (2003) 4717–4724.
- [9] T. Ikawa, T. Shiga, A. Okada, Fluorescence from poly(N-vinylcarbazole) in uniaxially stretched polymer films, *J. Appl. Polym. Sci.* 66 (1997) 1569–1573.
- [10] J. Yang, H. Li, G. Wang, B. He, Excimer formation in uniaxially stretched polymer films, *J. Appl. Polym. Sci.* 82 (2001) 2347–2351.
- [11] C. Löwe, C. Weder, Oligo(p-phenylene vinylene) Excimers as Molecular Probes: Deformation-Induced Color Changes in Photoluminescent Polymer Blends, *Adv. Mater.* 14 (2002) 1625–1629.
- [12] S.-J. Kim, D.H. Reneker, A mechanochromic smart material, *Polym. Bull.* 31 (1993) 367–374.
- [13] S.H. Foulger, P. Jiang, A.C. Lattam, Smith, J. Ballato, Mechanochromic Response of Poly(ethylene glycol) Methacrylate Hydrogel Encapsulated Crystalline Colloidal Arrays, *Langmuir*. 17 (2001) 6023–6026.
- [14] J.E. Comrie, W.T.S. Huck, Exploring Actuation and Mechanotransduction Properties of Polymer Brushes, *Macromol. Rapid Commun.* 29 (2008) 539–546.
- [15] O. Azzaroni, B. Trappmann, P. van Rijn, F. Zhou, B. Kong, W.T.S. Huck, Mechanically Induced Generation of Counterions Inside Surface-Grafted Charged Macromolecular Films: Towards Enhanced Mechanotransduction in Artificial Systems, *Angew. Chem. Int. Ed.* 45 (2006) 7440–7443.
- [16] C.R. Hickenboth, J.S. Moore, S.R. White, N.R. Sottos, J. Baudry, S.R. Wilson, Biasing reaction pathways with mechanical force, *Nature*. 446 (2007) 423–427.
- [17] D.A. Davis, A. Hamilton, J. Yang, L.D. Cremer, D. Van Gough, S.L. Potisek, *et al.*, Force-induced activation of covalent bonds in mechanoresponsive polymeric materials, *Nature*. 459 (2009) 68–72.
- [18] M.J. Kryger, M.T. Ong, S.A. Odom, N.R. Sottos, S.R. White, T.J. Martinez, *et al.*, Masked Cyanoacrylates Unveiled by Mechanical Force, *J. Am. Chem. Soc.* 132 (2010) 4558–4559.
- [19] J.M. Lenhardt, A.L. Black, S.L. Craig, gem-Dichlorocyclopropanes as Abundant and Efficient Mechanophores in Polybutadiene Copolymers under Mechanical Stress, *J. Am. Chem. Soc.* 131 (2009) 10818–10819.
- [20] K.L. Berkowski, S.L. Potisek, C.R. Hickenboth, J.S. Moore, Ultrasound-Induced Site-Specific Cleavage of Azo-Functionalized Poly(ethylene glycol), *Macromolecules*. 38 (2005) 8975–8978.
- [21] C.E. Diesendruck, B.D. Steinberg, N. Sugai, M.N. Silberstein, N.R. Sottos, S.R. White, *et al.*, Proton-Coupled Mechanochemical Transduction: A Mechanogenerated Acid, *J. Am. Chem. Soc.* 134 (2012) 12446–12449.

- [22] J.N. Brantley, K.M. Wiggins, C.W. Bielawski, Polymer mechanochemistry: the design and study of mechanophores, *Polym. Int.* 62 (2013) 2–12.
- [23] E.W. Flosdorf, L.A. Chambers, The Chemical Action of Audible Sound, *J. Am. Chem. Soc.* 55 (1933) 3051–3052.
- [24] M.M. Caruso, D.A. Davis, Q. Shen, S.A. Odom, N.R. Sottos, S.R. White, *et al.*, Mechanically-Induced Chemical Changes in Polymeric Materials, *Chem. Rev.* 109 (2009) 5755–5798.
- [25] A.L. Black, J.M. Lenhardt, S.L. Craig, From molecular mechanochemistry to stress-responsive materials, *J. Mater. Chem.* 21 (2011) 1655–1663.
- [26] K.M. Wiggins, J.N. Brantley, C.W. Bielawski, Methods for activating and characterizing mechanically responsive polymers, *Chem. Soc. Rev.* (2013).
- [27] T.J. Kucharski, R. Boulatov, The physical chemistry of mechanoresponsive polymers, *J. Mater. Chem.* 21 (2011) 8237–8255.
- [28] A.L. Black, J.A. Orlicki, S.L. Craig, Mechanochemically triggered bond formation in solid-state polymers, *J. Mater. Chem.* 21 (2011) 8460–8465.
- [29] H.M. Klukovich, Z.S. Kean, S.T. Iacono, S.L. Craig, Mechanically Induced Scission and Subsequent Thermal Remending of Perfluorocyclobutane Polymers, *J. Am. Chem. Soc.* 133 (2011) 17882–17888.
- [30] H.M. Klukovich, Z.S. Kean, A.L.B. Ramirez, J.M. Lenhardt, J. Lin, X. Hu, *et al.*, Tension Trapping of Carbonyl Ylides Facilitated by a Change in Polymer Backbone, *J. Am. Chem. Soc.* 134 (2012) 9577–9580.
- [31] A. Piermattei, S. Karthikeyan, Rint P. Sijbesma, Activating catalysts with mechanical force, *Nat Chem.* 1 (2009) 133–137.
- [32] A.G. Tennyson, K.M. Wiggins, C.W. Bielawski, Mechanical Activation of Catalysts for C–C Bond Forming and Anionic Polymerization Reactions from a Single Macromolecular Reagent, *J Am Chem Soc.* 132 (2010) 16631–16636.
- [33] K.M. Wiggins, T.W. Hudnall, A.G. Tennyson, C.W. Bielawski, Selective scission of pyridine-boronium complexes: mechanical generation of Bronsted bases and polymerization catalysts, *J. Mater. Chem.* 21 (2011) 8355–8359.
- [34] K.M. Wiggins, J.A. Syrett, D.M. Haddleton, C.W. Bielawski, Mechanically Facilitated Retro [4 + 2] Cycloadditions, *J. Am. Chem. Soc.* 133 (2011) 7180–7189.
- [35] X. Chen, A Thermally Re-mendable Cross-Linked Polymeric Material, *Science.* 295 (2002) 1698–1702.
- [36] J.N. Brantley, K.M. Wiggins, C.W. Bielawski, Unclicking the Click: Mechanically Facilitated 1,3-Dipolar Cycloreversions, *Science.* 333 (2011) 1606–1609.
- [37] J.N. Brantley, S.S.M. Konda, D.E. Makarov, C.W. Bielawski, Regiochemical Effects on Molecular Stability: A Mechanochemical Evaluation of 1,4- and 1,5-Disubstituted Triazoles, *J. Am. Chem. Soc.* 134 (2012) 9882–9885.
- [38] M.F. Rubner, Synthesis and characterization of polyurethane-diacetylene segmented copolymers, *Macromolecules.* 19 (1986) 2114–2128.

- [39] M.F. Rubner, Novel optical properties of polyurethane-diacetylene segmented copolymers, *Macromolecules*. 19 (1986) 2129–2138.
- [40] R.A. Nallicheri, M.F. Rubner, Investigations of the mechanochromic behavior of poly(urethane-diacetylene) segmented copolymers, *Macromolecules*. 24 (1991) 517–525.
- [41] J.L. Stanford, R.J. Young, R.J. Day, Formation and properties of urethane-diacetylene segmented block copolymers, *Polymer*. 32 (1991) 1713–1725.
- [42] R.A. Koevoets, S. Karthikeyan, P.C.M.M. Magusin, E.W. Meijer, R.P. Sijbesma, Cross-Polymerization of Hard Blocks in Segmented Copoly(ether urea)s, *Macromolecules*. 42 (2009) 2609–2617.
- [43] P.T. Hammond, R.A. Nallicheri, M.F. Rubner, An examination of the strain-induced orientation of hard segment domains in 4,4'-methylenebis(phenyl isocyanate)-based polyurethane-diacetylene segmented copolymers, *Mat Sci Eng -Struc.* 126 (1990) 281–287.
- [44] B.R. Crenshaw, C. Weder, Self-Assessing Photoluminescent Polyurethanes, *Macromolecules*. 39 (2006) 9581–9589.
- [45] Y. Chen, A.J.H. Spiering, S. Karthikeyan, G.W.M. Peters, E.W. Meijer, R.P. Sijbesma, Mechanically induced chemiluminescence from polymers incorporating a 1,2-dioxetane unit in the main chain, *Nat. Chem.* 4 (2012) 559–562.
- [46] Y. Hirshberg, Reversible Formation and Eradication of Colors by Irradiation at Low Temperatures. A Photochemical Memory Model, *J. Am. Chem. Soc.* 78 (1956) 2304–2312.
- [47] Y. Hirshberg, E.B. Knott, E. Fischer, Environmental influences and the colour of some merocyanines, *J. Chem. Soc. Resumed.* 0 (1955) 3313–3321.
- [48] V.I. Minkin, Photo-, Thermo-, Solvato-, and Electrochromic Spiroheterocyclic Compounds, *Chem. Rev.* 104 (2004) 2751–2776.
- [49] D.S. Tipikin,, Mechanochromism of organic compounds by the example of spiropyran., *Zhurnal Fiz. Khimii.* 75 (2001) 1876–1880.
- [50] S.L. Potisek, D.A. Davis, N.R. Sottos, S.R. White, J.S. Moore, Mechanophore-Linked Addition Polymers, *J. Am. Chem. Soc.* 129 (2007) 13808–13809.
- [51] B.A. Beiermann, D.A. Davis, S.L.B. Kramer, J.S. Moore, N.R. Sottos, S.R. White, Environmental effects on mechanochemical activation of spiropyran in linear PMMA, *J Mater Chem.* (2011).
- [52] C.K. Lee, D.A. Davis, S.R. White, J.S. Moore, N.R. Sottos, P.V. Braun, Force-Induced Redistribution of a Chemical Equilibrium, *J. Am. Chem. Soc.* 132 (2010) 16107–16111.
- [53] C.M. Kingsbury, P.A. May, D.A. Davis, S.R. White, J.S. Moore, N.R. Sottos, Shear activation of mechanophore-crosslinked polymers, *J Mater Chem.* (2011).
- [54] G. O'Bryan, B.M. Wong, J.R. McElhanon, Stress Sensing in Polycaprolactone Films via an Embedded Photochromic Compound, *Acs Appl. Mater. Interfaces.* (2010).
- [55] B.A. Beiermann, S.L.B. Kramer, J.S. Moore, S.R. White, N.R. Sottos, Role of Mechanophore Orientation in Mechanochemical Reactions, *ACS Macro Lett.* 1 (2012) 163–166.

- [56] C. Hepburn, Polyurethane elastomers, Applied Science Publishers, London; New York, 1982.
- [57] Z.S. Petrović, J. Ferguson, Polyurethane elastomers, Prog. Polym. Sci. 16 (1991) 695–836.
- [58] P. Król, Linear polyurethanes synthesis methods, chemical structures, properties and applications, VSP, Leiden; Boston, 2008.
- [59] R. Bonart, X-ray investigations concerning the physical structure of cross-linking in segmented urethane elastomers, J. Macromol. Sci. Part B. 2 (1968) 115–138.
- [60] J.T. Koberstein, R.S. Stein, Small-angle X-ray scattering studies of microdomain structure in segmented polyurethane elastomers, J. Polym. Sci. Polym. Phys. Ed. 21 (1983) 1439–1472.
- [61] H.S. Lee, S.L. Hsu, An analysis of phase separation kinetics of model polyurethanes, Macromolecules. 22 (1989) 1100–1105.
- [62] F. Yeh, B.S. Hsiao, B.B. Sauer, S. Michel, H.W. Siesler, In-Situ Studies of Structure Development during Deformation of a Segmented Poly(urethane–urea) Elastomer, Macromolecules. 36 (2003) 1940–1954.
- [63] C.W. Meuse, X. Yang, D. Yang, S.L. Hsu, Spectroscopic analysis of ordering and phase-separation behavior of model polyurethanes in a restricted geometry, Macromolecules. 25 (1992) 925–932.
- [64] P.J. Flory, J. Rehner, Statistical Mechanics of Cross-Linked Polymer Networks II. Swelling, J. Chem. Phys. 11 (1943) 521.
- [65] L. Leibler, Theory of Microphase Separation in Block Copolymers, Macromolecules. 13 (1980) 1602–1617.
- [66] T.P. Lodge, Block Copolymers: Past Successes and Future Challenges, Macromol. Chem. Phys. 204 (2003) 265–273.

CHAPTER 2

FORCE-INDUCED REDISTRIBUTION OF A CHEMICAL EQUILIBRIUM[‡]

2.1 Introduction

Mechanophores, molecules that respond in a productive fashion to mechanical stimuli, have the potential to dramatically increase the functionality of polymeric systems [1]. Davis *et al.* [2] first reported on covalently linked spiropyrans (SP) as highly effective color-generating mechanophores that can provide visible detection and mapping of mechanical stresses through their mechanically induced transformation to the merocyanine (MC) conformation in glassy and elastomeric chain growth polymers in the solid state. While the polymer systems explored by Davis *et al.* were quite successful in demonstrating a mechanochemically induced visible color change, the physical properties of these polymers were not ideal for investigation of the kinetics or thermodynamics of the mechanically induced transformation of SP mechanophore in bulk polymers.

The incorporation of SP mechanophore into step-growth polyurethane (PU) has a number of characterization advantages over previous polymer systems. The inherent mechanical toughness, elasticity, and low glass transition temperature ($T_g = -60\text{ }^{\circ}\text{C}$) of PU enable the effects of mechanical force on the SP-MC equilibrium (Figure 2.1a) to be studied. The initial polymer systems studied were not amenable to kinetic analysis because they were either too soft (elastomeric poly(methyl acrylate)), or too glassy (poly(methyl methacrylate) (PMMA)), $T_g =$

[‡]Results presented in this chapter were previously published in: C.K. Lee, D.A. Davis, S.R. White, J.S. Moore, N.R. Sottos, P.V. Braun, Force-Induced Redistribution of a Chemical Equilibrium, *JACS*. 132 (2010) 16107–16111.
DOI: 10.1021/ja106332g

105 °C. In PMMA, because of the high T_g , the rate of the conversion between the MC to SP form could not be investigated at room temperature and laboratory time scales [2]. The following chapter demonstrates that the SP mechanophore is mechanochromic in PU, and that the equilibrium between the colored MC and colorless SP form can be directly controlled by mechanical strain. Due to PU's low T_g , equilibrium is reached in experimentally accessible times at room temperature. Studies on the kinetics of the mechanically activated SP to MC conversion, as well as the thermally activated reversion of MC to SP in bulk polymer are conducted. PU is of specific interest not only because it is a ubiquitous engineering polymer, but also because it is synthesized via a step growth polymerization, and therefore the mechanophore concentration can be modulated independent of molecular weight or cross-linking density.

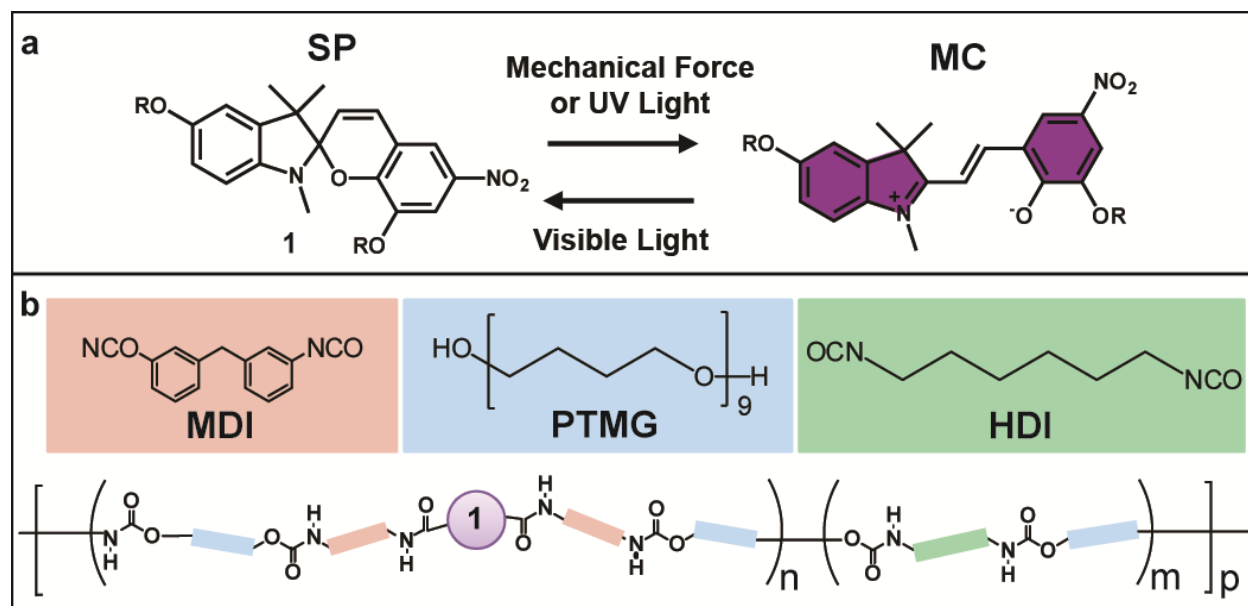


Figure 2.1 – a) Chemical structures of spiropyran (SP) and merocyanine (MC) and the mechanically or optically triggered conversion equilibrium between the colorless SP and colored MC forms. b) Schematic of the incorporation of SP mechanophore **1** into PU via step growth polymerization where $m \gg n$.

2.2 Experimental Methods

2.2.1 Materials and Synthesis

Materials: 1,6 Hexamethylene diisocyanate (HDI), 4,4'-methylenebis(phenyl isocyanate) (MDI), poly(tetramethylene oxide) (PTMO) ($M_n \approx 650\text{g/mol}$), and 1,4-diazabicyclo [2.2.2]octane (DABCO) were purchased through Sigma Aldrich. The PTMG was dried under high vacuum at 70 °C for 1-2 h before use. Hydroxyl functionalized spiropyran (SP) was synthesized according to the procedure outlined in literature [3]. Anhydrous tetrahydrofuran (THF) was obtained from an Anhydrous Engineering Solvent Delivery System (SDS) equipped with activated alumina columns. Reactions were performed under a N_2 atmosphere unless otherwise specified.

Polyurethane Synthesis: SP mechanophore incorporated polyurethane (PU) was a soft segment only material. Dihydroxy spiropyran **1** ($R=H$) (3mg, $8.5\mu\text{mol}$) was first reacted with an excess of MDI (125mg, 0.5mmol) in anhydrous THF (5mL) using DABCO (8mg, $71\mu\text{mol}$) as a catalyst, resulting in a diisocyanate functionalized mechanophore. Still in solution, the functionalized spiropyran was then reacted with PTMO ($M_n = 650\text{g/mol}$) (6.7g, 10.3mmol). The polymer was then put under vacuum at 70 °C to remove the solvent. Finally, HDI (1.86g, 11mmol) was added reacting with the PTMO to form PU. Tensile specimens were prepared by pouring the polymer into Delrin, “dog bone” shaped molds, and cured under a N_2 atmosphere at 60 °C for two days to yield the mechanophore containing polymer (PU-**1**) with the general structure shown in Figure 2.1b. Different concentrations of **1** were incorporated (0.015wt% - 0.06wt%). The resulting mechanochromic PUs all had similar molecular weights of 50-70kDa, and polydispersity indices of 3-6. For the following discussions PU-**1** with an optimized concentration of 0.03 wt% **1** was used for fluorescence and absorbance experiments.

2.2.2 Mechanical Testing

Tensile testing was done at room temperature on a rail frame with load data determined using a 50 lb. capacity Futek LSB300 load cell via a panel meter (Omega Engineering Inc., DP25B-S-A), DAQ card (National Instruments), and Labview software from National Instruments. Before absorbance and fluorescence testing, the tensile specimens were pre-strained to a length five times the initial gauge section, which caused the samples to neck and cold draw (Figure 2.2a, left). The pre-strained specimens were then reloaded to increasing levels of stretch, where stretch is defined as the final length over the initial length (after pre-straining). Typical load-stretch plots (Figure 2.2) of PU-1 (red line) and plain PU (black line) were very similar, suggesting that the low concentration of SP had negligible effects on the tensile properties of the polymer.

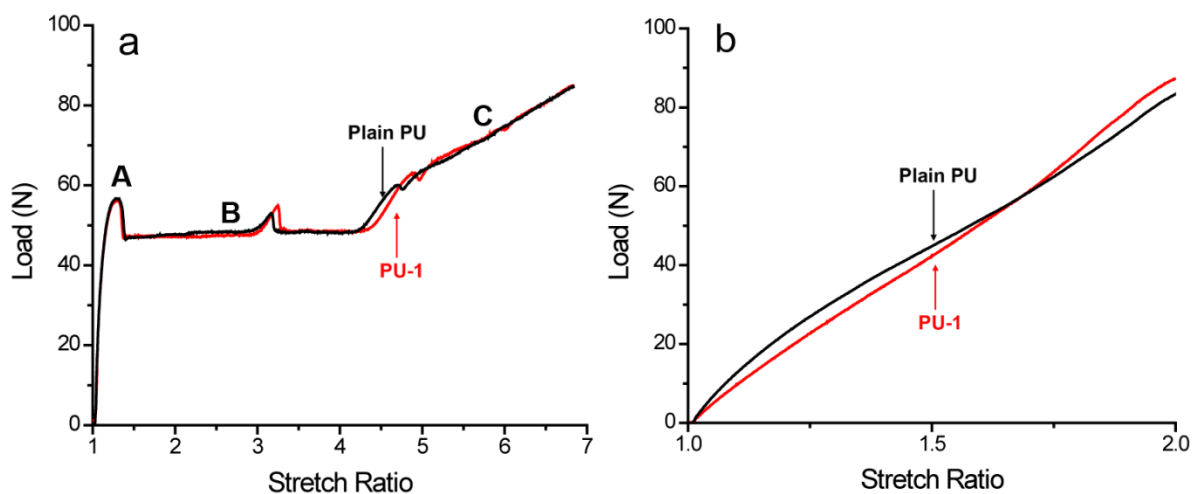


Figure 2.2 – a) Typical load-stretch plots of the first stretching of the PU samples, “pre-strain”. The polymer forms a stable neck just after the yield point (A), it draws with constant force (B) until the neck propagates along the gauge length and finally goes through an extended period of strain hardening (C). b) Load-displacement plots of a stretch after pre-straining.

2.2.3 Absorbance and Fluorescence Measurements

After pre-straining of tensile specimen absorbance data was collected using an Ocean Optics HL-2000 Tungsten Halogen light source and Ocean Optics HR2000+ spectrometer. For

collection of absorbance data the samples were mechanically tested on custom built rail frame. Displacement control was established through a bidirectional screw driven Lintech rail table. A fluorescence light microscope (Zeiss Axiovert 200M) was used to capture fluorescence images and ImageJ was used for image analysis.

2.3 Mechanical Activation and Controls

When the polymer was uniaxially stretched, a deep purple coloration appeared along the entire gauge section of the PU-1 sample (Figure 2.3a), demonstrating the stress-induced formation of the open MC form of the mechanophore. To confirm that activation of the SP mechanophore was indeed mechanical and not due to thermal or photo means of activation a difunctional control SP molecule **2** (Figure 2.3c) was synthesized and incorporated into PU (PU-2) using the same synthetic procedure as PU-1. The control SP was a hydroxyl functionalized version of the difunctional control used by Davis *et al.* [2], where the SP is coupled into the polymer backbone in such a fashion such that force is not transferred to the spiro C-O bond, and thus conversion from the SP to MC form is not mechanically triggered. When uniaxially stretched no color change was observed for plain PU (containing no mechanophore) or PU containing the difunctional control SP (PU-2) (Figure 2.3b). Absorbance measurements confirmed the lack of mechanical activation displaying no MC peak for both unstretched and stretched spectra (Figure 2.3d). In the control system, the difunctional control samples could be activated with ultraviolet (UV) light, thus confirming the presence and photochemical activity of the spiropyran (Figure 2.3b and 2.3d).

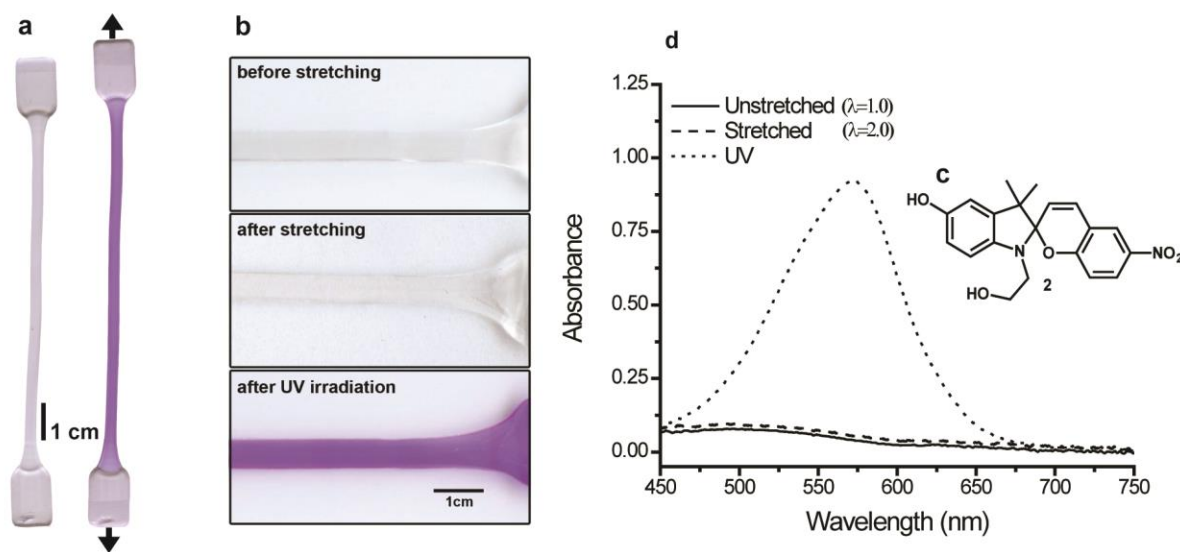


Figure 2.3 – a) Optical images of pre-stretched PU-1 “dog bone” containing 0.03wt% SP before (left) and after (right) being stretched to a stretch ratio (final length/ initial length) of 2.0 and released. b) Optical images of PU-2 before and after stretching and UV activation c) Chemical structure of difunctional control SP mechanophore. d) Absorbance spectra of PU-2 showing no mechanical activation, but a clear MC peak at about 575nm after UV irradiation.

2.4 Activation with Increasing Stretch

The mechanical activation of the PU-1 as a function of stretch was studied. It was observed that the MC absorbance peak centered on 575nm grew as a function of strain (Figure 2.4a and 2.4b), supporting the hypothesis that mechanical forces are directly responsible for converting the mechanophore from the SP to MC form. Increasing levels of strain correlate to larger amounts of mechanical force on the mechanophore, which in turn opens an increasing percentage of the mechanophores from SP to MC resulting in the growing MC peak centered at about 575nm. PU-2 was also tested with varying strain levels and resulted as expected, with no change in absorbance (Figure 2.4b).

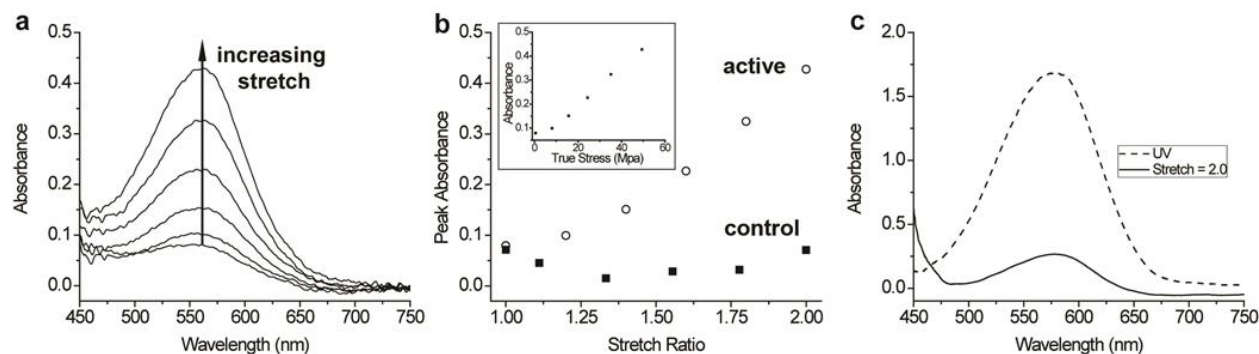


Figure 2.4 – a) Absorbance spectra of PU-1 as a function of increasing stretch ratio (1.0, 1.2, 1.4, 1.6, 1.8, 2.0). b) Peak absorbance (average of absorbance between 570 and 580nm) of PU-1 and difunctional control mechanophore as a function of stretch ratio. Inset: Peak absorbance as a function of true stress. Sufficient time was allowed between stretch steps for the mechanically induced SP to MC conversion to reach equilibrium. c) Absorbance spectra of a mechanically activated PU-1 stretched and held at a constant stretch of 2.0 compared to the same PU-1 sample irradiated with UV (365nm) for 5-10 min.

The increase of absorbance with strain as well with stress for the PU-1 appears linear at least up to a stretch of 2.0 (Figure 2.4b). Higher stretch values of about 2.3 were tested and resulted in continued increases in absorbance; however, higher stretch ratios led to slippage of the polymer samples in the testing grips. The linear increase of absorbance with strain leads us to believe we are far from activating all the mechanophore incorporated into the PU, since the absorbance must asymptotically reach some value. When the already mechanically activated PU-1 was held at a stretch of 2.0 and then irradiated with UV light ($\lambda \approx 365\text{nm}$) for 5 to 10 minutes, the polymer became noticeably darker purple and the MC absorbance peak increased (Figure 2.4c). Analysis of these results indicates that the mechanical activation of PU-1 activates ca. 20-30% of the SP relative to the amount activated by UV irradiation.

Nearly complete mechanophore activation must simply require levels of mechanical force on the mechanophore not attainable with the current experimental system. In part, this is an experimental problem in that the sample slips out of the grips at high strain, but also, on the

molecular level, this partial activation could reflect on the force distribution on individual mechanophores due to both the finite chain lengths in the sample and the distribution in mechanophore alignment in the sample. Significant color change was generally observed only after the necking event during the pre-strain step. Even though substantial plastic deformation and thus chain alignment takes place upon pre-straining, some fraction of mechanophores are likely to be oriented in such a direction that they do not activate under uniaxial tension. Overall this lends evidence to the hypothesis that chain alignment plays a key role in activation of the SP mechanophore as postulated by O'Bryan *et al.* [4] and demonstrated by Beiermann *et al.* [5]. It is also quite likely that the stress required for nearly complete activation would result in fracture of the polymer dog bone.

2.5 Kinetic Studies

In PU-1, which has a T_g of $-60\text{ }^{\circ}\text{C}$, the mechanically-induced $6-\pi$ electrocyclic ring-opening conversion from SP to MC fully reverts to the SP form after about one hour of exposure to fluorescent room light; this behavior can be repeated multiple times with the same sample. It was previously reported that the MC to SP reversion in elastomeric poly(methyl acrylate) ($T_g \approx 10\text{ }^{\circ}\text{C}$) occurred after approximately 6 hours of exposure to fluorescent room light, whereas reversion in glassy poly(methyl methacrylate) ($T_g \approx 105\text{ }^{\circ}\text{C}$) required several weeks [2]. The MC to SP ring closing kinetics appears to vary greatly with the local environment, with T_g being a major determinant.

Fluorescence imaging was used to quantify the time required for the MC to revert to SP under no load within PU. Taking advantage of the photochromic properties of SP [6], UV light was used to activate a solution casted film of PU-1, converting the SP mechanophore to the colored/fluorescent MC conformation. A thick film was used to eliminate any signal variation

from the slightly different thicknesses of the “dog bone” sample as well as scratches and defects on the surface which could lead to scattering. Over several hours, fluorescence images of the activated region were captured using brief exposures in the dark. The mean fluorescence intensity of the activated region was plotted versus time and fitted to a single exponential decay with a time constant of $\tau \approx 30\text{min}$ (Figure 2.5a). This shows that in just over an hour, kT at room temperature is sufficient to allow the MC form to revert back to the SP form favored at equilibrium.

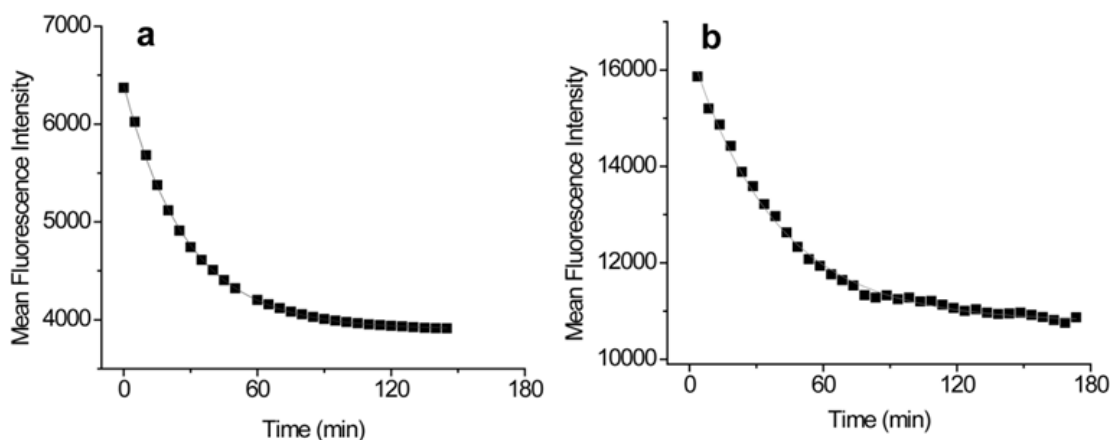


Figure 2.5 – a) Mean fluorescence intensity decay of UV activated PU-1 plotted against time and fitted to single exponential decay function with a $\tau \approx 30\text{min}$. b) Mean fluorescence intensity decay of mechanically activated PU-1 fitted to a single exponential with a $\tau \approx 38\text{min}$.

Fluorescence-based characterization was also performed on a mechanically activated PU-1 “dog bone” shaped sample. The sample was stretched to a stretch ratio of 2.0 then unloaded, placed in a dark container, and immediately taken to the fluorescence microscope. The time at which the sample was unloaded and removed from the rail frame was defined as time zero. Results for the mechanically activated PU-1 sample were similar except for a slightly longer time constant, $\tau \approx 38\text{min}$ (Figure 2.5b) when fitted to a single exponential decay function and slightly noisier due to thickness and imperfect surface of the “dog bone” shape. We suspect that the slight

increase in time constant τ could be a result of slowly relaxing residual strain in the polymer preventing the mechanophore from closing as quickly.

2.6 Mechanically Biased Equilibrium

The relatively rapid interconversion between the SP and MC form, coupled with the robust mechanical properties of PU-1 enable a quantitative analysis of the effects of strain on the equilibrium between the SP and MC forms. Visible color change of the PU-1 occurs immediately after mechanical activation, but the full color change is not instantaneous. When the sample is held at constant strain, over time it becomes increasingly purple and the MC peak (570-580nm) increases (Figure 2.6a). The peak absorbance versus time of the PU-1 sample held in the dark at a stretch of 2.0 shows the absorbance approaches a steady state value after 1-2 hours. In contrast to the mechanically activated PU-1 sample used for the fluorescence decay measurements (Figure 2.5b), which demonstrates the reversion of stress induced MC form back to the more thermally stable SP form; the mechanically activated MC in the PU-1 sample held under constant load does not revert. The plateau in absorbance seen in Figure 2.6a and lack of MC to SP reversion suggests that the mechanophore has reached a new mechanically biased equilibrium in the strained state.

After allowing the PU-1 to come to equilibrium, no change is expected to occur without changes to the ambient conditions, such as light exposure or temperature. For instance, irradiation with visible light should drive the equilibrium toward the closed SP form, even if the strain in the sample is held constant. If indeed the equilibrium ratio of MC to SP in the absence of light is determined by the force on the sample, upon removal of the visible light source, the amount of MC present should return to the no light levels. A PU-1 sample was mechanically activated in the dark to a stretch of 2.0 and allowed to equilibrate in the strained state

(approximately 1-2 hours). While still strained, the equilibrated sample was exposed to a bright visible light driving the sample towards the SP form. This could be observed as the color rapidly faded (≈ 30 min). Upon removal of the light, the color returned in 1-2 hours (the strain on the sample was constant over the entire experiment). This could be repeated multiple times, for as long as the sample stays in the strained state (Figure 2.6c). This not only provides further indication that the SP to MC conversion is induced by force, and not some other effect (e.g. effect during the initial mechanical deformation), but also shows that mechanical force is altering the potential energy surface such that the MC form becomes more favored under strain compared to the no strain situation.

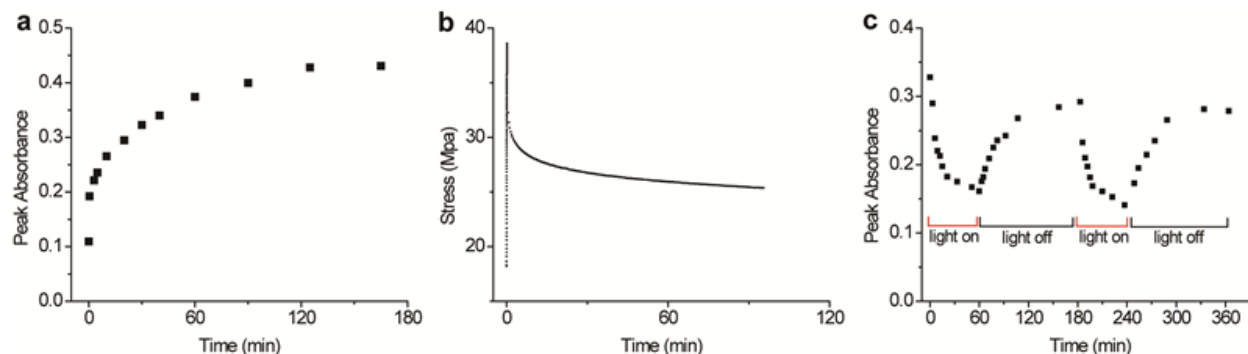


Figure 2.6 – a) Peak normalized absorbance at 570-580nm of mechanically activated PU-1 held at a constant stretch ratio of 2.0 vs. time. b) Typical stress relaxation of PU-1 held under constant strain. c) The peak absorbance (570-580nm) plotted versus time. The PU-1 sample had been held at constant stretch of 2.0 for 2 hours and at time = 0min a bright halogen light source is continuously irradiated onto the PU-1 sample for 1 hour, then removed for 2 hours, this is repeated demonstrating the altering of the equilibrium between SP and MC by strain.

Stress relaxation of the PU-1 tensile specimen was also monitored at different levels of strain (Figure 2.6b). The PU-1 was stretched at a strain rate of 1mm/sec to different levels of displacement. Between each increasing step of displacement sufficient time was allowed to ensure that the sample had relaxed and that the absorbance measurements were indeed taken at

the new equilibrium. After 90 minutes in constant strain the stress values were indeed close to a steady state value of stress relaxation, establishing that the dynamical values of stress in the tensile specimen had also equilibrated.

The thickness, cross-sectional area, and overall volume were monitored throughout the mechanical testing to ensure that measured physical dimensions of the sample over time remained constant. Thickness and cross-sectional area decrease correlated consistently with increases in gauge length of the tensile specimen, and the sample volume change remained fairly constant with only a slight increase in volume with stretch ratio. The minimal volume change indicates that although the sample is held under strain for long periods of time there is minimal grip slippage, which further supports that the measured equilibrium values are valid.

2.7 Conclusions

A new method of incorporating mechanophore into step-growth PU was developed. When uniaxially strained the SP-PU was shown to be mechanochromic. Visible spectroscopy was used to quantify the mechanical activation of SP to MC. The absorbance was shown to increase linearly with strain, and when held at constant strain, the MC form did not revert back to the thermodynamically preferred (under no load) SP form, indicating a strain-induced change in the energy landscape of the SP mechanophore system.

REFERENCES

- [1] M.M. Caruso, D.A. Davis, Q. Shen, S.A. Odom, N.R. Sottos, S.R. White, *et al.*, Mechanically-Induced Chemical Changes in Polymeric Materials, *Chem. Rev.* 109 (2009) 5755–5798.
- [2] D.A. Davis, A. Hamilton, J. Yang, L.D. Cremer, D. Van Gough, S.L. Potisek, *et al.*, Force-induced activation of covalent bonds in mechanoresponsive polymeric materials, *Nature*. 459 (2009) 68–72.
- [3] C.K. Lee, D.A. Davis, S.R. White, J.S. Moore, N.R. Sottos, P.V. Braun, Force-Induced Redistribution of a Chemical Equilibrium, *Journal of the American Chemical Society*. 132 (2010) 16107–16111.
- [4] G. O'Bryan, B.M. Wong, J.R. McElhanon, Stress Sensing in Polycaprolactone Films via an Embedded Photochromic Compound, *ACS Appl. Mater. Interfaces*. (2010).
- [5] B.A. Beiermann, S.L.B. Kramer, J.S. Moore, S.R. White, N.R. Sottos, Role of Mechanophore Orientation in Mechanochemical Reactions, *ACS Macro Letters*. 1 (2012) 163–166.
- [6] V.I. Minkin, Photo-, Thermo-, Solvato-, and Electrochromic Spiroheterocyclic Compounds, *Chem. Rev.* 104 (2004) 2751–2776.

CHAPTER 3

EXPLOITING FORCE SENSITIVE SPIROPYRANS AS MOLECULAR LEVEL PROBES[‡]

3.1 Introduction

Mechanochemistry [1] is a growing field of the study of force-induced productive chemical reactions. A considerable fraction of the research in mechanochemistry focuses on molecules that respond to external mechanical forces; such molecules are defined as mechanophores [2,3]. To date, a number of mechanophores have been developed which demonstrate force-triggered functionalities including color change [4,5], generation of reactive moieties [6–8], and catalyst activation [9,10]. While much attention has been focused on using mechanophores to add functionality to polymers, their inherent mechanochemical changes take place on the molecular scale making them attractive as localized force probes. Here we exploit the ability of a spiropyran mechanophore to react to local forces and demonstrate its use as a spatially-sensitive molecular probe in segmented polyurethane.

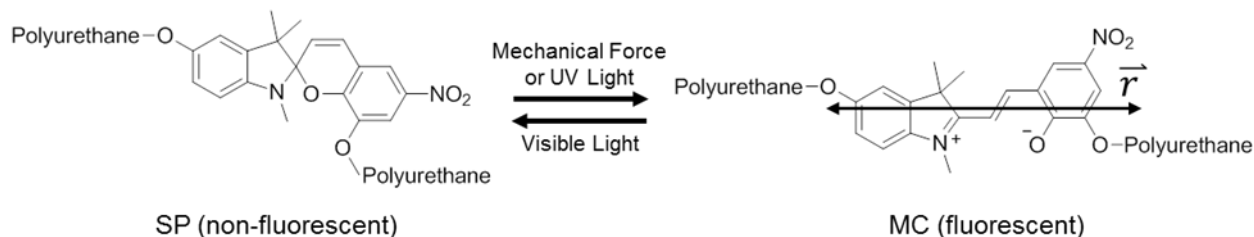


Figure 3.1 – Ring opening of SP to MC, with approximate MC transition dipole, (\vec{r}).

[‡]Results presented in this chapter were previously published in: C.K. Lee, B.A. Beiermann, M.N. Silberstein, J.Wang, J.S. Moore, N.R. Sottos, P.V. Braun, Exploiting Force Sensitive Spiropyrans as Molecular Level Probes. *Macromolecules*. 46 (2013) 3746-3752. DOI: 10.1021/ma4005428.

Spiropyran (SP), a popular mechanophore, is a well characterized molecule which undergoes a reversible 6- π electrocyclic ring opening reaction to a merocyanine (MC) form [11] (Figure 3.1). The SP mechanophore was first incorporated into solid state polymers by Davis *et al.* [5], who demonstrated stress induced ring opening of the SP within poly(methylacrylate) (PMA) into the highly colored and fluorescent MC form. More recently, mechanochemical reactivity of SP has been demonstrated in a number of different polymer systems [5,12–15], adding to the understanding of how time [13] and mobility [12,14] play important roles in the transmission of macroscopic force to these reactive moieties. Beiermann *et al.* [16] used the fluorescence anisotropy of MC [17] in PMA (elastomeric) and poly(methyl methacrylate) (PMMA) (glassy) to characterize the role of orientation in mechanically activated SP. Results showed that force-induced activation correlates to the mechanophore's state of alignment relative to the tensile direction. The fluorescence anisotropy method of characterizing SP mechanophore orientation is promising for probing orientation and force in distinct environments of a more complex polymer system, such as phase separated segmented polyurethane (SPU).

Polyurethanes are of particular interest not only because of their many useful engineering properties, but also due to their highly tunable mechanical properties, which enables a study on the effect of mechanics on mechanochemistry in a single class of polymers [18]. Polyurethanes have high abrasion and chemical resistance, excellent mechanical and elastic properties, and are blood and tissue compatible [19]. The typical segmented polyurethane elastomer is a linear block copolymer containing three primary components: a polyol, a diisocyanate, and a chain extender resulting in polymers of alternating hard (isocyanate and chain extender) and soft segments (long chain polyols). It is well recognized that the impressive combination of elasticity and strength of segmented polyurethanes is in large part due to the two-phase nature of these materials. The

thermodynamic incompatibility of the chemically distinct hard and soft segment microphase segregates into separate soft and hard segment domains. With increasing hard segment content the elastic modulus and degree of phase segregation both increase [20]. It is therefore of particular interest to study and understand how force is distributed over this two-phased morphology for a wide range of strain levels.

In part for the reasons described above, polyurethanes have been popular polymers for the incorporation and study of mechanochromic moieties. Rubner [21,22] first studied the color changing optical properties of polydiacetylene in a segmented polyurethane and reported on its thermochromic and mechanochromic properties. Since then, other reports [23–26] have described the use of mechanochromic polydiacetylenes to study the organization and role of the hard segment domains in segmented polyurethane during tensile deformation. Kim *et al.* [27] used the *trans*-to-*cis* isomerization of diaminoazobenzenes synthesized into segmented polyurethane as a “strain recording material.” Most recently Crenshaw and Weder [28,29] blended and covalently incorporated cyano-substituted oligo(*p*-phenylene vinylene) (cyano-OPV) into segmented polyurethane. Mechanical deformation of these systems led to irreversible phase separation exhibiting corresponding photoluminescent color change. Recently, we reported on the synthesis and properties of SP-linked polyurethane (not segmented) [13]. Here, using a similar step growth polymerization approach, a segmented polyurethane containing the SP mechanophore in either the soft or the hard segment is synthesized. The SP mechanophore’s sensitivity to molecular level forces will be used to probe each phase of segmented polyurethane during uniaxial tensile loading, providing information about the force and the molecular alignment within each phase.

3.2 Experimental Methods

3.2.1 Materials and Synthesis

Materials: 1,6 Hexamethylene diisocyanate (HDI), 4,4'-methylenebis(phenyl isocyanate) (MDI), poly(tetramethylene oxide) (PTMO) ($M_n \approx 1000$ g/mol), 1,4 butanediol (BD), and 1,4-diazabicyclo [2.2.2]octane (DABCO) were purchased through Sigma Aldrich. The PTMO and BD were dried under high vacuum at 70 °C for 1-2 h before use. Hydroxyl functionalized spiropyran (SP) was synthesized according to the procedure outlined by Davis *et al.* [5] Anhydrous tetrahydrofuran (THF) was obtained from an Anhydrous Engineering Solvent Delivery System (SDS) equipped with activated alumina columns. Reactions were performed under a N₂ atmosphere unless otherwise specified.

SP functionalization: Dihydroxy functionalized SP (3mg, 8.5μmol) and DABCO (8mg, 71μmol) were dissolved in anhydrous THF (5mL) to form solution A. MDI (125mg, 0.5mmol) was dissolved in an equal volume of anhydrous THF to form solution B. A large molar excess of MDI to SP was used to ensure diisocyanate functionalization of the SP, and to minimize the probability of SP-MDI oligomerization. Solution A was added dropwise to solution B, mixed and heated at 70 °C for 1 h.

SP in the soft segment (SPSS): For the 40 wt% hard segment SPU the functionalized SP solution was added to the PTMO soft segment (4.89g, 4.89mmol). While the SP mechanophore reacted with the PTMO at 70 °C, the THF solvent was simultaneously removed under high vacuum. Next, HDI (2.31g, 13.76mmol) was added to the PTMO and reacted at 70 °C for 2 h. Finally the hard segment chain extender BD (0.8g, 8.88mmol) was added, thoroughly mixed, degassed, poured into Delrin “dog bone”-shaped molds and cured in an N₂ purged oven at 60 °C for 2 d. The 22 wt% hard segment SPU was synthesized using the above procedure with the ratio of monomers as follows: PTMO: HDI: BD 6.25:8.92:2.66 mmol.

SP in the hard segment (SPHS): For the 40 wt% hard segment SPU, the functionalized SP solution was added to BD (0.8g, 8.88mmol) and reacted for 10-15 min. The SP-BD solution was then added to a soft segment prepolymer of PTMO (4.89g, 4.89mmol), HDI (2.31g, 13.76mmol) and DABCO (2mg, 1 μ mol) pre-synthesized for 1.5-2 h at 70 °C. While reacting, the polymer was put under high vacuum to remove the THF solvent. Finally, the polymer was poured into Delrin “dog bone”-shaped molds and cured in an N₂ purged oven at 60 °C for 2 d. The 22 wt% hard segment SPU was synthesized using the above procedure with the ratio of monomers as follows: PTMO: HDI: BD 6.25:8.92:2.66 mmol.

3.2.2 Sample Preparation

For UV activated experiments SPU samples were irradiated with UV light ($\lambda = 365\text{nm}$) for 10 min immediately prior to mechanical testing and imaging. For mechanically-activated experiments a halogen light source was used to irradiate visible light on the SPU samples for at least 10 min to drive the equilibrium toward the non-fluorescent SP form. This was to ensure that mechanically activated mechanophore in the fluorescent MC form would dominate the fluorescence response.

3.2.3 Optical Characterization

A circularly polarized 532 nm laser was used to excite the fluorescent SPU samples. Full field fluorescence was collected using a CCD camera (Allied Vision Technology model 145C) after passing through a linear polarizer positioned either parallel or perpendicular to the stretch direction. The red channel intensity of the CCD, corrected for background noise, was taken as the fluorescence intensity. The fluorescence intensities were averaged over each CCD pixel to

calculate an order parameter. Figure 3.2 shows a schematic of the experimental setup for fluorescence anisotropy collection which was also previously reported [16].

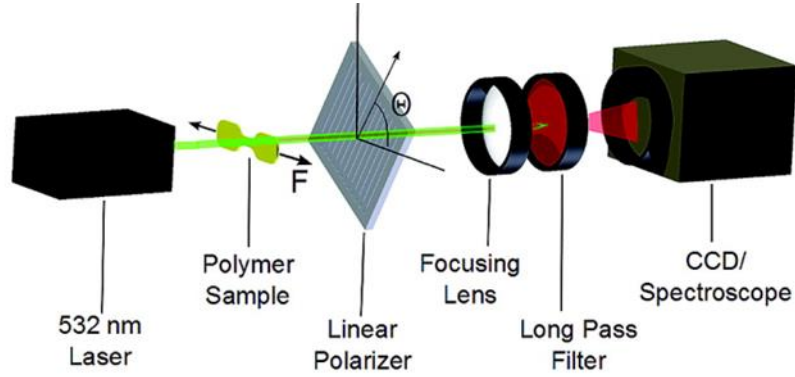


Figure 3.2 – Schematic of the experimental setup used to measure fluorescence polarization during deformation, adopted from Beiermann *et al.* [16]. Full field fluorescence images taken using a CCD camera focused on the sample and the red channel intensity of the CCD, corrected for background noise, was taken as the quantitative fluorescence intensity.

3.2.4 Mechanical Testing

SPU samples were strained incrementally, with steps of 25% strain with respect to the initial length, at a strain rate of 0.004 s^{-1} using a bi-directional screw driven rail table. Force was measured using a Honeywell Sensotech load cell with load capacity of 220 N. Between each motion step, a fluorescent image was taken with a linear polarizer in either the parallel or perpendicular orientation, the polarizer was then rotated 90° , and a fluorescent image was taken at the second polarizer orientation. The elongation was reported using a stretch ratio (λ) where stretch ratio is defined as the final length over the initial length. True stress is defined assuming incompressibility as:

$$\sigma_{True} = \frac{P}{A_0} \lambda \quad (1)$$

where P is defined as the load, A_0 is the initial cross-sectional area, and λ is the stretch ratio.

3.2.5 Order Parameter

The relative orientation was determined using an order parameter (S) based on the second-order Legendre polynomial P_2 : [30]

$$\langle P_2 \rangle = \frac{\langle 3 \cos^2(\beta) - 1 \rangle}{2} \equiv S \quad (2)$$

where β is the angle between the stretch direction and the predominant emission dipole moment (\vec{r}) of the MC molecule (Figure 3.1). From eq (2), order parameter values vary between 0 (random distribution) and 1 (perfect alignment). The order parameter is derived from eq (2) based on the measured parallel and perpendicular fluorescence intensities with respect to the stretch direction [31,32]:

$$S = \frac{(I_{\parallel} - I_{\perp})}{(I_{\parallel} + 2I_{\perp})} \quad (3)$$

where I_{\parallel} and I_{\perp} represent the total fluorescence intensity with the linear polarizer parallel and perpendicular to the stretch direction respectively. Eq (3) assumes that the mechanophore is rotationally fixed during each set of parallel and perpendicular measurements.

3.2.6 Optical Corrections

Fluorescence images of SPU samples, after visible light exposure and under no load, showed a small level of inherent fluorescence. The inherent fluorescence is a result of a small population of mechanophore in the MC form at equilibrium in SPU ($I_{eq.}$). While the equilibrium form of the mechanophore is predominantly the colorless SP constitution [13], this small population of randomly oriented MC prior to stretching lowers the calculated “mechanically activated” order parameter. We define the measured fluorescence intensity as the sum of fluorescence from mechanically activated mechanophore (I_{mech}) and the mechanophore in the MC form at equilibrium ($I_{eq.}$) seen in eq (4).

$$I_{meas} = I_{mech} + I_{eq}. \quad (4)$$


To determine order parameters for only mechanically activated mechanophore, the measured fluorescence intensity (I_{meas}) is first corrected for the inherent fluorescence and scattering due to changes in sample thickness during testing using experimental data collected from a non-mechanically activated difunctional control SP mechanophore [5,13] synthesized into SPU (see Figure 3.3 for detailed chemistry). Its fluorescence behavior with stretch was measured and $T_{correction}$ is defined as the normalized fluorescence intensity from the difunctional control SP in SPU during stretching seen in Figure 3.7a and 3.7b (“22 wt% HS Control” and “40 wt% HS Control”). The measured fluorescence with the correction factor is defined in eq (5).

$$\frac{I_{meas.}}{T_{correction}} = I_{mech} + I_{eq.} * (1 - x) \quad (5)$$

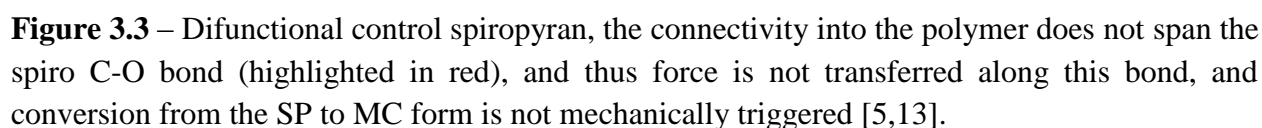
$T_{correction}$ is the thickness and scattering correction factor and x is the fraction of mechanophore which mechanically activate relative to the total concentration of mechanophore. From previous studies [13] we can assume that the number of mechanically activated mechanophore is low compared to the total concentration of mechanophore, and therefore this term is dropped and the fluorescence correction equation, solving for I_{mech} can be approximated as:

$$I_{mech} = \frac{I_{meas.}}{T_{correction}} - I_{eq}. \quad (6)$$

Eq (6) is applied to the measured fluorescence data of all mechanically activated tests and the order parameters were calculated using I_{mech} values. While the resulting order parameters are a more accurate representation of mechanically activated mechanophore orientation, the equation does not account for the orientation effects on $I_{eq.}$ at different stretch ratios (the effect of strain on the angular distribution of the equilibrium population of mechanophores in the MC form). We simply assume any changing orientation of $I_{eq.}$ at different stretch ratios are negligible for this



The chemical structure shows a bis-benzoxazine resin. It consists of two benzoxazine rings linked by a central carbon atom. Each benzoxazine ring has a polyurethane group attached to the nitrogen atom. The structure is labeled with "Polyurethane-O" and "Polyurethane". A red dashed line highlights the benzoxazine ring system.



Thermal properties of the SPUs were determined using differential scanning calorimetry (DSC) with a Mettler-Toledo model DSC821. Each sample was first heated from room temperature (25 °C) to 200 °C, and then cycled from -150 °C to 200 °C at 20 °C min⁻¹.

Segmented polyurethane (SPU) with spiropyran (SP) mechanophore (SP-SPU) incorporated into either the soft segment (SPSS) or hard segment (SPHS) was synthesized at a low (22 wt%) and high (40 wt%) hard segment (HS) composition. Thermal analysis using DSC shows a soft segment glass transition temperature (T_g) of ca. $-70\text{ }^{\circ}\text{C}$ for both hard segment compositions (Figure 3.5). In the 40 wt% sample, there is a clear hard domain melting endotherm at T_m ca. $160\text{ }^{\circ}\text{C}$, while in the 22 wt% sample the melting endotherm is shifted to a lower temperature and is broader (T_m ca. $85\text{ }^{\circ}\text{C}$). The literature T_m of pure HDI-BD hard segment is $180\text{ }^{\circ}\text{C}$ [33], so the shifted T_m in the 22 wt% material is most likely due to partial miscibility of hard and soft

segments at this lower hard segment content [34]. The location of the SP does not measurably influence T_g or T_m in either material (Figure 3.4).

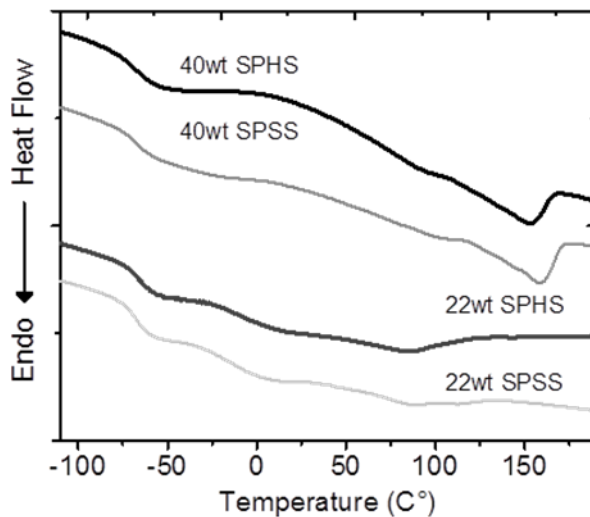


Figure 3.4 – Heating curves (2nd heating) of low (22 wt%) and high (40 wt%) hard segment content SPU of SPSS and SPHS.

Stress-stretch curves are presented in Figure 3.5a. As expected, higher hard segment content increases stiffness and strain hardening response. Drops in the stress are due to polymer relaxation at each stop in deformation to capture the fluorescence images. The relaxation appears to be minimal, and the overall stress in the SPU is comparable to SPU stretched at a continuous strain rate (Figure 3.5b). The location of the SP (incorporation into the hard or soft segment) does not induce statistically significant changes in the mechanical behavior of the material (Figure 3.5a). The lack of change enabled direct SP-based comparisons of the two segments within each material.

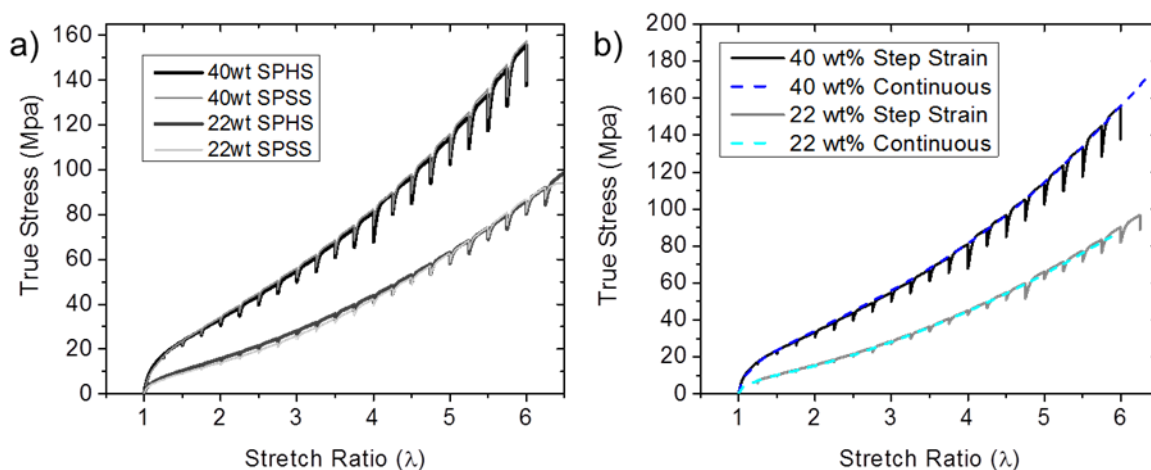


Figure 3.5 – a) Typical step loading stress vs. stretch ratio curves of the low (22 wt%) and high (40 wt%) hard segment compositions with the (SP) incorporated in either the hard segment (SPHS) or the soft segment (SPSS). b) True stress versus stretch ratio of both 40 wt% and 22 wt% comparing step strain loading and continuous loading (using SPSS material).

When the SP-SPU was stretched monotonically, the coloration of the polymer changed to a deep purple due to the force-induced activation of SP to MC (Figure 3.6c). *In situ* fluorescence images were collected during SPU stretching, and normalized average fluorescence intensities (I/I_0) were plotted against stretch ratio (Figure 3.6a and 3.6b). The normalized fluorescence (I/I_0) of the active sample decreases, increases, and then, for the 40 wt% case, levels off. This non-monotonic behavior results from specimen thickness and scattering changes during stretching. Normalized fluorescence for the non-mechanically active difunctional control SP-SPU (Figure 3.6a and 3.6b, “22 wt% Control” and “40 wt% Control”) is assumed to remain constant during deformation, and was used to quantify the strain induced optical (primarily thickness and scattering) effects on fluorescence. When evaluating the SP to MC activation, the mechanophore is assumed to exist primarily in the SP form below a critical force and in the MC form above this critical force [13]. Therefore, the increasing fluorescence values with stretch represent an increasing population of mechanophore above this critical force.

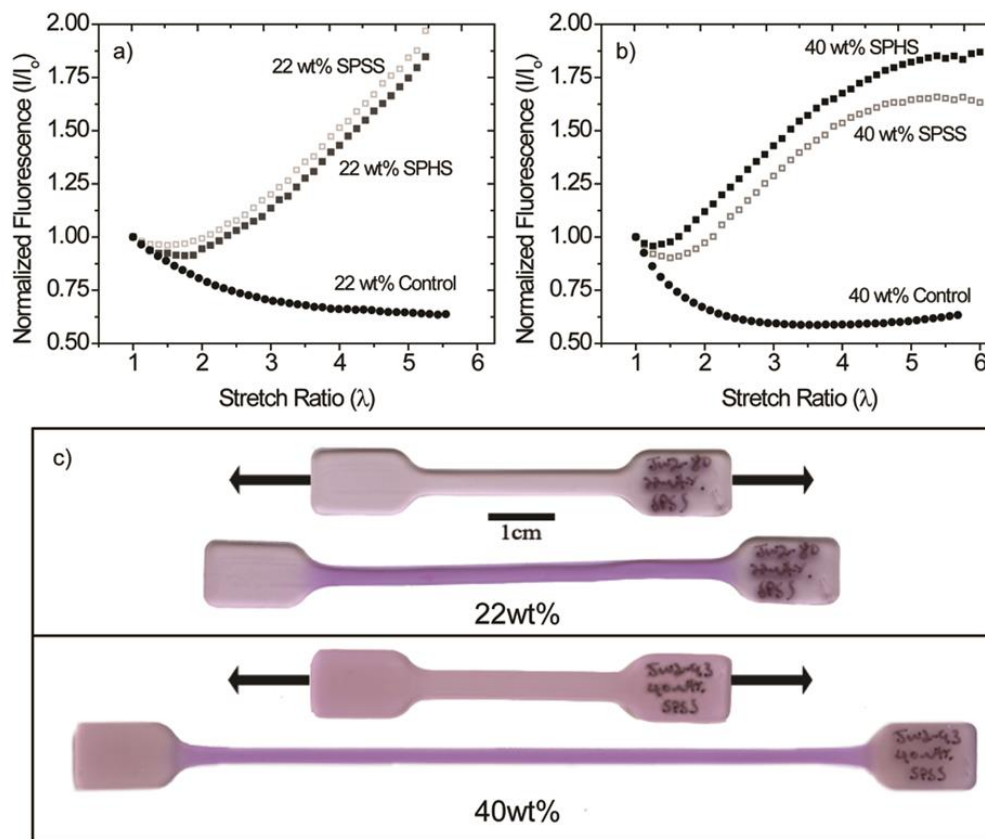


Figure 3.6 – Normalized fluorescence during monotonic stretching of active and control SP-SPU in a) 22 wt% hard segment SPU and b) 40 wt% hard segment SPU c) Optical images of mechanically activated SP-SPU (after unloading), both strained to a stretch ratio of at least 5.5. Higher strain recovery in the 22 wt% HS SPU is due to the lower HS content resulting in its more elastomeric nature.

3.4 UV-Activated Spiropyran-linked Segmented Polyurethane

UV activated material was used to track orientation during uniaxial deformation. The SP incorporated SPU samples were irradiated with UV light ($\lambda=365\text{nm}$) prior to stretching to convert a large population of the colorless SP mechanophore to the fluorescent MC form. By monitoring the UV activated MC form, the calculated order parameters represent the average orientation of all the mechanophores in the SPU. The UV activated samples were then incrementally strained to a stretch ratio of 6. Figure 3.7 shows the calculated order parameters for both compositions of hard segment with SP in the soft segment (SPSS) and SP in the hard

segment (SPHS). Not surprisingly, for all samples, the order parameter under no load ($\lambda=1$) is nearly 0 indicating that the MC (i.e., from UV activation) are initially randomly oriented. The order parameters for both the 22 wt% and 40 wt% hard segment SP-SPU samples show an increase in orientation of the MC molecules in the direction of tensile stretch as a function of increasing stretch ratio, with the 22 wt% always more oriented than the 40 wt% hard segment material. In the 22 wt% hard segment SPU, the SP in the soft and hard segments exhibit the same orientation, with order parameters increasing from near zero to ca. 0.25 with increasing stretch ratio. The similarity between the two materials suggests that at this low quantity of hard segment, the majority of the hard segment is miscible with the soft segment. The shallow and broad melting endotherm seen in Figure 3.4 for the 22 wt% material supports this assumption.

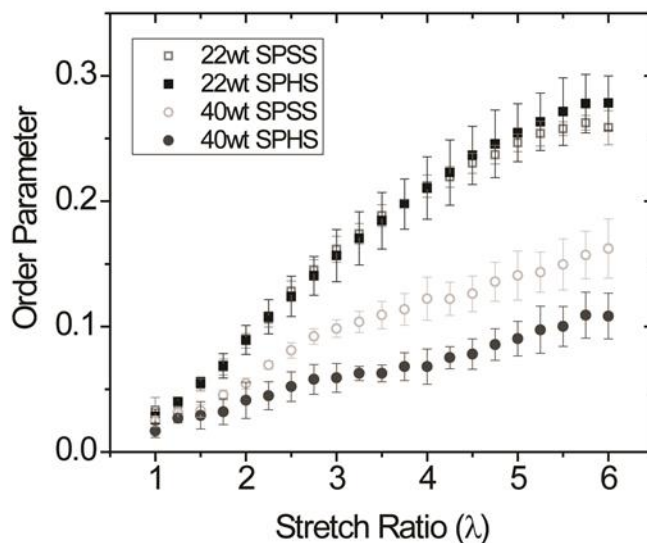


Figure 3.7 – Average order parameter as a function of stretch ratio of UV activated SP-SPU. Error bars represent standard deviation of three samples tested.

In the 40 wt% material, the orientation of the mechanophore also increases with stretch ratio and shows that the SPSS is always more oriented than the SPHS. The SPSS order parameter increases from near zero to ca. 0.15, whereas the SPHS only increases to ca. 0.10 (Figure 3.7).

The differing order parameters for SP in the two segments is consistent with the notion that these two segments are phase separated. Assuming that orientation of the MC is directly related to the orientation and alignment of the polymer chains, the higher order parameter in the SPSS implies that rotation and alignment of the soft segment polymer chains occurs before rotation and alignment of the hard segment domains.

3.5 Mechanically Activated Spiropyran-linked Segmented Polyurethane

The force induced conversion of the initially colorless SP to the fluorescent MC form was used to track orientation of the mechanophores, in which force at the molecular level was sufficient to drive the SP-to-MC conversion during uniaxial deformation. Figure 3.8a and 3.8b show typical parallel and perpendicular fluorescence values for 22 wt% and 40 wt% hard segment SPU samples. While fluorescence parallel and perpendicular to the stretch direction both increase as a function of strain, the parallel fluorescence is much higher indicating that there are more MC mechanophores that were mechanically activated when oriented parallel to the stretch direction relative to the perpendicular stretch direction. Using the fluorescence data in Figure 3.8a and 3.8b, order parameters were calculated and are shown in Figure 3.8c. The order parameters follow the same trends with stretch as in the UV activated cases.

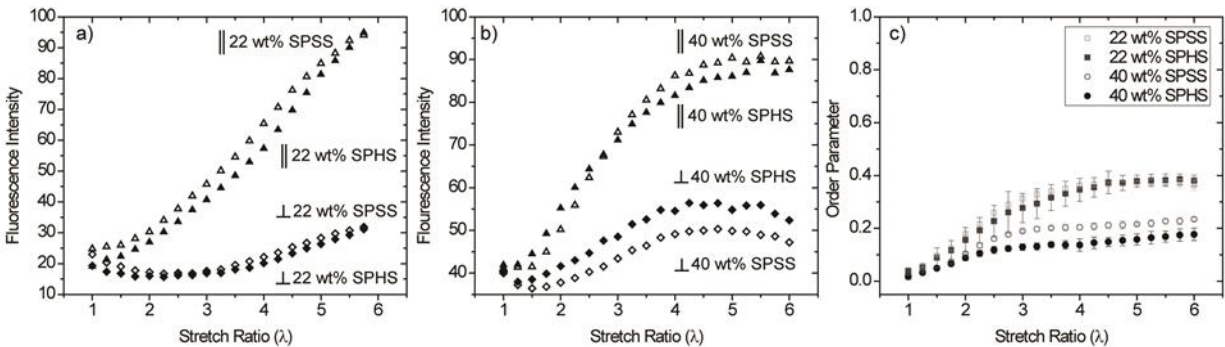


Figure 3.8 – Typical parallel and perpendicular fluorescence intensities from a) 22 wt% and b) 40 wt% hard segment SPSS and SPHS both stretched to a stretch ratio of at least 5.5. c) Mechanically-activated order parameter vs. stretch ratio of SPSS and SPHS for both 22 wt% and 40 wt% hard segment content SPU.

The orientation of mechanophores at sufficient force to mechanically activate SP is somewhat obscured by the initially non-zero (and randomly oriented) fluorescence (Figure 3.8a and 3.8b). In order to isolate only the mechanically activated MC, we corrected the measured fluorescence intensities for thickness and scattering changes using the fluorescence behavior of a non-mechanically active difunctional control SP mechanophore synthesized into SPU. We assume that the thickness and optical changes during stretching of this control is similar to the active SP-SPU materials. The 22 wt% and 40 wt% hard segment SPUs corrected fluorescence intensities (I_{mech}) isolating mechanically induced fluorescence are shown for both the SPSS and SPHS in Figure 3.9a and 3.9b. The corrected parallel and perpendicular fluorescence now start at zero and increase with stretch for both hard segment concentrations. In Figure 3.9b, the fluorescence appears to increase up to $\lambda \approx 4$, where it then levels off, and then decreases. The origin of this decrease stems from the $T_{\text{correction}}$ curve used in the fluorescence correction (see 3.2.6 *Optical Corrections*). While the fluorescence for the difunctional control samples show an overall decrease with fluorescence due to sample thinning (Figure 3.6a and 3.6b, “22 wt% HS Control” and “40 wt% HS Control”), in the 40 wt% HS Control around $\lambda \approx 4$ there is a slight upturn in

fluorescence. The increase in fluorescence in the 40 wt% HS Control at high order parameters is not fully understood, but does result in the decrease in fluorescence seen in Figure 3.9b. We believe the decrease in fluorescence at high λ to be unphysical and not representative of SP mechanophore activation or orientation with mechanical force. Though the fluorescence data appears to decrease, the overall conclusions drawn from order parameter calculations, which are a ratio of the parallel and perpendicular fluorescence, are not affected. Order parameters from the isolated mechanically activated fluorescence (Figure 3.9c) are significantly higher than the uncorrected order parameters (Figure 3.8c). Order parameter values at $\lambda < 2$ were omitted due to insufficient fluorescence. For the single phase 22 wt% hard segment SPU order parameter values range from ca. 0.7 to ca. 0.5. In the 40 wt% hard segment SPU, a clear difference in the SPSS and SPHS order parameters is still present, but now the corrected fluorescence results in greater values, ca. 0.2 to ca. 0.4.

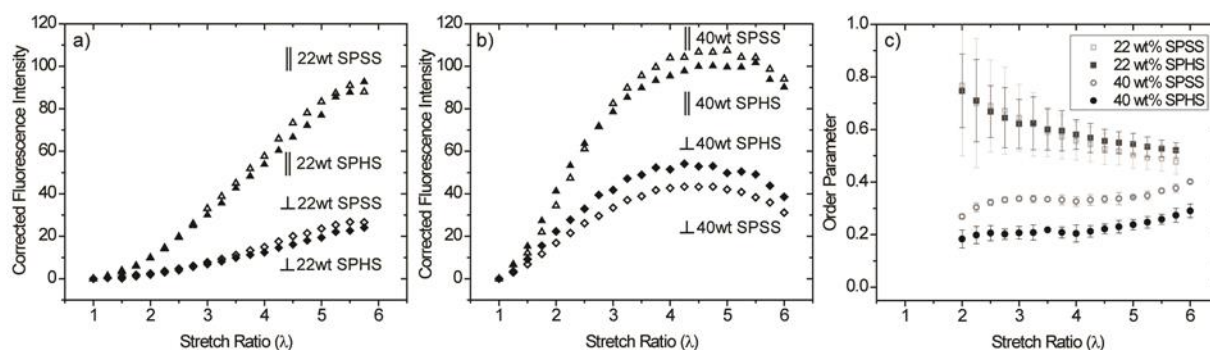


Figure 3.9 – Representative corrected parallel and perpendicular fluorescence intensities for a) 22 wt% and b) 40 wt% hard segment SPSS and SPHS. c) Mechanically activated order parameters calculated from parallel and perpendicular intensities corrected for thickness and optical changes.

The low glass transition temperature (T_g ca. -70 °C) and elastomeric nature of the soft segment results in a very mobile phase, while the high melting temperature (T_m ca. 160 °C) of the hard

segment domains (Figure 3.4) results in a glassy, more constraining local environment. It is for this reason that we assume SP in the soft segments will have greater mobility than SP in the glassier hard segment, affecting the overall ability of SP mechanophores to align under stress. The high level of orientation for mechanically activated SP (Figure 3.9c) in the 22 wt% hard segment compared to the 40 wt% hard segment SPU may be related to the microstructure of each material. In the 22 wt% SPU, the hard segment is miscible, thus, the load is distributed equally across the hard and soft segments, and the hard segments do not constrain rotation of the SP. The high levels of orientation then result from the soft and hard segments jointly undergoing elastomeric stretching and alignment. The miscibility of the hard and soft blocks explains the similar order parameters for the 22 wt% SPHS and 22 wt% SPSS. In the 40 wt% SPU, the hard domains are likely phase separated and may not deform equivalently with the soft domains due to the difference in mobility in each segment, resulting in the possibility of hard domains constraining the rotation of the SP. And, at a given stretch ratio, more of the strain may be across the soft segments, resulting in the observed higher order parameter for the SPSS than the SPHS (Figure 3.8c and Figure 3.9c).

The corrected mechanically activated SP-SPU order parameters also show interesting trends as a function of stretch ratio. In the UV activated cases (Figure 3.7), the order parameters all increased with increasing stretch ratio, representing the effect of the macroscopic deformation on the orientation of all mechanophores. The order parameters in the mechanically activated case (Figure 3.9c) decrease with increasing stretch ratio for the 22 wt% hard segment and only modestly increase with increasing stretch ratio in the 40 wt% hard segment SPU. The difference between the UV activated (all mechanophores activated) and the mechanically activated (only mechanophores which feel sufficient local force activated) results demonstrate the orientation-

dependent effect of force on mechanophore activation. Essentially, mechanophores oriented perpendicular to the applied force are unlikely to activate, while the UV activates mechanophores regardless of orientation.

The decreasing order parameter with increasing stretch ratio seen in the 22 wt% hard segment SPU can likely be attributed to increasing levels of force at higher stretch ratios. A similar trend in mechanophore orientation was seen in elastomeric PMA [16]. At low stretch ratios those mechanophores which are highly aligned with the direction of stretch activate first. As the sample is strained, the stress in the SPU increases, and force across the polymer chains increases, which in turn causes mechanophores that are increasingly off-axis to also activate, lowering the overall average calculated order parameter. The trend in the 40 wt% hard segment SPU is also different than the more homogenous 22 wt% hard segment SPU. The order parameter initially shows slight increases, plateaus from $\lambda \approx 3$ to $\lambda \approx 4$, and then again increases slightly to $\lambda = 6$. The origins of non-continuous changes in the order parameter in the 40 wt% SPU could be a combination of factors; we hypothesize the observation may be related to the “hard segment break-up” phenomena common in SPUs [35,36]. As the SPU is initially stretched, most of the deformation is likely carried by the soft segment, seen by the higher increase in order parameter for the SPSS from $\lambda \approx 2$ to $\lambda \approx 3$. From $\lambda \approx 3$ to $\lambda \approx 4$, deformation may become more distributed between both segments, possibly the origin of the slight plateau, and finally at $\lambda > 4$, the hard segment domains begin to break up due to higher levels of stress. As the hard segment domains break up, soft segment chains which were previously un-stretched chains connecting hard domains can now stretch and orient, supported by the slight increase in orientation for the SPSS (Figure 3.9c). The slight increase in the orientation seen in the SPHS material at $\lambda > 4$ may be due to more alignment of the SPHS because the hard domains break up in the direction of stretch.

The order parameters determined for the mechanically-activated SPU samples are ratios of the parallel and perpendicular fluorescence; therefore, to determine a degree of activation for the SP mechanophore, the measured fluorescence intensities rather than the order parameters need to be compared. In the 22 wt% material, the change in fluorescence intensity with stretch ratio for both the SPSS and SPHS are about the same (Figure 3.8a and Figure 3.9a). This similarity is evidence that the SP mechanophore at this low hard segment content is essentially in the same local environment, independent of whether SP was synthesized into the hard segment or soft segment. Therefore, at this concentration of hard segment, the SPSS and SPHS have a similar degree of mechanical activation.

Since the SPHS in 40 wt% hard segment SPU had a lower average order parameter, the SP is less mobile in the hard segment and is expected to show a lower degree of activation compared to the more aligned SPSS. Figure 3.8b and 3.9b, presents the 40 wt% hard segment SPU fluorescence data for the parallel fluorescence and perpendicular fluorescence for both the SPSS and SPHS. The parallel fluorescence intensity is about the same for both the SPSS and the SPHS, indicating that while the SPHS is in a less mobile environment, it does have enough mobility to mechanically activate. The degree of activation of the SP in both the hard and soft segment is comparable when the mechanophore is oriented in the direction of stretch, but the SP in the hard segment are capable of mechanically activating at much lower levels of alignment relative to the direction of stretch. These results suggest that force is carried differently in the elastomeric soft segment and the glassy hard segment. In the elastomeric soft-segment force is translated into simultaneous stretching and rotating. SP in chains that are not aligned do not activate because those chains do not carry significant force. The hard segment chains, having a higher glass transition temperature, do not undergo the same elastomeric-like chain deformation as the soft

segment does. The force on the SP mechanophore causing activation in the hard segment may be more dominated by intermolecular chain forces, allowing activation of mechanophore which are not fully aligned with the direction of stretch.

3.6 Conclusions

The SP mechanophore was incorporated into either the soft or hard segment phase of segmented polyurethane, and shown to be mechanochromic. Using the SP mechanophore as a molecular level probe, the orientation and force-induced activation of the mechanophore in each phase at two different hard segment compositions (22 wt% and 40 wt%) of SPUs were studied. When the SP mechanophore was synthesized into either the soft segment (SPSS) or hard segment phase (SPHS) of the 22 wt% material, the same levels of activation and orientation for both SPSS and SPHS are seen in UV activated and mechanically-activated experiments, suggesting a lack of phase segregation. In the mechanically activated experiments, this single phase material also demonstrated high levels of alignment (order parameter ca. 0.5-0.7) with the direction of stretch. In the 40 wt% material, segregation of the hard and soft segments was evident, and the SPSS and SPHS show different average order parameters as a function of increasing stretch ratio. The higher level of orientation for the SPSS in 40 wt% material compared to the SPHS suggests that the force felt by the mechanophore in each phase is different. Similar levels of fluorescence in the parallel direction indicate that while the hard segment phase is glassy, there is still enough mobility for force-induced activation of the mechanophore. The higher perpendicular fluorescence for SPHS indicates that SP mechanically activates in the hard segment at lower levels of alignment. The different mechanism by which force is transferred to the mechanophore in each phase provides insight into force distribution in each local environment.

REFERENCES

- [1] M.M. Caruso, D.A. Davis, Q. Shen, S.A. Odom, N.R. Sottos, S.R. White, *et al.*, Mechanically-Induced Chemical Changes in Polymeric Materials, *Chem. Rev.* 109 (2009) 5755–5798.
- [2] C.R. Hickenboth, J.S. Moore, S.R. White, N.R. Sottos, J. Baudry, S.R. Wilson, Biasing reaction pathways with mechanical force, *Nature*. 446 (2007) 423–427.
- [3] J.N. Brantley, K.M. Wiggins, C.W. Bielawski, Polymer mechanochemistry: the design and study of mechanophores, *Polym. Int.* 62 (2013) 2–12.
- [4] S.L. Potisek, D.A. Davis, N.R. Sottos, S.R. White, J.S. Moore, Mechanophore-Linked Addition Polymers, *J. Am. Chem. Soc.* 129 (2007) 13808–13809.
- [5] D.A. Davis, A. Hamilton, J. Yang, L.D. Cremer, D. Van Gough, S.L. Potisek, *et al.*, Force-induced activation of covalent bonds in mechanoresponsive polymeric materials, *Nature*. 459 (2009) 68–72.
- [6] M.J. Kryger, M.T. Ong, S.A. Odom, N.R. Sottos, S.R. White, T.J. Martinez, *et al.*, Masked Cyanoacrylates Unveiled by Mechanical Force, *J. Am. Chem. Soc.* 132 (2010) 4558–4559.
- [7] J.M. Lenhardt, A.L. Black, B.A. Beiermann, B.D. Steinberg, F. Rahman, T. Samborski, *et al.*, Characterizing the mechanochemically active domains in gem-dihalocyclopropanated polybutadiene under compression and tension, *J Mater Chem.* 21 (2011) 8454–8459.
- [8] C.E. Diesendruck, B.D. Steinberg, N. Sugai, M.N. Silberstein, N.R. Sottos, S.R. White, *et al.*, Proton-Coupled Mechanochemical Transduction: A Mechanogenerated Acid, *J. Am. Chem. Soc.* 134 (2012) 12446–12449.
- [9] A.G. Tennyson, K.M. Wiggins, C.W. Bielawski, Mechanical Activation of Catalysts for C–C Bond Forming and Anionic Polymerization Reactions from a Single Macromolecular Reagent, *J Am Chem Soc.* 132 (2010) 16631–16636.
- [10] J.M.J. Paulusse, R.P. Sijbesma, Selectivity of mechanochemical chain scission in mixed palladium(ii) and platinum(ii) coordination polymers, *Chem. Commun.* (2008) 4416–4418.
- [11] V.I. Minkin, Photo-, Thermo-, Solvato-, and Electrochromic Spiroheterocyclic Compounds, *Chem. Rev.* 104 (2004) 2751–2776.
- [12] B.A. Beiermann, D.A. Davis, S.L.B. Kramer, J.S. Moore, N.R. Sottos, S.R. White, Environmental effects on mechanochemical activation of spiropyran in linear PMMA, *J Mater Chem.* (2011).
- [13] C.K. Lee, D.A. Davis, S.R. White, J.S. Moore, N.R. Sottos, P.V. Braun, Force-Induced Redistribution of a Chemical Equilibrium, *J. Am. Chem. Soc.* 132 (2010) 16107–16111.
- [14] C.M. Kingsbury, P.A. May, D.A. Davis, S.R. White, J.S. Moore, N.R. Sottos, Shear activation of mechanophore-crosslinked polymers, *J Mater Chem.* (2011).
- [15] G. O'Bryan, B.M. Wong, J.R. McElhanon, Stress Sensing in Polycaprolactone Films via an Embedded Photochromic Compound, *Acs Appl. Mater. Interfaces.* (2010).
- [16] B.A. Beiermann, S.L.B. Kramer, J.S. Moore, S.R. White, N.R. Sottos, Role of Mechanophore Orientation in Mechanochemical Reactions, *Acs Macro Lett.* 1 (2012) 163–166.

- [17] M. Bletz, U. Pfeifer-Fukumura, U. Kolb, W. Baumann, Ground- and First-Excited-Singlet-State Electric Dipole Moments of Some Photochromic Spirobenzopyrans in Their Spiropyran and Merocyanine Form, *J Phys Chem.* 106 (2002) 2232–2236.
- [18] C. Hepburn, *Polyurethane elastomers*, Applied Science Publishers, London; New York, 1982.
- [19] Z.S. Petrović, J. Ferguson, *Polyurethane elastomers*, *Prog. Polym. Sci.* 16 (1991) 695–836.
- [20] J.A. Miller, S.B. Lin, K.K.S. Hwang, K.S. Wu, P.E. Gibson, S.L. Cooper, Properties of polyether-polyurethane block copolymers: effects of hard segment length distribution, *Macromolecules.* 18 (1985) 32–44.
- [21] M.F. Rubner, Synthesis and characterization of polyurethane-diacetylene segmented copolymers, *Macromolecules.* 19 (1986) 2114–2128.
- [22] M.F. Rubner, Novel optical properties of polyurethane-diacetylene segmented copolymers, *Macromolecules.* 19 (1986) 2129–2138.
- [23] R.A. Nallicheri, M.F. Rubner, Investigations of the mechanochromic behavior of poly(urethane-diacetylene) segmented copolymers, *Macromolecules.* 24 (1991) 517–525.
- [24] J.L. Stanford, R.J. Young, R.J. Day, Formation and properties of urethane-diacetylene segmented block copolymers, *Polymer.* 32 (1991) 1713–1725.
- [25] R.A. Koevoets, S. Karthikeyan, P.C.M.M. Magusin, E.W. Meijer, R.P. Sijbesma, Cross-Polymerization of Hard Blocks in Segmented Copoly(ether urea)s, *Macromolecules.* 42 (2009) 2609–2617.
- [26] P.T. Hammond, R.A. Nallicheri, M.F. Rubner, An examination of the strain-induced orientation of hard segment domains in 4,4'-methylenebis(phenyl isocyanate)-based polyurethane-diacetylene segmented copolymers, *Mat Sci Eng -Struc.* 126 (1990) 281–287.
- [27] S.-J. Kim, D.H. Reneker, A mechanochromic smart material, *Polym. Bull.* 31 (1993) 367–374.
- [28] B.R. Crenshaw, C. Weder, Deformation-Induced Color Changes in Melt-Processed Photoluminescent Polymer Blends, *Chem. Mater.* 15 (2003) 4717–4724.
- [29] B.R. Crenshaw, C. Weder, Self-Assessing Photoluminescent Polyurethanes, *Macromolecules.* 39 (2006) 9581–9589.
- [30] M. Gurr, The use of rotation matrices in the mathematical description of molecular orientations in polymers, *Colloid Polym. Sci.* 273 (1995) 607–625.
- [31] G. Baur, A. Stieb, G. Meier, Polarized Fluorescence of Dyes Oriented in Room Temperature Nematic Liquid Crystals, *Mol. Cryst. Liq. Cryst.* 22 (1973) 261–269.
- [32] T. Damerau, M. Hennecke, Determination of orientational order parameters of uniaxial films with a commercial 90°-angle fluorescence spectrometer, *J. Chem. Phys.* 103 (1995) 6232.
- [33] Y. Li, Z. Ren, M. Zhao, H. Yang, B. Chu, Multiphase structure of segmented polyurethanes: effects of hard-segment flexibility, *Macromolecules.* 26 (1993) 612–622.

- [34] L.M. Leung, J.T. Koberstein, Small-angle scattering analysis of hard-microdomain structure and microphase mixing in polyurethane elastomers, *J. Polym. Sci. Polym. Phys. Ed.* 23 (1985) 1883–1913.
- [35] F. Yeh, B.S. Hsiao, B.B. Sauer, S. Michel, H.W. Siesler, In-Situ Studies of Structure Development during Deformation of a Segmented Poly(urethane–urea) Elastomer, *Macromolecules*. 36 (2003) 1940–1954.
- [36] H. Sup Lee, S. Ra Yoo, S. Won Seo, Domain and segmental deformation behavior of thermoplastic elastomers using synchrotron SAXS and FTIR methods, *J. Polym. Sci. Part B Polym. Phys.* 37 (1999) 3233–3245.

CHAPTER 4

SOLVENT SWELLING ACTIVATION OF MECHANOPHORE CROSSLINKED POLYMERS

4.1 Introduction

Solvent swelling is a common process in polymeric materials [1]. In thermoplastics, it can be the first step in the dissolution of a polymer, while in thermosets, swelling leads to the formation of gels (Figure 4.1a). In both cases, understanding the mechanical processes associated with swelling may provide new insights for engineering design. Understanding the solvent swollen state of gels is of particular importance given how ubiquitous gels are for applications including biomedical [2–4], where they are used in tissue engineering, drug delivery and contact lenses; and engineering, where they can be found in valves, sealants, and membranes [5–7].

Solvents swell crosslinked polymer networks to a degree determined by both the solvent-polymer interactions and the polymer network structure [8]. As solvent enters the network, the polymer network progressively expands. According to the Flory-Rehner theory the degree of swelling is a balance between 1) the entropy of the polymer and solvent mixing, 2) the entropy change caused by reduction in the number of polymer chain conformations upon swelling, and 3) the heat of mixing of the polymer and solvent [9]. The energetic driving forces behind these processes have been well-studied [9,10], but new models are still being established to describe this complex process of polymer-solvent interactions [11–13]. While the description of the system as a whole has been fairly well developed, the forces induced at the molecular level in gels are not well understood.

Deformation and failure of crosslinked polymers has been extensively studied [14–16]. Hickenboth *et al.* used the worm-like chain model [17] as a qualitative method to estimate the force caused by chain extension during swelling of crosslinked poly(methyl methacrylate) (PMMA) beads [18]. Their calculations suggest that forces resulting from polymer swelling are not sufficient to cause significant covalent bond scission, but were in a range of force capable of triggering a Bergmann rearrangement. Experimentally they were unable to demonstrate mechanophore (force sensitive molecule) activation through swelling of the PMMA beads. Plunkett *et al.* [19] showed no evidence of accelerated bond scission when a force sensitive disulfide [20] crosslinked hydrogel was swollen in methanol. While these experiments gave no additional information on the forces during swelling, recently, forces in solid polymers have been investigated using mechanically induced chemical reactions (mechanochemistry) [21–23].

The spiropyran (SP) mechanophore has been used in the past to study mechanical forces in polymers in solution [24] and the solid state including elastomers [25,26], glassy polymers [27,28], and crosslinked polymers [25,29]. Under mechanical force, UV light, or heat, SP undergoes an electrocyclic ring-opening to the colored and fluorescent merocyanine (MC) form (Figure 4.1b). Here, we use the SP mechanophore incorporated as a crosslinker, to study forces in swelled crosslinked PMMA (Figure 4.1a). Using fluorescence imaging, we perform a systematic study of SP activation during the swelling of polymers with varying crosslinking density in different solvents to gain insights into the swelling conditions required for mechanochemical activation of the SP mechanophore. Control experiments, using a non-mechanically active SP mechanophore (Figure 4.1c), confirmed that activation of the mechanophore is due to force across the spiro-junction, and not due to mechanophore-solvent interactions.

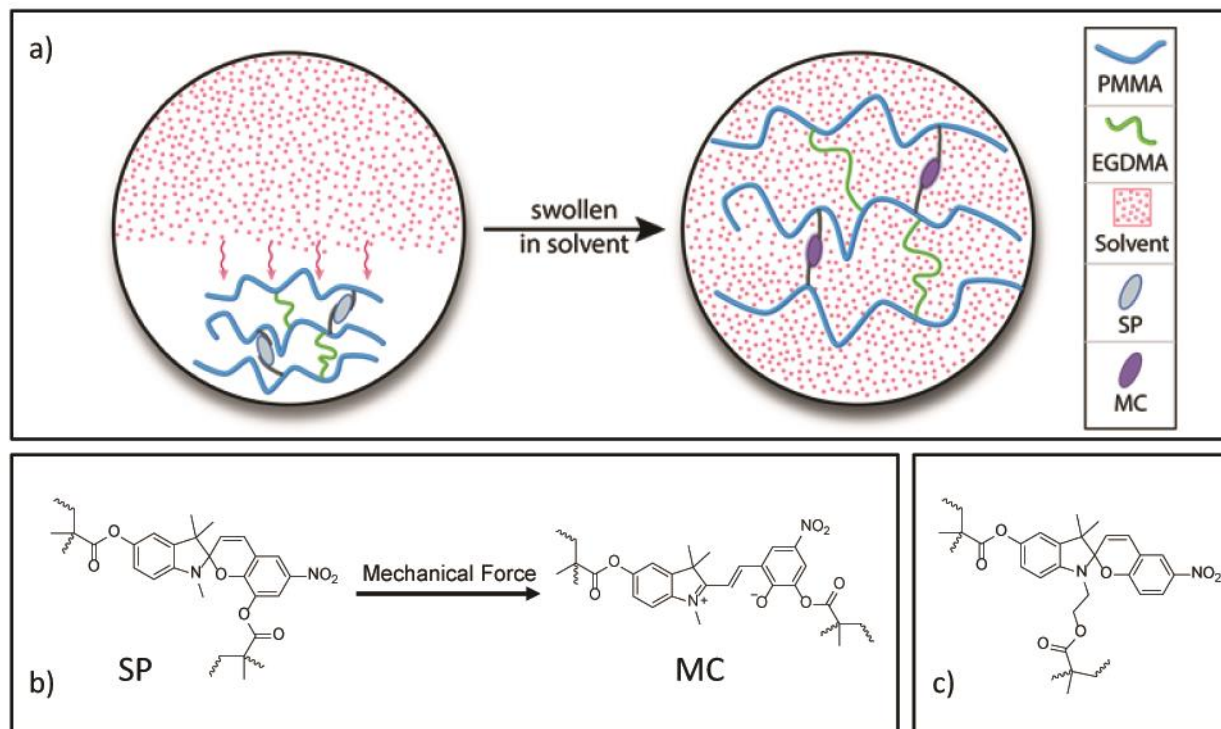


Figure 4.1 – a) Schematic of mechanical activation of SP crosslinker in crosslinked PMMA via polymer swelling b) Chemical structures of active (mechanically triggered) colorless spiropyran (SP) mechanophore and its conversion to the colored and fluorescent merocyanine (MC) conformation c) Chemical structure of the non-mechanically active control SP mechanophore.

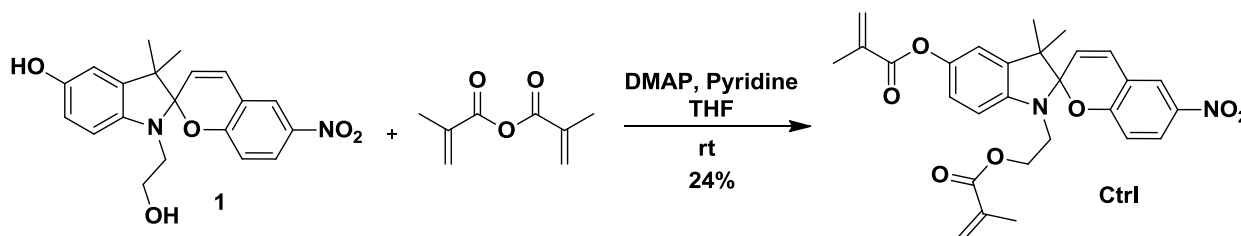
4.2 Experimental Methods

4.2.1 Synthesis and Polymerization

General experimental details: Unless otherwise stated, all starting materials were obtained from commercial suppliers and used without purification. Benzoyl peroxide (BPO) was reprecipitated from acetone using water and dried under vacuum. Methyl methacrylate (MMA) monomer was filtered through a basic alumina plug to remove the inhibitor, and degassed with argon for 30 minutes. All polymerization reactions were performed under argon atmosphere. Flash column chromatography was conducted with silica gel 60 (230-400 mesh) from Silicycle.

Active spiropyran: Active spiropyran (SP) was synthesized according to the procedure outlined by Davis *et al.* [25].

Di-functional control spiropyran: Synthesis of (\pm)-2-(5'-(methacryloyloxy)-3',3'-dimethyl-6-nitrospiro [chromene-2,2'-indolin]-1'-yl)ethyl methacrylate (**Ctrl**)



Dihydroxy-spiropyran 12 (113mg, 0.31mmol, 1eq) and 4-(dimethylamino)pyridine (20.0mg, 0.16mmol, 0.5equiv) were dissolved in 500 μ L of pyridine. A solution of methacrylic anhydride (137 μ L, 0.92mmol, 3equiv) in 1.70mL THF was added, and the reaction mixture was stirred at room temperature for 24 h. The reaction mixture was then diluted with 25mL of CH_2Cl_2 and washed twice with 20mL of NaHSO_4 (1 M), then with 20mL of saturated Na_2CO_3 and then 20mL of brine. The organic phase was dried using MgSO_4 , filtered, and evaporated to dryness. The crude product was purified by column chromatography eluting with 0.5% MeOH in CH_2Cl_2 to yield the dimethacrylate spiropyran as a tan solid: 38 mg, (24%).

^1H NMR (500 MHz, CDCl_3) δ 8.03 (dd, J = 8.9, 2.7 Hz, 1H), 8.00 (d, J = 2.8 Hz, 1H), 6.95 – 6.84 (m, 3H), 6.77 (d, J = 8.9 Hz, 1H), 6.66 (d, J = 8.4 Hz, 1H), 6.33 (s, 1H), 6.07 (s, 1H), 5.86 (d, J = 10.4 Hz, 1H), 5.74 (s, 1H), 5.57 (s, 1H), 4.29 (td, J = 6.3, 2.7 Hz, 2H), 3.61 – 3.32 (m, 2H), 2.07 (s, 3H), 1.92 (s, 3H), 1.25 (s, 3H), 1.18 (s, 3H).

^{13}C NMR (125 MHz, CDCl_3) 167.3, 166.6, 159.4, 144.7, 144.5, 141.3, 137.1, 136.2, 136.2, 128.6, 127.1, 126.2, 126.1, 123.0, 121.6, 120.5, 118.5, 116.0, 115.7, 106.9, 106.7, 62.7, 53.0,

42.8, 25.9, 19.9, 18.6, 18.5. HRMS-ESI (m/z): $[M+H]^+$ calcd. for $C_{28}H_{29}N_2O_7$, 505.1975 ; found, 505.1980.

SP crosslinked PMMA synthesis: For 1 mol% crosslinker PMMA, benzoyl peroxide (BPO) (15mg, 62 μ mol, 0.00662equiv) and SP (0.83mg, 1.7 μ mol, 0.00018equiv) were combined in a vial sealed with a septum and flushed with argon for 5 min. Ethylene glycol dimethylacrylate (EGDMA) (17.4 μ L, 92 μ mol, 0.00982equiv) and methyl methacrylate (MMA) (1.0mL, 9.4mmol, 1.0equiv) were then added. Once the components were fully dissolved, dimethylaniline (DMA) (6 μ L, 47 μ mol, 0.00506equiv) was added and the vial was sealed and mixed. The reaction mixture was allowed to pre-polymerize for 5 min to increase the viscosity of the mixture and then injected into rectangular molds (Figure 4.2) (27 x 8.5 x 0.75 mm). The molds were kept in an ultrasound bath to remove trapped gases and ensure consistent polymerization. After injection, the upper atmosphere of the mold was filled with a blanket of argon and sealed with a rubber cap. The mold up to the cap was submerged in a 25 °C water bath to dissipate the exotherm of the polymerization. The samples were removed from the molds after 26 h polymerization.

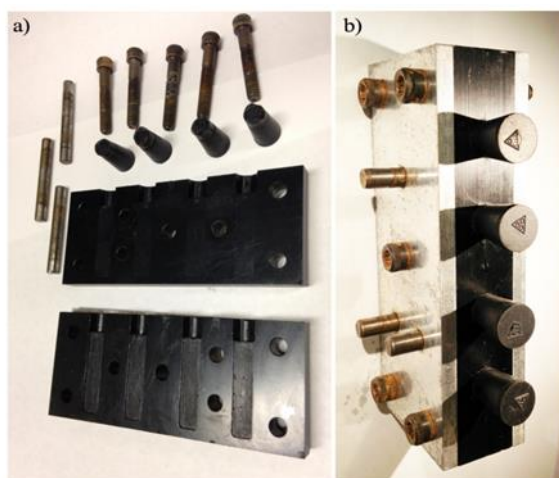


Figure 4.2 – Pictures of Delrin molds used in the synthesis of crosslinked PMMA samples a) mold taken apart showing rectangular mold area b) mold fully assembled.

4.2.2 Characterization Methods

Nuclear Magnetic Resonance: ^1H and ^{13}C NMR spectra were obtained using a Varian 500 MHz spectrometer in the VOICE NMR laboratory at the University of Illinois; the residual solvent protons were used to reference the chemical shift. Coupling constants (J) are reported in Hertz (Hz), and splitting patterns are designated as s (singlet), d (doublet), t (triplet), q (quartet), dd (double doublet), dt (double triplet), m (multiplet), and br (broad).

Swelling and Fluorescence Measurements: 10-30mg rectangular samples were cut and irradiated with a halogen pipe light (21V / 150W) for 2 h to revert any mechanophores converted to the MC form during polymerization to the colorless SP form prior to testing. Each sample was weighed and placed in a 20mL vial with 5mL of solvent. Samples were kept in the dark, and removed for analysis at defined time intervals. Fluorescence images (Figure 4.3) were captured through the bottom of the vial with an inverted fluorescence microscope (Zeiss Axiovert 200M, 560EX/620EM Rhodamine Chroma Filter), using exposure time of 5 s for all samples except for active SP in DMF, where 3 s was used to avoid saturation of the signal. The degree of swelling was determined by gravimetric methods and defined as $((m-m_0)/m_0)$ [1]. For each measurement, a sample was removed from the vial, excess solvent was wicked away from the surface, and the sample was weighed.

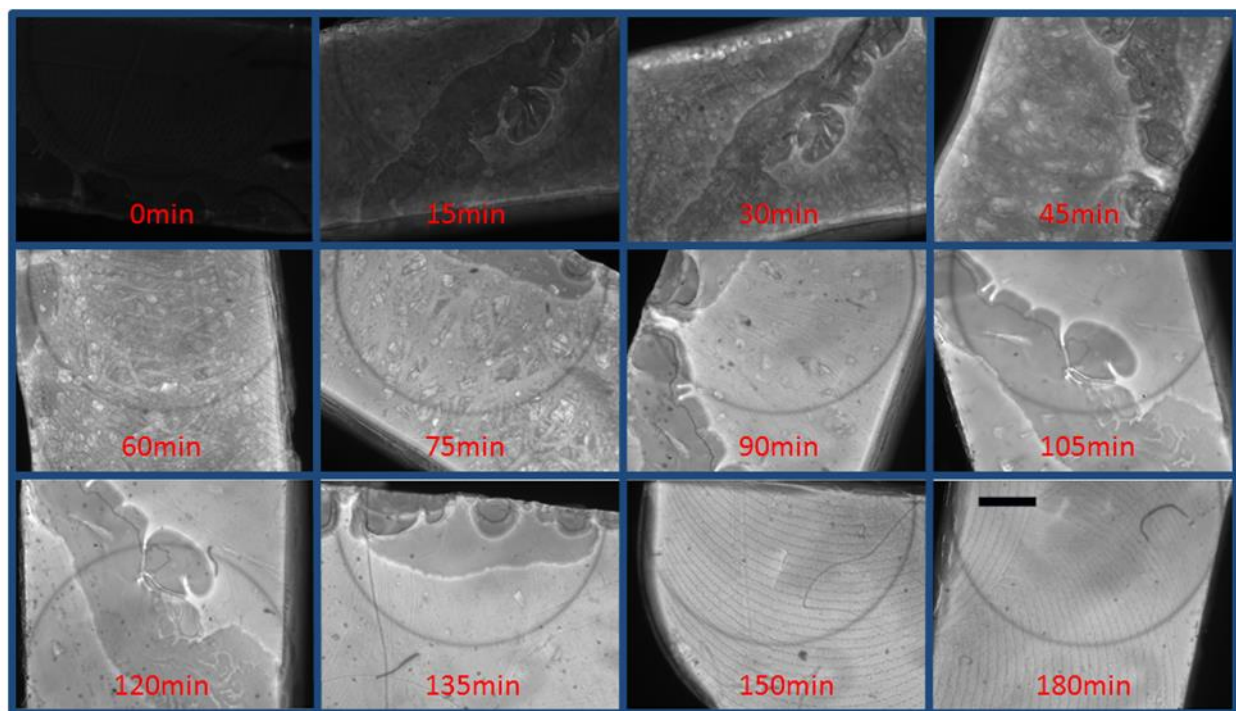


Figure 4.3 – Fluorescence images of a sample of active SP crosslinked PMMA swollen in acetone over the course of 3 h. Scale bar = 500 μm .

4.3 Polymer Swelling and Spiropyran Activation

The prepared SP crosslinked PMMA (1 mol% crosslinker) samples were submerged in solvents and left to swell for several hours. As the samples increase in mass and volume (ca. 100%), they develop a vibrant purple coloration (Figure 4.4), indicating that some of the mechanophore is now in the open MC form (Figure 4.1b). To verify that the conversion of SP crosslinker to MC is due to mechanical force and not solvent interactions, a control SP was prepared. The active SP's crosslinker connectivity allows force from the swollen network to be effectively transmitted to the spiro C-O bond, which is cleaved in an electrocyclic ring-opening reaction (Figure 4.1b). In the control SP crosslinker, the connectivity into the polymer does not span the spiro C-O bond (Figure 4.1c), and thus force is not effectively transferred across this bond; conversion to the MC form for the control SP is not mechanically triggered [25].

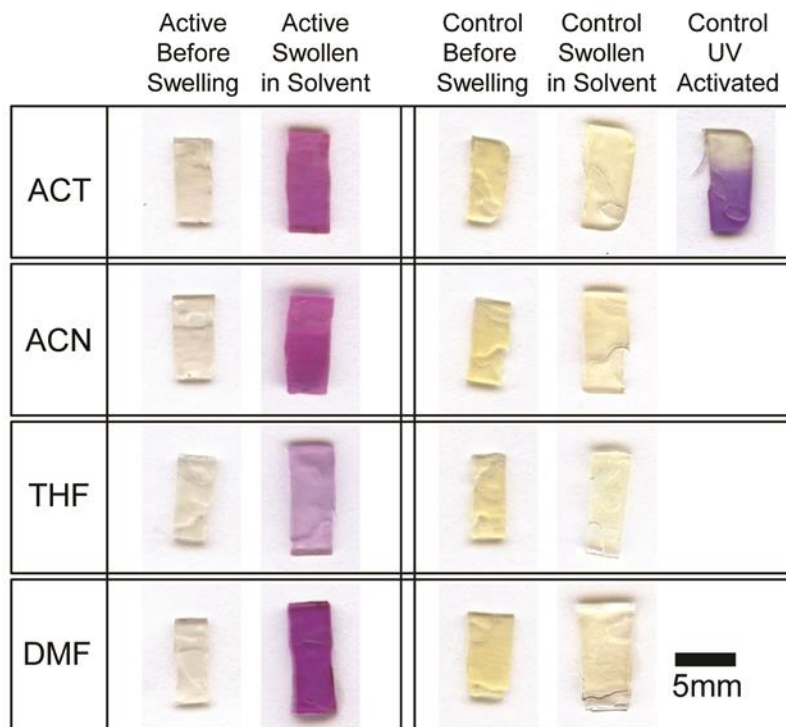


Figure 4.4 – Active SP crosslinked PMMA (1 mol% crosslinker) samples before and immediately after swelling in acetone (ACT), acetonitrile (ACN), tetrahydrofuran (THF), and dimethylformamide (DMF); the purple color indicates conversion of SP to the colored MC form. Control SP crosslinked PMMA samples swell similarly to the active samples, but display no color change unless irradiated by UV light (shown for acetone swollen control sample only). Only the bottom half of the “Control UV Activated” sample was irradiated with UV.

Control samples were prepared by the same method as the active samples, but using the control SP (Figure 4.1c). When this crosslinked PMMA is swollen in the same organic solvents, similar volume changes are observed, but with no color change, indicating that the control SP crosslinker did not convert to the MC form. When a portion of the swollen control sample is irradiated with UV light (365 nm), the exposed area turns a deep purple; confirming the presence and photochemical activity of the SP mechanophore (Figure 4.4). The absence of color in the swollen controls confirms that the rearrangement of the SP to MC in the samples containing the

active mechanophore was not caused by the change in solvent polarity that results when the polymer is swollen.

To obtain quantitative swelling data, the degree of swelling, $((m-m_o)/m_o) = (\Delta m/m_o)$ [1], of the polymer was measured as a function of time. High and low polarity solvents, such as water and toluene, respectively, were very slow to induce swelling (toluene) or did not cause swelling (water), and no color change was observed. Other solvents such as chloroform caused extremely fast swelling [15,16] and color change for the active sample, leading to fragmentation of the sample in a matter of minutes, and therefore were not adequate for further studies. The polar aprotic solvents acetone, tetrahydrofuran, acetonitrile, and dimethylformamide resulted in a slower and more controlled swelling behavior, and were therefore used in this study. During swelling, *in-situ* fluorescence imaging was used to quantify activation of the mechanophore to the MC form. Plotted in Figure 4.6 are the results of both the degree of swelling (black symbol) and the fluorescence change (blue symbol) of the active (closed symbol) and control (open symbol) SP crosslinked PMMA.

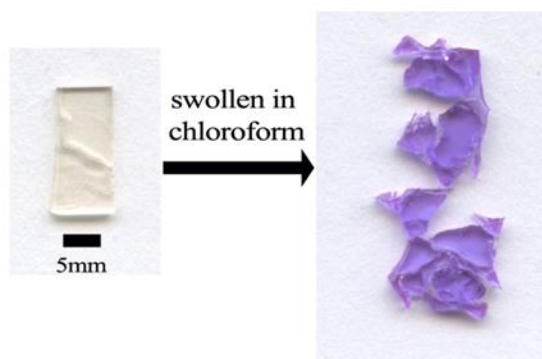


Figure 4.5 – SP crosslinked PMMA swollen in chloroform, resulting in extremely fast swelling and fragmentation of the polymer sample.

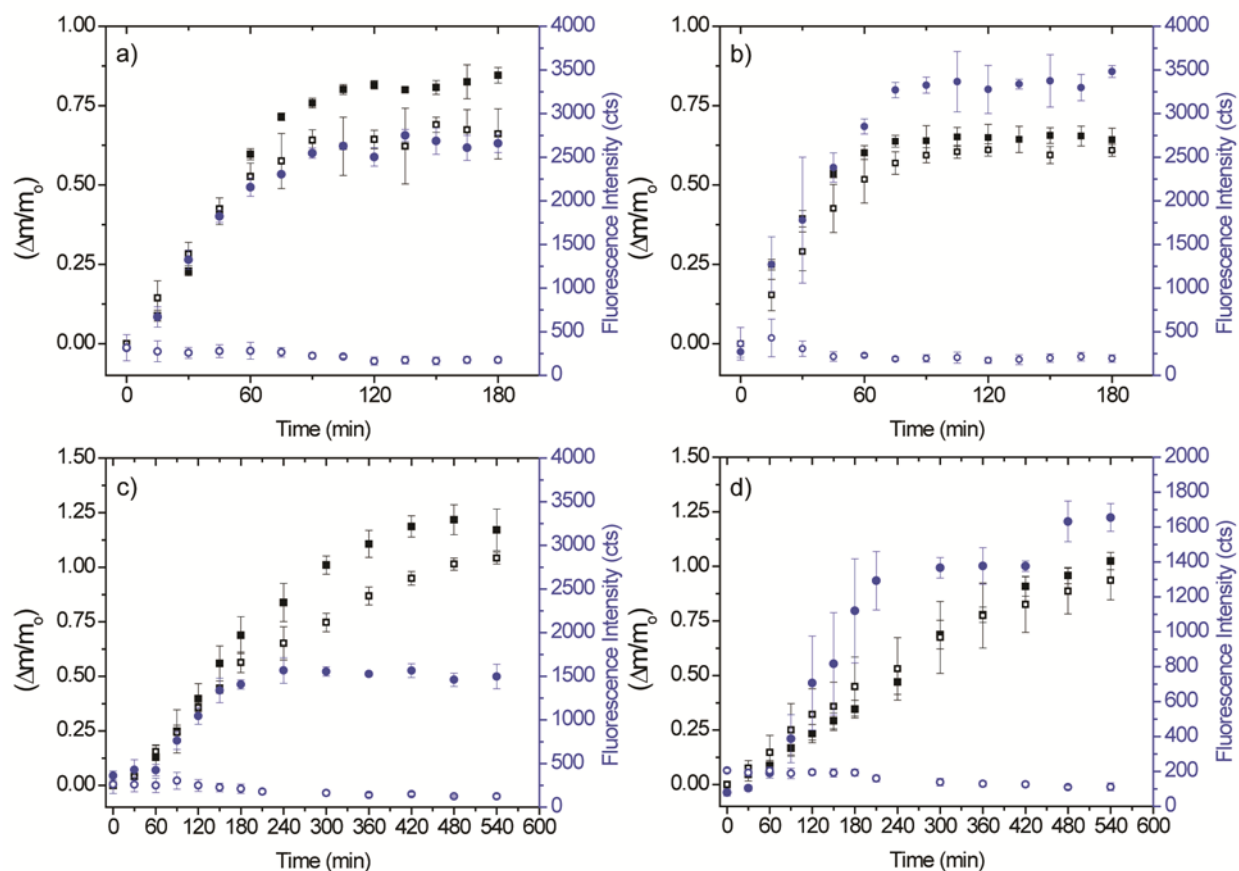


Figure 4.6 – Degree of swelling (black squares) and fluorescence intensity (blue circles) from active SP (closed square or circle) and control SP (open square or circle) crosslinked PMMA swollen in a) acetone, b) acetonitrile, c) tetrahydrofuran, d) dimethylformamide.

In acetone (Figure 4.6a) the polymer swelling increase begins to plateau shortly after 90 min, equilibrating at 1.75-1.8 times its original mass. The fluorescence intensity follows an almost identical trend, also reaching equilibrium around 90 min. The polymer degree of swelling in ACN (Figure 4.6b) was similar to acetone, but began to equilibrate sooner, at around 75 min. The fluorescence also followed the swelling trend, increasing up to about 75 min and then remaining fairly unchanged. Swelling of the SP crosslinked PMMA in THF and DMF is much slower, requiring over 8 h before reaching equilibrium. The degree of swelling is greater, equilibrating at values around 2.2 (THF) and 2.1 (DMF). In DMF, while the rate of swelling was

slower, the fluorescence intensity was exceptionally high. To capture the change in fluorescence for swelling in DMF, the exposure time for fluorescence imaging was reduced, resulting in lower fluorescence intensity while still capturing the overall fluorescence change (Figure 4.6d). The fluorescence again increases and plateaus at a very similar time scale as the degree of swelling. In THF the fluorescence plateaus around 4 h, about 4 h before the mass stopped increasing. The source of this fluorescence plateau was further investigated and is described in section 4.4. In all solvents except THF, the degree of swelling and fluorescence intensity increase appears to be closely correlated, suggesting that the polymer swelling and mechanical activation of the SP mechanophore into the MC form are closely correlated.

In ACN and DMF the degree of swelling is essentially identical for both the active and control polymer (Figure 4.6b and Figure 4.6d), and in acetone and THF the control swells slightly less than the active polymer, however, the swelling is still comparable (Figure 4.6a and Figure 4.6c). The similar swelling of the active and control materials indicates their crosslink densities are similar. The fact that no significant fluorescence change is observed for the control samples is strong evidence that force across the C-O bond is required to cause mechanochemical activation of the SP, and that the SP is not activated by solvent interactions.

4.4 Solvent Interaction Studies

The absence of color change in the control SP containing crosslinked PMMA after swelling suggests that the activation seen in the active SP crosslinked PMMA is only caused by mechanical force. Solvent interactions can influence the equilibrium between SP and MC (affecting the total fluorescence observed). In addition, solvatochromic effects could also be altering the absorbance, and therefore fluorescence, of the merocyanine [30–32]. To rigorously determine if solvent interactions have any effect on the equilibrium between SP and MC, the

absorbance spectra of the active and control MC was studied in different organic solvents as both a small molecule and as a crosslinker in PMMA.

The spiropyran molecule was dissolved in organic solvents, irradiated by UV light (254 nm) to convert to the MC form, and then UV-Vis spectroscopy was performed to determine the absorbance in each solvent (Table 4.1). As expected, clear solvatochromic effects were observed both in the active and control SP molecules (Figure 4.7). UV-Vis spectroscopy of the SP crosslinker, attached into the PMMA network and subjected to swelling-based activation, did not display the same solvatochromic effects seen in the dissolved SP molecule. SP crosslinked PMMA swollen in acetone, ACN, and DMF, all had the same maximum absorption of 565 nm (Figure 4.7); suggesting that after swelling in these solvents, the chemical environment of the mechanophore is similar to that of PMMA. In THF, the maximum absorbance is red-shifted to 579 nm. This value is very close to the value observed for MC molecules in THF environment (581 nm), indicating a strong solvent-mechanophore interaction after 9 h of swelling, even when linked in as a crosslinker in PMMA. This solvent-mechanophore interaction may explain the early plateauing of the fluorescence values observed during swelling in THF even though the degree of swelling measured in THF was comparable to the other solvents, suggesting that the force caused by swelling should be similar. To investigate this phenomenon the peak absorbance of active SP crosslinked PMMA swelled in THF was collected as a function of time (Figure 4.8). Initially the peak absorbance was constant, centered around 571 nm, but after approximately 3 h a red-shift in the peak absorbance was observed, representing interaction of THF with the MC. This red-shift in absorbance occurs around the time when the fluorescence increase of polymers swelled in THF began to plateau (Figure 4.6c). Since strong solvent interactions may facilitate the ring-closure of the MC to SP, it is reasonable to conjecture that when this solvent interaction

begins, mechanical force is no longer the only factor influencing the SP-MC equilibrium. Consequently, SP crosslinked PMMA swelled in THF cannot be compared to the other solvents (acetone, ACN, or DMF), since there are possibly two different effects (solvent interactions and mechanical forces) influencing the relative concentration of MC.

Table 4.1 – Peak Absorbance of SP Mechanophore in Organic Solvents

<i>Solvent</i>	<i>Active SP (nm)</i>	<i>Control SP (nm)</i>	<i>X-linked PMMA (nm)</i>
ACT	561	578	565
ACN	552	565	565
THF	581	595	579
DMF	551	567	565

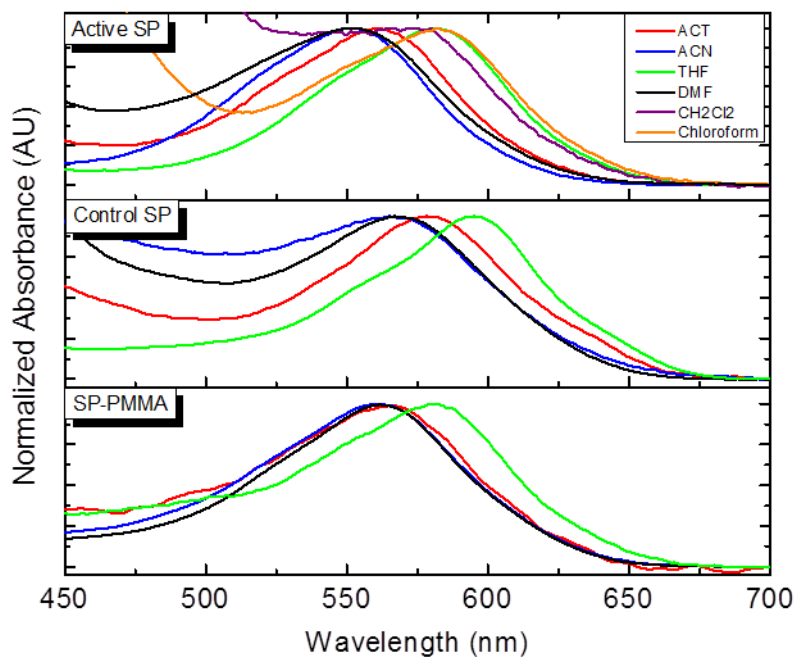


Figure 4.7 – Absorbance spectra in different solvents of the merocyanine form of active and control SP and SP crosslinked PMMA after solvent swelling experiments.

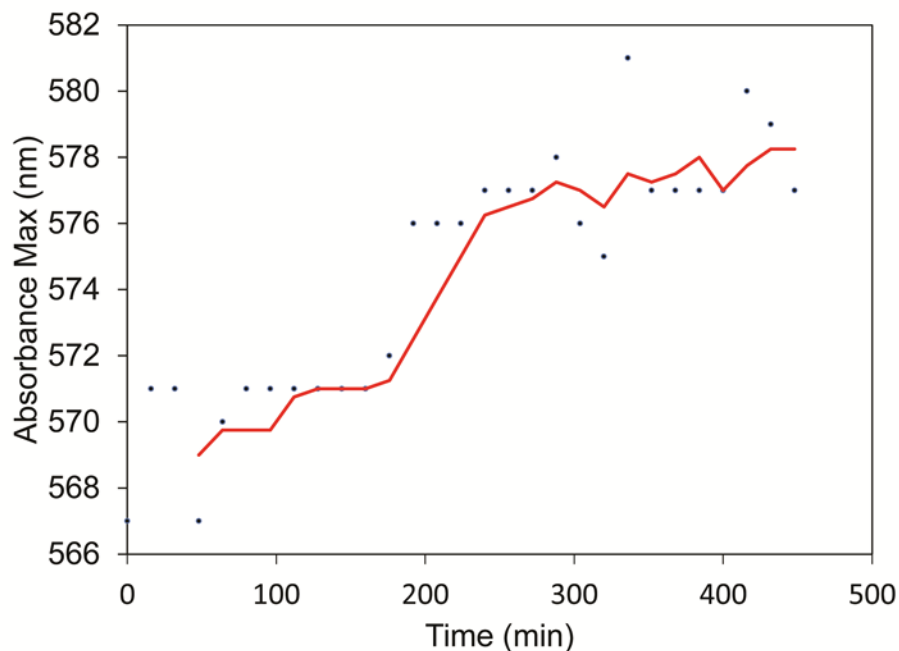


Figure 4.8 – Peak absorbance of active SP crosslinked PMMA swollen in THF; there is a red shift in the peak absorbance at about 180 min. Red line represents 3-point average of data points.

4.5 Crosslink Density vs. Activation

PMMA containing three different crosslink densities were synthesized and used to investigate the forces at the crosslinks caused by swelling. The SP concentration in all three polymers remained the same, only the concentration of the EGDMA crosslinker was varied. In Figure 4.9, the degree of swelling (black closed symbols) and fluorescence intensity (open blue symbols) for crosslink densities of 1, 5, and 10 mol% are compared during swelling in acetone. As expected, the swelling decreased with increasing crosslink density. In 3 h the 1% crosslinked PMMA swelled the most, to ca. 1.8 times its initial mass. The 5% crosslink density PMMA swelled to ca. 1.4 times the initial mass and the 10% crosslink swelled even less, reaching only 1.1 times its initial mass. The more crosslinked samples take a longer time to reach equilibrium, as demonstrated by the 10% crosslinker, which has not reached equilibrium within 3 h (Figure 4.9).

As was previously shown for swelling in acetone, the increase in fluorescence intensity is directly correlated to the degree of swelling.

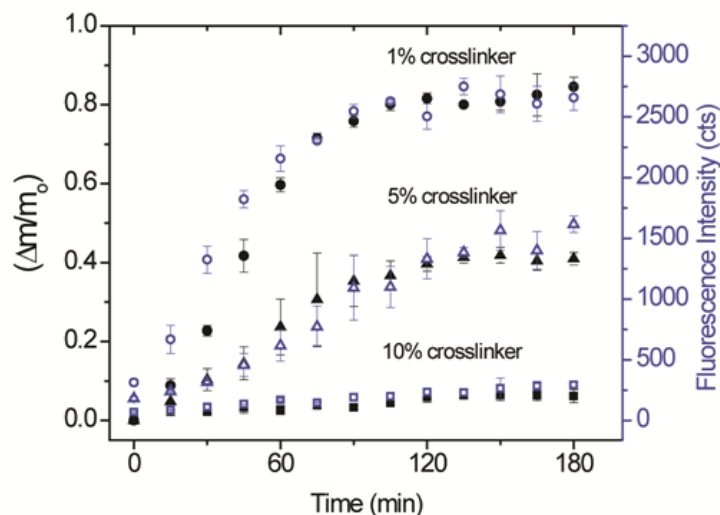


Figure 4.9 – Degree of swelling (closed symbols) and fluorescence intensity (open symbols) from active SP crosslinked PMMA swollen in acetone at crosslink densities of 1, 5, and 10 mol%

The data presented in Figure 4.9 has motivated further studies to try and relate the force during polymer swelling to established polymer models (Rubber Elasticity Theory). Since fluorescence is correlated to mechanical force, the fluorescence intensity from mechanically activated mechanophores and the corresponding equilibrium swelling values will be used to relate strain on the material (from swelling) directly to the molecular level forces on the polymer chains.

In Figure 4.9, only the 1% and 5% crosslinked material has reached equilibrium, resulting in only two data points (data after ≈ 120 minutes), which could be used to fit polymer models. Other experiments related to the time dependence of SP activation in swollen crosslinked PMMA confirmed that the activation of the SP mechanophore lags the solvent swelling. In an attempt to attain different equilibrium swelling values with corresponding fluorescence response from mechanically activated SP, variation in solvent quality was used. Mixtures of acetonitrile

and H₂O were first attempted, and while different equilibrium swelling ratios were attained, small amounts of H₂O which entered the polymer network resulted in strong solvatochromic effects. While the polymer samples swollen in 100% acetonitrile swelled the most, they did not result in the highest “measured” fluorescence. When UV-Vis spectroscopy was conducted on the polymers swelled in these mixtures there was a clear difference in the peak absorbance. In addition, solvent mixtures of acetone and hexane as well as a polymer mixture of poly(ethylene oxide) (10,000 g/mol) and acetonitrile were also attempted, but again resulted in solvatochromic effects.

Next, we swelled the polymer in a single solvent, and removed the polymer sample at different time intervals. The swollen polymer sample was placed in an empty vial, sealed, and left to equilibrate for a few hours before the fluorescence image was collected. When using acetonitrile, there was significant solvent evaporation over the course of 1 h, in addition, the fluorescence images were significantly brighter, saturating the fluorescence signal. We hypothesize that the evaporation from the surface causes an imbalance of force between the bulk polymer and the surface, possibly activating more SP. Since, acetonitrile evaporated, DMF was next attempted. Polymer samples swollen in DMF when removed and left to equilibrate did not lose mass over the equilibration time, but the fluorescence and swelling followed an opposite trend, where increased swelling resulted in a decrease in fluorescence. The sample which swelled the least was the sample that equilibrated the longest. It is possible that small amounts of water vapor could be affecting the fluorescence intensity during the hours of equilibration.

Finally, a variation of the previous method was attempted, but rather than letting the sample equilibrate in an empty vial, the sample was placed in silicone oil. This was to facilitate better imaging, as the silicone oil was used as index matching fluid. Data collected by this method

displayed two major issues. The first was that after equilibrating in silicone oil for an hour, there was significant mass loss from the polymer sample. The second was that the same fluorescence value was attained for both the sample swollen for 6 h and 8 h, but the swelling ratio for each was different (6 h \approx 1.14; 8 h \approx 1.35). The fluorescence values were also very low compared to previous data collected with similar imaging conditions. While the color of the samples were a deep dark purple, fluorescence intensity was only around 2000 counts, where previous experiments with swelling in DMF was so high that lower exposure times had to be used (Figure 4.6d). This type of plateau fluorescence may be due to fluorescence quenching in the sample.

Many different methods were used to collect different equilibrium swelling and fluorescence values. While all of the methods did attain different equilibrium swelling, the fluorescence values were inaccurate due to solvatochromic effects. Moving forward there are a number of current engineering issue, which remain unanswered or unconfirmed. First, is the control of the optics, there needs to be confirmation that the collection of fluorescence data is reproducible and accurate. A second is the possibility of fluorescence quenching, synthesis of a crosslinked sample with lower SP concentration should be tested. A third possible source of inconsistent fluorescence measurements is the fluorescence lamp itself, the current lamp used is old and likely needs a new bulb. A possible solution to the inconsistent fluorescence is to use an internal standard. A fluorescent dye at a known concentration could be synthesized into the PMMA backbone, and its fluorescence could be compared to the fluorescence from the SP. Once these current challenges are addressed, equilibrium swelling values and their corresponding fluorescence intensities can be used to relate force to the mechanophore activation.

4.6 Conclusions

In conclusion, we used SP, a force-sensitive molecule, to study mechanical forces in crosslinked polymers during solvent swelling. In the case of PMMA, several solvents of mid-polarity induced adequate force to activate the electrocyclic ring-opening of spiropyran crosslinks, while more polar and apolar solvents, which swell very slowly or not at all, do not activate the mechanophore. Using gravimetric analysis and fluorescence imaging, we demonstrated that in most cases, swelling and activation are directly correlated, demonstrating that the forces due to polymer swelling are causing mechanical activation of the SP mechanophore. A SP control in which the force does not pass through the spiro C-O bond was prepared and used to confirm this assumption. Also, solvatochromic effect of the MC molecule in different solvents was used to investigate the role of solvent-mechanophore interactions. In most cases, the solvent-mechanophore interactions of the SP crosslinker in PMMA are minimal, with the exception of THF, where the solvent-mechanophore interaction influences the SP-MC equilibrium, limiting the study of the swelling forces in this solvent. Finally, the effect of different crosslink densities was studied. We demonstrated that less swelling, from increased crosslink density), resulted in less force and therefore less mechanophore activation. This study has described a simple method to study the forces occurring inside a crosslinked polymer during swelling, a field still open in materials science. Moreover, it demonstrates a new simple method to activate and test new mechanophores on crosslinked polymers.

REFERENCES

- [1] A.A. Tager, Physical Chemistry of Polymers 2nd. ed., Mir Publishers, 1978.
- [2] O. Wichterle, D. LiM, Hydrophilic Gels for Biological Use, *Nature*. 185 (1960) 117–118.
- [3] R.V. Ulijn, N. Bibi, V. Jayawarna, P.D. Thornton, S.J. Todd, R.J. Mart, *et al.*, Bioresponsive hydrogels, *Mater. Today*. 10 (2007) 40–48.
- [4] M. Blondeau, T. Coradin, Living materials from sol–gel chemistry: current challenges and perspectives, *J. Mater. Chem.* 22 (2012) 22335.
- [5] D.J. Beebe, J.S. Moore, J.M. Bauer, Q. Yu, R.H. Liu, C. Devadoss, *et al.*, Functional hydrogel structures for autonomous flow control inside microfluidic channels, *Nature*. 404 (2000) 588–590.
- [6] M.L. Kraft, J.S. Moore, n-Alkyl Fatty Acid-Modified Microgels: Ion Permeation as a Function of Chain Length, *Langmuir*. 19 (2002) 910–915.
- [7] I. Tokarev, S. Minko, Multiresponsive, Hierarchically Structured Membranes: New, Challenging, Biomimetic Materials for Biosensors, Controlled Release, Biochemical Gates, and Nanoreactors, *Adv. Mater.* 21 (2009) 241–247.
- [8] M. Rubinstein, *Polymer Physics*, Oxford University Press, Oxford ; New York, 2003.
- [9] P.J. Flory, J. Rehner, Statistical Mechanics of Cross-Linked Polymer Networks II. Swelling, *J. Chem. Phys.* 11 (1943) 521.
- [10] H.M. James, E. Guth, Theory of the Elastic Properties of Rubber, *J. Chem. Phys.* 11 (1943) 455.
- [11] S. Nandi, H.H. Winter, Swelling Behavior of Partially Cross-Linked Polymers: A Ternary System, *Macromolecules*. 38 (2005) 4447–4455.
- [12] S.K. De, N.R. Aluru, B. Johnson, W.C. Crone, D.J. Beebe, J. Moore, Equilibrium swelling and kinetics of pH-responsive hydrogels: models, experiments, and simulations, *J. Microelectromechanical Syst.* 11 (2002) 544–555.
- [13] W. Hong, X. Zhao, J. Zhou, Z. Suo, A theory of coupled diffusion and large deformation in polymeric gels, *J. Mech. Phys. Solids*. 56 (2008) 1779–1793.
- [14] J. Scheirs, *Compositional and failure analysis of polymers: a practical approach*, Wiley, Chichester ; New York, 2000.
- [15] D. Cohn, G. Marom, Deformation and failure of polymeric matrices under swelling conditions, *J. Appl. Polym. Sci.* 28 (1983) 1981–1992.
- [16] T. Alfrey, E.F. Gurnee, W.G. Lloyd, Diffusion in glassy polymers, *J. Polym. Sci. Part C Polym. Symp.* 12 (1966) 249–261.
- [17] *Polymer handbook*, 4th edition, 4th ed, Wiley, New York ; Chichester, 2004.
- [18] C.R. Hickenboth, J.D. Rule, J.S. Moore, Preparation of enediyne-crosslinked networks and their reactivity under thermal and mechanical conditions, *Tetrahedron*. 64 (2008) 8435–8448.
- [19] K.N. Plunkett, M.L. Kraft, Q. Yu, J.S. Moore, Swelling Kinetics of Disulfide Cross-Linked Microgels, *Macromolecules*. 36 (2003) 3960–3966.

- [20] I. Park, S.S. Sheiko, A. Nese, K. Matyjaszewski, Molecular Tensile Testing Machines: Breaking a Specific Covalent Bond by Adsorption-Induced Tension in Brushlike Macromolecules, *Macromolecules*. 42 (2009) 1805–1807.
- [21] M.M. Caruso, D.A. Davis, Q. Shen, S.A. Odom, N.R. Sottos, S.R. White, *et al.*, Mechanically-Induced Chemical Changes in Polymeric Materials, *Chem. Rev.* 109 (2009) 5755–5798.
- [22] K.M. Wiggins, J.N. Brantley, C.W. Bielawski, Polymer Mechanochemistry: Force Enabled Transformations, *Acs Macro Lett.* 1 (2012) 623–626.
- [23] S.L. Craig, Mechanochemistry: A tour of force, *Nature*. 487 (2012) 176–177.
- [24] S.L. Potisek, D.A. Davis, N.R. Sottos, S.R. White, J.S. Moore, Mechanophore-Linked Addition Polymers, *J. Am. Chem. Soc.* 129 (2007) 13808–13809.
- [25] D.A. Davis, A. Hamilton, J. Yang, L.D. Cremer, D. Van Gough, S.L. Potisek, *et al.*, Force-induced activation of covalent bonds in mechanoresponsive polymeric materials, *Nature*. 459 (2009) 68–72.
- [26] C.K. Lee, D.A. Davis, S.R. White, J.S. Moore, N.R. Sottos, P.V. Braun, Force-Induced Redistribution of a Chemical Equilibrium, *J. Am. Chem. Soc.* 132 (2010) 16107–16111.
- [27] G. O'Bryan, B.M. Wong, J.R. McElhanon, Stress Sensing in Polycaprolactone Films via an Embedded Photochromic Compound, *Acs Appl. Mater. Interfaces*. (2010).
- [28] B.A. Beiermann, D.A. Davis, S.L.B. Kramer, J.S. Moore, N.R. Sottos, S.R. White, Environmental effects on mechanochemical activation of spiropyran in linear PMMA, *J Mater Chem.* (2011).
- [29] C.M. Kingsbury, P.A. May, D.A. Davis, S.R. White, J.S. Moore, N.R. Sottos, Shear activation of mechanophore-crosslinked polymers, *J Mater Chem.* (2011).
- [30] S.-R. Keum, M.-S. Hur, P.M. Kazmaier, E. Buncel, Thermo- and photochromic dyes: indolino-benzospiropyrans. Part 1. UV–VIS spectroscopic studies of 1,3,3-spiro(2H-1-benzopyran-2,2'-indolines) and the open-chain merocyanine forms; solvatochromism and medium effects on spiro ring formation, *Can. J. Chem.* 69 (1991) 1940–1947.
- [31] I.D.L. Albert, T.J. Marks, M.A. Ratner, Rational Design of Molecules with Large Hyperpolarizabilities. Electric Field, Solvent Polarity, and Bond Length Alternation Effects on Merocyanine Dye Linear and Nonlinear Optical Properties, *J. Phys. Chem.* 100 (1996) 9714–9725.
- [32] G. Favaro, F. Masetti, U. Mazzucato, G. Ottavi, P. Allegrini, V. Malatesta, Photochromism, thermochromism and solvatochromism of some spiro [indolinoxazine]-photomerocyanine systems: effects of structure and solvent, *J. Chem. Soc. Faraday Trans.* 90 (1994) 333.

CHAPTER 5

CONTACT MECHANOCHEMISTRY: POLYACIDS AND POLYAMINES

5.1 Introduction

5.1.1 Concept and Motivation

This chapter sets out to investigate a new concept known as contact mechanochemistry, where two reactive phases with complimentary functionality are separated physically by thermodynamic phase segregation. When the two phases are brought in contact with each other through means of mechanical force, the initially isolated reactive domains now exposed to complimentary functionalities can react, ultimately inducing polymer property changes. Block copolymers and polymer blends are a unique class of materials with both tunable mechanical and chemical properties [1,2]. The inherent nature of these materials to phase separate into microdomains [3,4] is a very appealing property, one we intend to harness and use for mechanochemistry.

In order to achieve such a system, we propose to prepare a block copolymer with two blocks that have complimentary reactive functionalities, but with one block initially chemically protected during synthesis and processing. After synthesis and processing, the protected chemical functionality in the material will undergo a deprotection, producing a microdomain with a functionality that compliments that of the second block. When the material undergoes mechanical deformation in such a way that breaks up the phase separated microstructure, the complimenting functionalities come in contact and are capable of reacting with each other, resulting in a polymer with potentially improved mechanical properties after deformation. This

concept is visually laid out in Figure 5.1. The work presented in this chapter explores the use of poly(acid) and poly(amine) block copolymers for this new concept, and evaluates the viability of this chemistry for contact mechanochemistry.

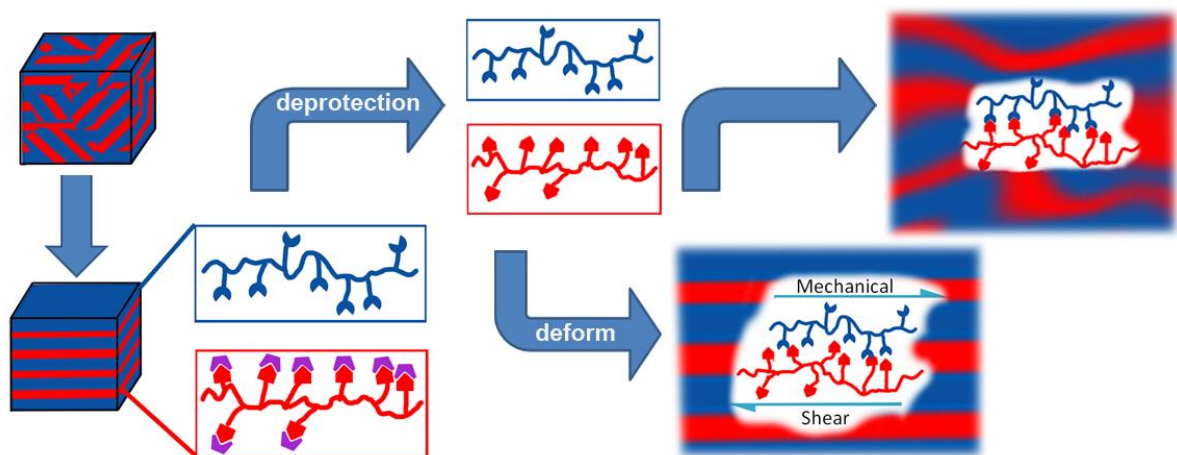


Figure 5.1 – Schematic of proposed contact mechanochemistry in block copolymers concept.

5.2 Poly(*tert*-butyl acrylate) and Poly(2-(dimethylamino)ethyl methacrylate) Copolymers

5.2.1 Motivation

As a simple system to test the concept of contact mechanochemistry in block copolymers, poly(acid)s and poly(amine)s were selected as the two complimentary phases. Poly(acids) and poly(amines) are known to readily form stable complexes due to strong hydrogen-bonding with partial charge transfer [5,6]. In addition, the protection and deprotection of carboxylic acids have been largely explored in the context of organic and bioorganic synthesis, providing a large variety of possibilities to choose from [7]. A protected carboxylic acid that has been largely used in the context of polymer synthesis is *tert*-butyl acrylate (tBA), which can easily be polymerized into poly(*tert*-butyl acrylate) (PTBA) by known control radical polymerization techniques [8]. PTBA is also a well-studied polymer, known for its ability to thermally deprotect into poly(acrylic acid) (PAA) via cleavage of the *tert*-butyl ester linkage [9–12] (Figure 5.2a).

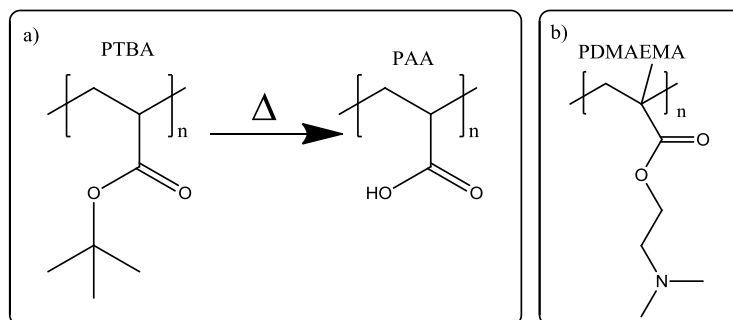


Figure 5.2 – a) Schematic of poly(*tert*-butyl acrylate) (PTBA) thermal deprotection to poly(acrylic acid) (PAA) b) Polymeric chemical structure of poly(dimethylamino-ethyl methacrylate) (PDMAEMA).

Poly(dimethylamino-ethyl methacrylate) (PDMAEMA) was selected for the second phase (Figure 5.2b). PDMAEMA is a methacrylate with a pendent tertiary amine which is easily protonated [13,14], it is commonly synthesized as a block in amphiphilic block copolymers and studied for its applications as stabilizers, emulsifiers, and dispersants [15–21]. In addition, PDMAEMA is also a good second phase candidate because there is established literature on the synthesis of this particular block copolymer (PAA-b-PDMAEMA) [20–22]. Preliminary experiments mixing polymer solutions of PAA and PDMAEMA demonstrated rapid complex formation and immediate precipitation of a white solid (Figure 5.3), which supports the proposal of this PAA and PDMAEMA as a chemistry to investigate in the solid state.



Figure 5.3 – Mixing of polymer solutions: PTBA and PDMAEMA in THF (left) resulting in no reaction, PDMAEMA and PAA in H₂O (right) resulting in white precipitate.

5.2.2 Polymer Synthesis

Materials: *tert*-butyl acrylate (tBA), methyl acrylate (MA), and 2-(dimethylamino)ethyl methacrylate (DMAEMA) were filtered through basic alumina to remove inhibitor and then sparged with N₂ for 10-15 minutes. Solvents used in polymerizations, such as acetone and 1,2-dichlorobenzene were also sparged with N₂ for 10-15 minutes before use. CuBr, CuCl, Methyl 2-bromopropionate, *N,N,N',N',N'*-pentamethyldiethylenetriamine (PMDETA), 1,1,4,7,10,10-Hexamethyltriethylenetetramine (HMTETA), and 2,2'-bipyridal were all used as received.

For a typical tBA polymerization [8]: A 100mL Schlenk flask equipped with a Teflon stir bar was purged with Argon for 10-15 minutes followed by the addition of tBA monomer (21.0g, 164mmol), CuBr (25.0mg, 0.171mmol), PMDETA ligand (32.2mg, 0.186mmol), and 6mL of acetone. The flask was immediately sealed and three freeze-pump-thaw cycles were applied to remove dissolved oxygen. The flask was backfilled with argon, and methyl 2-bromopropionate initiator (32.2mg, 0.186mmol) was then added. Finally, the flask was placed in an oil bath thermostated at 60°C for 5 h. The polymerization was opened to air, acetone was added and the polymer was filtered through a silica plug to remove CuBr. After the solvent was removed *in vacuo*, the polymer was precipitated by drop wise addition to stirring 1:1 cold mixture of H₂O:methanol. The resulting white solid polymer was collected and dried under vacuum at room temperature. $M_n \approx 30,000$ and $M_w/M_n \approx 1.2$

Poly(methyl acrylate) (PMA) macroinitiator [21,23]: A dried Schlenk flask equipped with a Teflon stir bar was purged with Argon for 10-15 minutes followed by the addition of MA monomer (9.56g, 111.1mmol), CuBr (0.132g, 0.926mmol), and 2,2'-bipyridal ligand (0.867g, 5.56mmol). The flask was immediately sealed and three freeze-pump-thaw cycles were applied to remove dissolved oxygen. The flask was backfilled with argon, and methyl 2-bromopropionate initiator (0.309g, 1.85mmol) was then added. The flask was placed in an oil

bath thermostated at 90°C for 2 h. The polymerization was opened to air, THF was added, and the polymer was filtered through a neutral alumina plug to remove the copper. Due to the polymer's low molecular weight it was redissolved in THF several times and the solvent was removed with a rotary evaporator, rather than precipitated, then dried under vacuum at room temperature. $M_n = 6,200$ g/mol and $M_w/M_n = 1.4$.

For a typical DMAEMA polymerization [24]: DMAEMA monomer (15.2g, 96.6mmol) was polymerized in the presence of PMA-macroinitiator in 20mL of 1,2-dichlorobenzene using CuCl (59.9mg, 0.605mmol) and HMTETA ligand (139mg, 0.605mmol). The PMA-macroinitiator was first dissolved in 1,2-dichlorobenzene and then remaining reactants were added into the Schlenk flask equipped with a stir bar, and was immediately sealed. Three freeze-pump-thaw cycles were applied to remove dissolved oxygen. The flask was backfilled with argon and placed in an oil bath thermostated at 90°C for 4 h. The polymerization was opened to air, THF was added, and the polymer was filtered through a fritted funnel of neutral alumina to remove the copper. After solvent was removed *in vacuo*, the polymer was precipitated by drop wise addition to stirring hexane. The resulting polymer was collected and dried under vacuum at room temperature.

For a typical block copolymer polymerization (PTBA-PMA-PDMAEMA) [8,20,21]: Bromo-terminated PTBA ($M_n \approx 30,000$, 2 g, 0.065 mmol), CuBr (4.5mg, 0.032mmol), PMDETA (5.5mg, 0.032mmol) and MA monomer (0.33g, 3.56mmol) were added to a Schlenk flask equipped with a stir bar, and was immediately sealed. Three freeze-pump-thaw cycles were applied to remove dissolved oxygen. The flask was backfilled with argon and the flask was placed in an oil bath thermostated at 70°C for 2 h. The polymerization was opened to air, THF was added, and the polymer was filtered through a neutral alumina plug to remove the copper. Polymer was precipitated by drop wise addition to stirring 1:1 cold mixture of H₂O:methanol,

isolated by vacuum filtration, collected and dried under vacuum at room temperature ($M_n \approx 35,000$). The dried P(TBA)-PMA-macroinitiator (1.5g, 0.043mmol) was then dissolved in 1,2-dichlorobenzene and then the remaining reactants, DMAEMA monomer (1.35g, 8.57mmol), CuCl (5.3mg, 0.0537mmol) and HMTETA ligand (12.4mg, 0.0537mmol) were added into the Schlenk flask equipped with a stir bar, and was immediately sealed. Three freeze-pump-thaw cycles were again applied to remove dissolved oxygen. The flask was backfilled with argon and the flask was placed in an oil bath thermostated at 90°C for 4 h. The polymerization was opened to air, THF was added, and the polymer was filtered through a neutral alumina plug to remove the copper. After solvent was removed *in vacuo*, the polymer was precipitated by drop wise addition to 1:1 cold mixture of H₂O:methanol, which resulted in a only semi-solid polymer flakes. The precipitated solution was stored in the freezer to allow the polymer to settle to the bottom, and then the solvent was decanted off the top. To isolate the polymer, the precipitate was centrifuged at 4500rpm for 5 min. The solid was collected and the resulting polymer was dried under vacuum at room temperature. Due to PDMAEMA adsorption to GPC columns, which result in increased retention times and lead to lower detected molecular weights, the molecular weight was determined using ¹H NMR, which is further described in *section 5.2.3*.

5.2.3 Characterization Methods

Gel Permeation Chromatography (GPC): Analytical GPC analyses were performed with a Waters 1515 Isocratic HPLC pump, a Waters (2998) Photodiode Array Detector, a Waters (2414) Refractive Index Detector, a Waters (2707) 96-well autosampler, and a series of 4 Waters HR Styragel columns (7.8 X 300mm, HR1, HR3, HR4, and HR5) in THF at 30°C. The GPC was calibrated using monodisperse polystyrene standards.

Differential Scanning Calorimetry (DSC): Glass transition temperatures of homopolymers and block copolymers were determined using DSC, performed on a Mettler-Toledo model DSC82. Polymer samples (5-10mg) were first heated from 25°C to 100°C to clear any thermal history, and then cycled 2 times from -100°C to 150°C at 20°/min. The second heating was used to determine the glass transition temperature.

Thermal Gravimetric Analysis (TGA): TGA was used to confirm the thermal deprotection of PTBA to PAA. For typical isothermal experiments the samples were held at 160°C for 5 h, and for typical temperature ramp experiments sample were ramped from 25°C to 300°C at 10°C/min.

Molecular Weight Determination by ^1H NMR: ^1H NMR in CDCl_3 on a Varian 500MHz spectrometer was carried out to determine the composition of block copolymers, which contained PDMAEMA blocks. The macroinitiators (PMA or PTBA-PMA) molecular weights were first determined by GPC. Then the integrated signal at δ 4.0-4.2 ppm which arise from the methoxy protons of PDMAEMA was compared to either the signal at δ 3.6-3.8 ppm from methoxy protons for PMA or at δ 1.4 ppm from the *tert*-butyl group. Using the known molecular weight of the macroinitiator the molecular weight of the PDMAEMA block could be determined.

Fourier Transform Infrared Spectroscopy (FTIR): Spectra was recorded using a Thermo Nicolet NEXUS 670 FT-IR spectrometer representing the sum of 64 scans at a resolution of 4 cm^{-1} from 800-4000 cm^{-1} . Samples were prepared by solvent casting a thin layer of polymer on NaCl salt plates. When polymers were insoluble samples were prepared using KBr and a pellet press.

5.2.4 Homopolymers and Block Copolymer Characterization

All polymers were synthesized by atom transfer radical polymerization (ATRP). Since the end goal is to induce phase separation and also to mechanically deform these materials, high molecular weight polymers (higher than molecular weight of entanglement) were targeted. A typical PTBA homopolymer, which is also the macroinitiator had a $M_n \approx 30,000$ g/mol determined by GPC. To ensure that the two complimentary phases were separated and to avoid possible interface interactions prior to deformation, a tri-block copolymer was synthesized. PMA, a low T_g polymer ($T_g \approx 10^\circ\text{C}$), was chosen as a soft middle phase, which may be easily deformed in later steps during mechanical mixing of the complimentary phases. The goal was to synthesize a very short middle block to provide a physical barrier between the two reactive blocks after thermal deprotection. A typical PMA block grown from the PTBA macroinitiator had a $M_n \approx 5,000$ g/mol, confirmed by both GPC and ^1H NMR analysis. From the PTBA-PMA macroinitiator, PDMAEMA the polymer with the pendent tertiary amine (Figure 5.2b) was grown. It has been reported in literature [25–27] that GPC analysis of PDMAEMA results in lower than expected molecular weight values, this is often attributed to PDMAEMA adsorption onto GPC columns, increasing retention time and therefore leading to false lower molecular weights. Therefore, the molecular weight of the PDMAEMA block was determined by ^1H NMR analysis (5.2.3 *Characterization Methods*). By comparing the protons from the methoxy protons of PDMAEMA to the known number of protons in the *tert*-butyl group in PTBA, the PDMAEMA had a $M_n \approx 25,700$ g/mol. This resulted in a final block copolymer of PTBA-PMA-PDMAEMA with a total $M_n \approx 60,000$ g/mol. A homopolymer of PDMAEMA was also synthesized with a $M_n \approx 27,500$ g/mol.

Thermal analysis of the polymers synthesized was conducted using DSC. The PTBA homopolymer had a $T_g \approx 40^\circ\text{C}$, which was similar to previously reported literature value of $T_g =$

36°C [28,29]. The T_g for PDMAEMA was $\approx -30^\circ\text{C}$. This value is much lower than previous reports in literature. The T_g for PDMAEMA ($M_n = 49,000$ g/mol) was reported as 6.7°C [30], while the T_g for PDMAEMA ($M_n = 242,000$ g/mol) was reported as 19°C [28]. These are higher values than the T_g determined for the PDMAEMA synthesized. It is possible that residual solvent (1,2-dichlorobenzene, BP = 180.5°C), may be plasticizing the PDMAEMA resulting in the T_g discrepancy. The heating curves for the block copolymer (PTBA-PMA-PDMAEMA) in Figure 5.4 shows two thermal transitions, both similar to the T_g values determined for the homopolymers (40°C for PTBA and -30°C for PDMAEMA). The lack of any PMA thermal transition is likely due to the low quantity of PMA in the block copolymer.

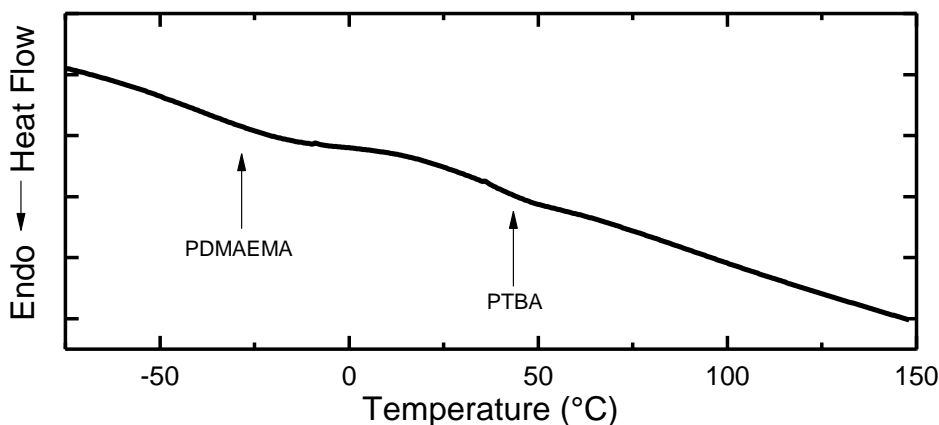


Figure 5.4 – DSC curve (2nd heating) of block copolymer (PTBA-PMA-PDMAEMA) showing the glass transition (T_g) of the two major blocks, PDMAEMA $T_g \approx -30^\circ\text{C}$ and PTBA $T_g \approx 40^\circ\text{C}$

5.2.5 Poly(*tert*-butyl acrylate) Thermal Deprotection

To confirm that the labile ester linkage of PTBA could be thermally removed, the thermal behavior and stability was examined by TGA. In Figure 5.5 the mass loss of TBA as function of temperature is shown. The character of this TGA curve is similar to literature [10,12], including one of the earliest reports by Wallraff *et al.*, where they studied thermal and acid-catalyzed deprotection kinetics of poly(*tert*-butyl methacrylate) (PTBMA). Their report demonstrated that

thermal cleavage of the *tert*-butyl ester linkage follows two reaction steps of a slow unimolecular thermolysis followed by a fast auto-acceleration step in which the deprotected groups catalyze further deprotection. In Figure 5.5 a small decrease in mass begins around 160°C, while significant mass loss likely related to the auto-acceleration step occurs around 225°C. The molecular weight of the tBA repeat unit (128.17 g/mol) compared to the acrylic acid (72.06 g/mol) after deprotection results in a theoretical mass loss of 44%, which is similar to the mass loss seen in Figure 5.5.

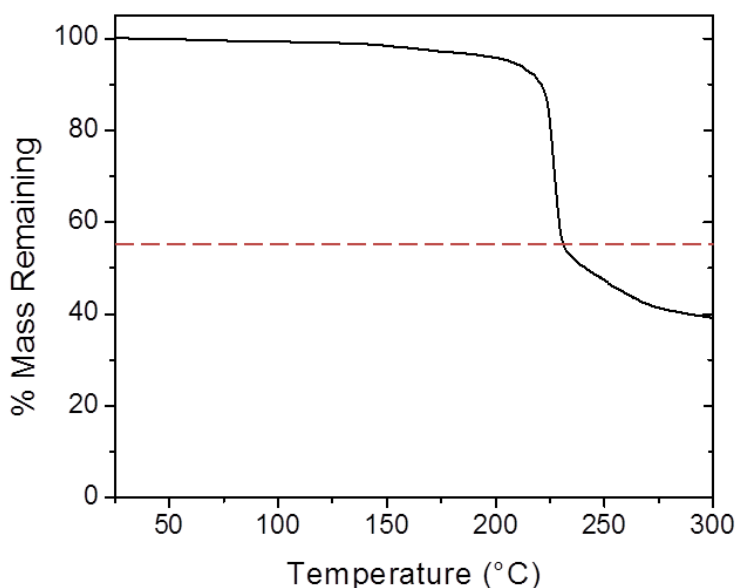


Figure 5.5 – Thermal behavior of PTBA during temperature ramp from 25°-300°C (10°/min), the dashed red line represents the expected theoretical mass loss of 44%.

Detailed information on the structural change of the PTBA was obtained by casting a thin film of PTBA onto a NaCl salt plate and analyzing by FTIR. Spectra were taken before and after annealing the PTBA on the NaCl salt plate at 160°C for 1 day in air and are shown in Figure 5.6. Before annealing, the spectrum shows absorption bands associated with the *tert*-butyl acrylate functionality from C=O ester stretching at 1730 cm⁻¹, CH₃ bending at 1394/1368 cm⁻¹, C-C-O

stretching at $1277/1258\text{ cm}^{-1}$, and C-O stretching at 1160 cm^{-1} [31,32]. After annealing, the peaks attributed to the t-butoxy group almost entirely disappear, in addition the sharp peak due to the carbonyl group (C=O) from the ester linkage is broadened. This confirms the thermolysis and deprotection of the PTBA into PAA.

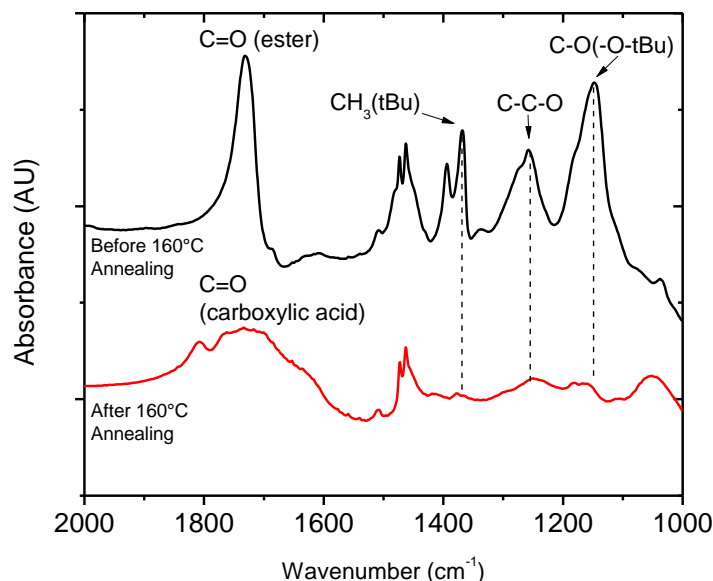


Figure 5.6 – FTIR spectra of PTBA obtained before and after annealing at 160°C for 1 day confirming thermal deprotection to PAA.

5.2.6 Intermolecular Crosslinking of PDMAEMA

The PTBA-PMA-PDMAEMA block copolymer was annealed at 160°C for 1 day, in order to deprotect the PTBA, transforming the block copolymer into PAA-PMA-PDMAEMA. After annealing, the block copolymer turned a dark brown, was more brittle and glassy, and also became insoluble. There were two possible explanations for the change in polymer properties. The first is that the block copolymer is not phase separated prior to thermal deprotection, and when the PTBA becomes PAA, due to the high heat (160°C), which likely facilitates extra mobility and reactivity, the PDMAEMA and PAA react with each other. The second possibility

is that the PDMAEMA is not thermally stable at temperature required for PTBA deprotection. The second possibility has been reported in literature [27], and therefore seemed most likely. In order to test this possibility, the thermal stability of PDMAEMA was investigated. A sample of PDMAEMA homopolymer was heated at 160°C for 1 day. Prior to heating the PDMAEMA, samples of the polymer easily dissolved in H₂O (Figure 5.7a), but after heating it was no longer soluble and instead swelled (Figure 5.7b), suggesting that heating at 160°C resulted in intermolecular crosslinking of PDMAEMA, which is similar to observations by Lowe *et al.*[27]. Other studies on the thermolysis of PTBA has shown that a minimum temperature of 160°C is required to cleave the ester linkage, converting PTBA to PAA. Heating to lower temperatures (130°C) did not achieve ester cleavage [12].

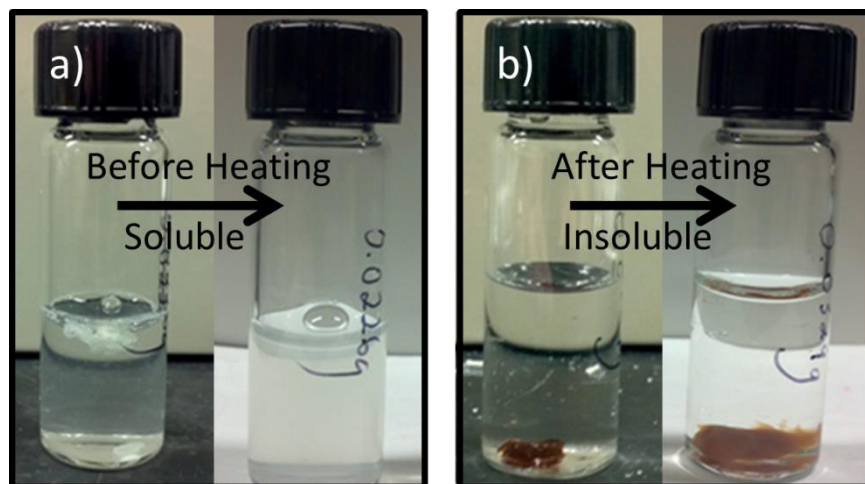


Figure 5.7 – a) PDMAEMA prior to heating fully soluble in H₂O b) PDMAEMA after heating at 160°C is no longer soluble due to crosslinking.

5.2.7 Summary

A tri-block copolymer of PTBA-PMA-PDMAEMA was synthesized with the intention of investigating the mechanochemistry in block copolymers, via disruption of phase separation by

mechanical force. The block copolymer was successfully synthesized using ATRP with a good molecular weight of $M_n \approx 60,000$ g/mol and the thermolysis of PTBA into PAA was confirmed using TGA and FTIR analysis. Upon thermal deprotection of the block copolymer at 160°C it was discovered that the PDMAEMA is not thermally stable and undergoes intermolecular crosslinking, resulting in a brittle insoluble polymer, not viable for further investigation as a system for block copolymer contact mechanochemistry. In the next section, acrylates with hemiacetal ester moieties will be investigated as a possible low temperature thermal deprotection alternative to PTBA.

5.3 Poly(1-ethoxyethyl methacrylate) and Poly(2-(dimethylamino) ethyl methacrylate) Copolymers

5.3.1 Motivation

In the previous section, poly(*tert*-butyl acrylate) (PTBA) and poly(2-(dimethylamino) ethyl methacrylate) (PDMAEMA) were investigated as a model system to investigate the concept of mechanochemistry in block copolymers. However, the high temperature (160°C) required for thermolysis of the *tert*-butyl protecting group resulted in crosslinking of the PDMAEMA block. In this section, an alternative to PTBA, poly(1-ethoxyethyl methacrylate) (PEEMA) is synthesized, characterized, and evaluated as a material suitable for block copolymer contact mechanochemistry.

Crosslinking reactions involving carboxyl groups are ubiquitous throughout chemistry [33–35], and thus motivated PAA's selection as one of the reactive phases for block copolymer mechanochemistry. Unfortunately, materials with high reactivity carboxyl groups have short shelf lives at room temperature, and also are only soluble in specific organic solvents, therefore it is common for the carboxyl group to be modified into a protected form. In addition to the *tert*-

butyl protecting group mentioned, benzyl methacrylates [36,37] and 2-tetrahydropyranyl methacrylates [27,38,39] are other common alternatives, but each still require high deprotection temperatures or are highly susceptible to significant anhydride formation during thermolysis.

Nakane *et al.* [40] developed the use of hemiacetal ester moieties as a new protection group. The advantage of hemiacetal esters is that while the PAA can be thermally deprotected in a few hours at 160°C, it can also be deprotected at temperatures as low as 80°C in 24 h (see Figure 5.8 for chemical structure) [40]. In addition, hemiacetal esters such as 1-ethoxyethyl methacrylate (EEMA), can be polymerized by both ATRP and reversible addition fragmentation chain transfer (RAFT) [22,41–44], which are common living polymerization methods used for the synthesis of block copolymers.

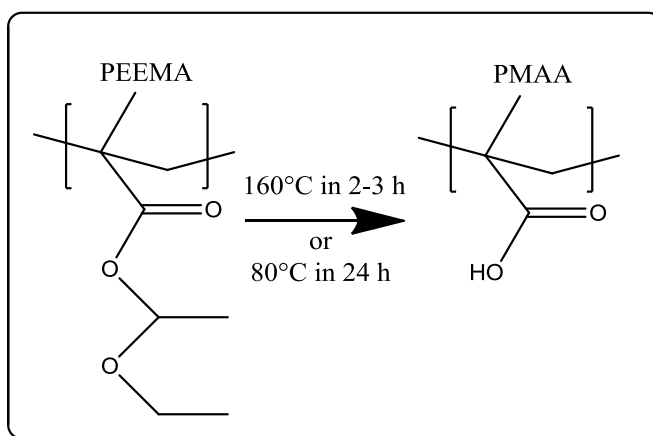


Figure 5.8 – Chemical structure of poly(1-ethoxyethyl methacrylate) (PEEMA) and its thermal deprotection to poly(methacrylic acid) (PMAA).

5.3.2 Monomer and Polymer Synthesis

Materials: *N,N*-(dimethylamino)ethyl methacrylate (DMAEMA) was filtered through basic alumina to remove inhibitor. Anisole and toluene used as a solvent during polymerization were sparged with N₂ for 10-15 minutes prior to use. Methacrylic acid, ethyl vinyl ether, phosphoric

acid, phenothiazine, azobis(isobutyronitrile) (AIBN) and 2-cyano-2-propyl benzodithioate (CPDB) were used as received.

Procedure for the synthesis of 1-ethoxyethyl (meth)acrylate (EE(M)A) [40,42]: Under a nitrogen atmosphere, 1.0mol (68.6 mL) of acrylic acid or 1.0mol (85.2 mL) of methacrylic acid was added slowly at 0°C to a mixture of 1.2mol (114.9mL) of ethyl vinyl ether and 0.002mol (0.2g) of phosphoric acid as a catalyst. The mixture was stirred at room temperature for 48 h. The catalyst was then absorbed on $\text{Mg}_6\text{Al}_2(\text{OH})_{16}\text{CO}_3 \cdot 4\text{H}_2\text{O}$. After filtration the excess vinyl ether was evaporated. The product was distilled at reduced pressure with phenothiazine as inhibitor.

Typical EEMA polymerization procedure by ATRP [42–44]: The monomer was first passed through a basic Al_2O_3 plug to remove traces of residual acid. A Schlenk flask equipped with a Teflon stir bar was purged with Argon for 10-15 minutes followed by the addition of EEMA monomer (5g, 31.6mmol), CuCl (7.8mg, 0.079mmol), PMDETA ligand (24.8μL, 0.12mmol) and 10mL anisole. The flask was immediately sealed and three freeze-pump-thaw cycles were applied to remove oxygen. The flask was backfilled with argon, and ethyl 2-bromoisobutyrate initiator (EBIB) (23.1μL, 0.158mmol) was then added. Finally, the flask was placed in an oil bath thermostated at 55°C for 24 h. The polymerization was opened to air, THF was added and the polymer was filtered through a neutral alumina plug to remove CuBr. After evaporating the excess solvent, polymer precipitation into cold methanol as stated in literature was attempted, resulting in no solid polymer. The remaining solvent was removed under vacuum leaving 200-300mg of polymer.

Typical EEMA polymerization procedure by RAFT [22,41]: A 100mL Schlenk flask equipped with a Teflon stir bar was purged with Argon for 10-15 minutes followed by the

addition of EEMA monomer (5mL, 29.5mmol), AIBN (6.1mg, 0.037mmol), CPDB RAFT agent (30.3 μ L, 0.147mmol) and 10mL of toluene. The flask was immediately sealed and three freeze-pump-thaw cycles were applied to remove dissolved oxygen. The flask was backfilled with argon and placed in an oil bath thermostated at 70°C for 20 h. The polymerization was opened to air, and excess solvent was removed *in vacuo*. The remaining polymer solution was precipitated into stirring cold methanol, collected, redissolved in ether and reprecipitated in methanol. A solid polymer was collected and dried under vacuum.

Typical DMAEMA polymerization procedure by RAFT [45]: A 100mL Schlenk flask equipped with a Teflon stir bar was purged with Argon for 10-15 minutes followed by the addition of DMAEMA monomer (4.65g, 5mL, 29.5mmol), AIBN (6.1mg, 0.037mmol), CPDB RAFT agent (30.3 μ L, 0.147mmol) and 10mL of toluene. The flask was immediately sealed and three freeze-pump-thaw cycles were applied to remove dissolved oxygen. The flask was backfilled with argon and placed in an oil bath thermostated at 90°C for 20 h. The polymerization was opened to air to stop the reaction. After solvent was removed *in vacuo*, the polymer was precipitated by drop wise addition to stirring hexane. The resulting polymer was collected and dried under vacuum at room temperature.

For a typical block copolymer polymerization (PEEMA-PDMAEMA): PEEMA or PDMAEMA macroinitiators synthesized still have the thiocarbonyl-thio chain transfer agent as an end group. This CPDB end group is utilized to synthesize the block copolymers. A 100mL Schlenk flask equipped with a Teflon stir bar was purged with argon for 10-15 minutes followed by the addition of PEEMA macroinitiator (4.85g, 0.148mmol) with 10mL of toluene. Once the macroinitiator had fully dissolved in the solvent AIBN (6.1mg, 0.037mmol) and DMAEMA monomer (4.66g, 5 mL, 29.5mmol) was added. The flask was immediately sealed and three

freeze-pump-thaw cycles were applied to remove dissolved oxygen. The flask was backfilled with argon and placed in an oil bath thermostated at 90°C for 4 h. The polymerization was opened to air, and excess solvent was removed *in vacuo*. The remaining block copolymer solution was precipitated into stirring cold methanol, and a solid polymer was collected and dried under vacuum.

Sample Molding: Polymer powder was molded into approximately 1mm thick disk with a diameter of 25 mm via compression molding. A pressure of 200 psi was applied to the mold at a temperature of 80°C for 8 minutes. Example of a molded sample can be seen in Figure 5.12.

Characterization Methods: The characterization methods used in this section are the same as those used for the PTBA block copolymer systems and can be found in “*Characterization Methods 5.2.3*”

5.3.3 Homopolymers and Block Copolymer Characterization

PEEMA synthesized by ATRP produced very low polymer yield (<5%). Polymerizations with a different initiator (2,2,2-trichloroethanol) [42], with and without CuCl₂, as well as bulk polymerizations were also attempted, but all resulted in yields too low for practical mechanical testing.

PEEMA synthesized by RAFT, produced polymers improved yields (30-40%) and molecular weights. Typical PEEMA polymers synthesized by RAFT had a $M_n \approx 32,000$ g/mol with a PDI = 1.11 ($M_{n,theo} = 31,600$ g/mol), determined by GPC analysis. Homopolymers of PDMAEMA were also synthesized by RAFT, but molecular weights determined by GPC were low compared to theoretical calculations ($M_{n,exp} = 14,300$ g/mol, $M_{n,theo} = 31,400$ g/mol). This is a result of the DMAEMA sticking to the GPC columns, resulting in longer retention times and lower molecular weights [45]. A macroinitiator with known molecular weight is required to determine the

molecular weight of PDMAEMA by ^1H NMR. Poly(ethylene glycol) macroinitiators of 350 g/mol and also 1,100 g/mol were synthesized and used to polymerize PDMAEMA, but the protons from these macroinitiators lacked the resolution in ^1H NMR spectra and could not be compared to the PDMAEMA to determine the molecular weight. While a PEEMA macroinitiator is the next option, the PDMAEMA polymerization is carried out at 90°C , and possible deprotection of the PEEMA into PMAA during polymerization was an initial concern for use of PEEMA as the macroinitiator.

PEEMA, with known molecular weight of $M_n \approx 32,000$ g/mol was used as a macroinitiator for PDMAEMA polymerization. By comparing hemiacetal ester moiety in the side chain of PEEMA to the methoxy proton in PDMAEMA the molecular weight of the PDMAEMA and the block copolymer was determined. A typical block copolymer had a composition of about 50:50 PEEMA to PDMAEMA with a molecular weight between 40,000 – 50,000 g/mol.

5.3.4 Thermal Deprotection of PEEMA

Thermal deprotection of PEEMA into PMAA was tested using isothermal TGA at 160°C for 5 h. Figure 5.9 displays the mass loss for both PEEMA and PDMAEMA homopolymers and the block copolymer. The PDMAEMA over the course of 5 h does not show any significant mass loss, which was expected. The PEEMA as well as the block copolymers both showed mass loss values close to the calculated theoretical values in 2-3 h for the block copolymer and 3-4 h for the PEEMA homopolymer. The mass loss in the block copolymer does seem to go beyond the theoretical value (dashed line) but that calculated value is based on the composition of the block copolymer, which was assumed to be close to 50:50. Small deviations in the molecular weights of each block likely accounts for the appearance of greater than theoretical mass loss.

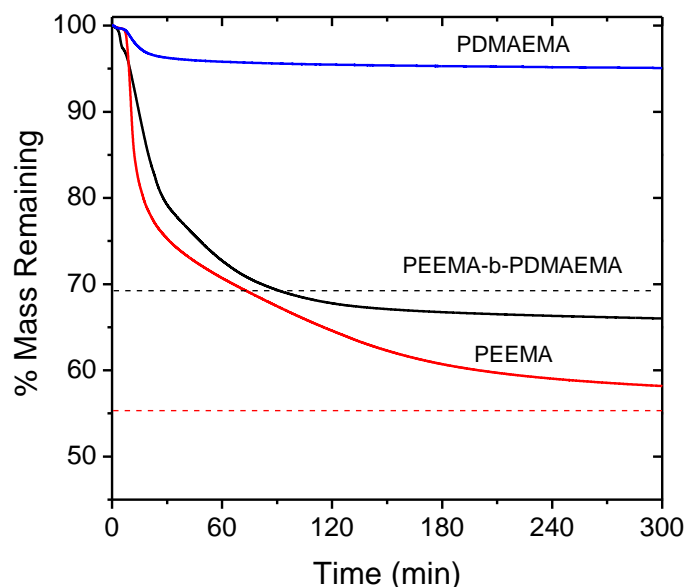


Figure 5.9 – Isothermal TGA of PDMAEMA, PEEMA-b-PDMAEMA block copolymer and PEEMA homopolymer heated at 160°C for 5 h. The dashed lines represent the theoretical mass loss.

To confirm low temperature deprotection of PEEMA, 10-20 mg samples of PEEMA polymer were placed in an oven at 90°C for 24 h. NMR spectra of PEEMA heated in an oven purging N₂ showed no change after 24 h (Figure 5.10b) from NMR spectra of PEEMA before heating (Figure 5.10a). The deprotection is likely acid catalyzed, and while heating in the N₂ purging oven there may have been a lack of moisture present to facilitate or catalyze deprotection. When the PEEMA was heated in the same oven with no N₂ purging for 24 h, NMR spectra showed the disappearance of two characteristic peaks for PEEMA at δ 5.6-5.8 ppm and at δ 3.85, 3.63 ppm from the hemiacetal ester moieties in the side chain (Figure 5.10c). In addition, there was the appearance of a methacrylic acid peak at δ 12.4 ppm, confirming the thermal deprotection of PEEMA to PMAA.

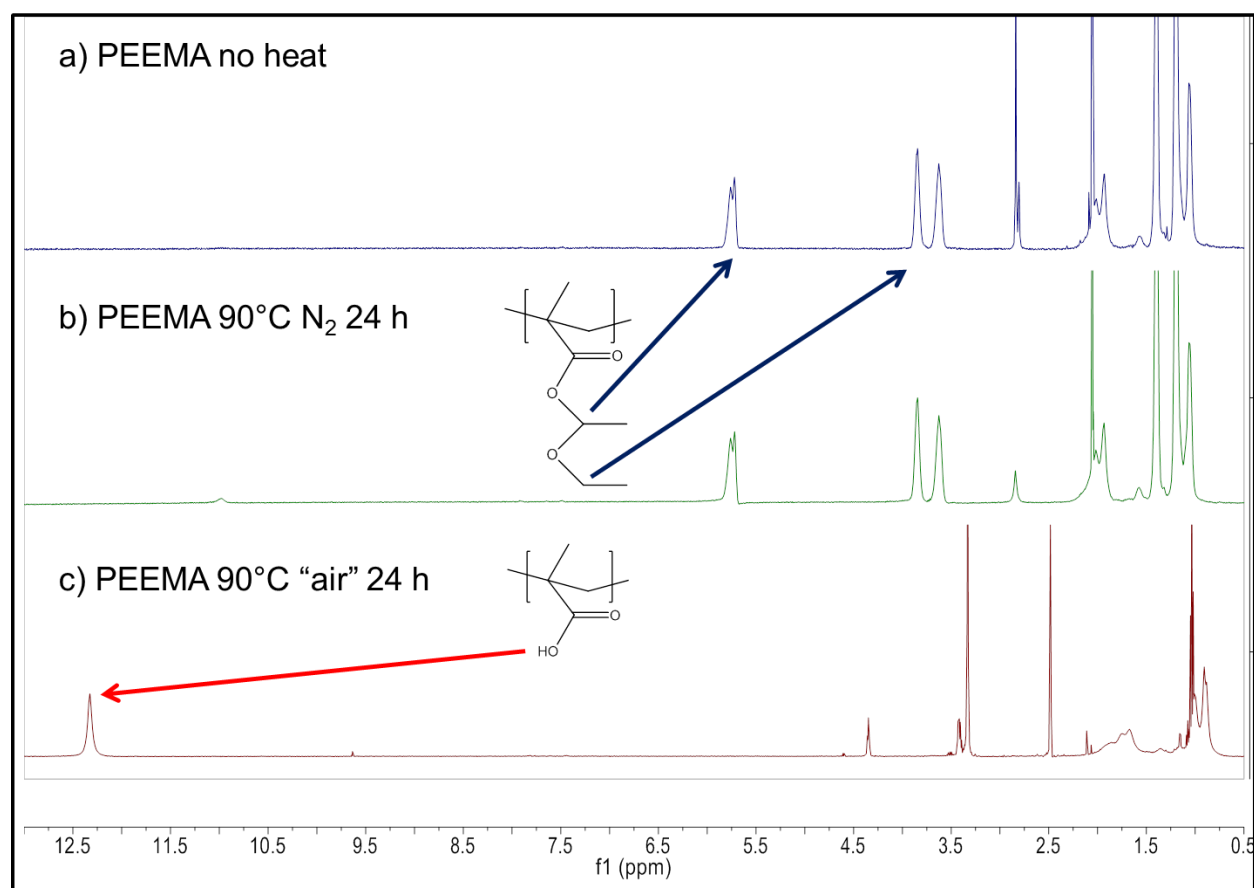


Figure 5.10 – ^1H NMR of PEEMA a) before heating, b) heated at 90°C under N₂ for 24 h, and c) heated at 90°C in “air” for 24 h.

5.3.5 Block Copolymer Deprotection Challenges

Thermal deprotection of the PEEMA as a block in the PEEMA-*b*-PDMAEMA block copolymer was confirmed by TGA at 160°C (Figure 5.9), but as discussed in *section 5.2.6*, the PDMAEMA block is susceptible to crosslinking at this high temperature. In Figure 5.11 the PEEMA homopolymer and block copolymer were heated at 90°C for 24 h and FTIR spectra is presented. The PEEMA after heating (Figure 5.11b) shows a broad band centered around 3300 cm⁻¹, corresponding to an OH stretch of PMAA, not present prior to heating (Figure 5.11a)

[40,46]. For the block copolymer, no OH stretching band appears after heating (Figure 5.11d), and the FTIR spectra before and after remain essentially the same.

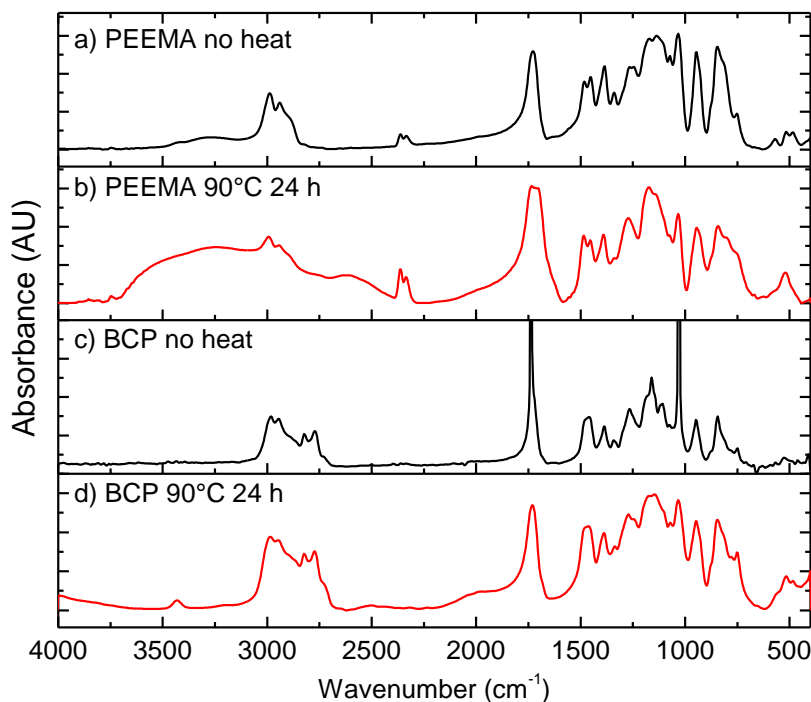


Figure 5.11 – FTIR spectra of PEEMA homopolymer a) before and b) after heating at 90°C for 24h and the PEEMA-b-PDMAEMA block copolymer (BCP) c) before and d) after heating at 90°C for 24 h.

While FTIR did not confirm the low temperature deprotection of the PEEMA when part of the block copolymer, bulk block copolymer samples of PEEMA-b-PDMAEMA did result in mass loss when annealed. In Figure 5.12, a block copolymer hot pressed into a disk (25 mm diameter) for rheological testing is shown before and after annealing. When the disk was heated at 90°C for 24h, large voids appear throughout the sample. The large voids are likely a product of the removal of the hemiacetal ester moieties as a gas. The block copolymer synthesized was about 50% PEEMA and 50% PDMAEMA, and the molecular weight of both monomers is very similar (PEEMA = 158.19 g/mol; PDMAEMA = 157.21 g/mol). Since the theoretical mass loss of

PEEMA to PMAA is 45%, if we assume exactly half the block copolymer is PEEMA, an expected mass loss would be $\approx 27\%$. Bulk block copolymer samples of PEEMA-b-PDMAEMA annealed in an oven at 90°C for 24h resulted in an average mass change of 15-20%. While, it appears that the PEEMA may not experience full deprotection, the significant mass loss measured, and void formation observed after heating is evidence of low temperature thermal deprotection of the PEEMA-b-PDMAEMA.

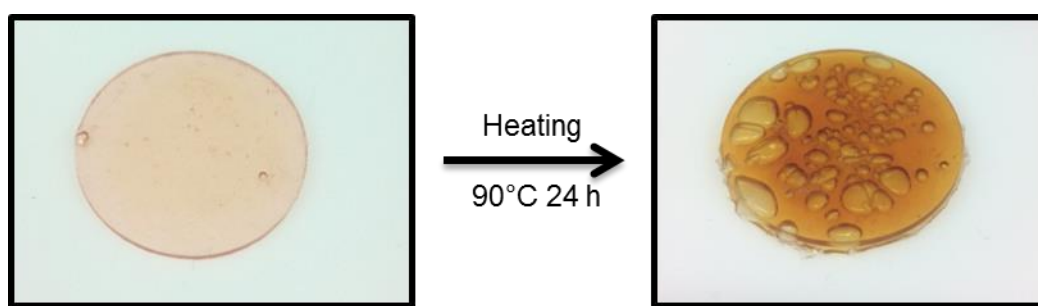


Figure 5.12 – PEEMA-b-PDMAEMA compression molded into 25mm diameter disk before and after thermal deprotection at 90°C for 24 h.

The FTIR spectra in Figure 5.11c and 5.11d did not show the appearance of the OH stretching band expected for the deprotected PMAA group. It is possible that while the PEEMA group did deprotect into PMAA, the block copolymer may not be phase separated, resulting in immediate reaction of the OH group formed. To confirm this, polymer films were solution casted onto glass slides. The films were very optically clear, and when viewed under a microscope with different phase condensers, showed no signs of phase separation.

5.3.6 Large Amplitude Oscillatory Shear Challenges

While traditionally tension and compression are used to mechanically deform mechanochemical systems [47], the deformations needed to break up and mix block copolymer

phases will likely result in polymer failure before morphology break up. Therefore, the use of large amplitude oscillatory shear (LAOS) was proposed as a means to induce mechanical mixing of the two complimentary phases after phase separation and thermal deprotection. LAOS in block copolymers is a well-studied method for inducing long range microdomain order [48–52]. We propose the use of LAOS to induce movement of the microdomains. When the block copolymer is protected, shear induced ordering should be possible, but once the protected phase is activated (by deprotection), LAOS can be used to induce movement of phases, which will be hindered by an interaction of the complimenting polymer functionalities. In the protected block copolymer mechanical properties (G' , G'') of the material should remain similar before and after shearing, while in the deprotected material fundamentally different mechanical properties should arise, from shear induced chemical reactions between the two phases.

In order to shear the samples, a rheometer (TA Instrument's AR-G2) was operated in parallel-plate geometry mode, requiring a small disk geometry. The final block copolymer disk (Figure 5.12), formed by compression molding, was glassy, and did not have good surface contact with the parallel-plates. This resulted in slipping during LAOS, not enabling accurate G' and G'' values to be determined. When the sample was heated to soften the polymer, better contact with the plates were achieved, but heating for long durations of time again resulted in the bubbling and void formation of the disk sample (Figure 5.12, right). The large void formation resulted in a non-uniform polymer sample surface making it unsuitable for accurate rheological data collection. In addition, results from the previous section (*section 5.3.5*) led to the conclusion that the block copolymer synthesized in this study is not phase separated.

Traditional block copolymer systems studied by LAOS are often a combination of glassy and rubbery polymers, such as poly(styrene)-b-poly(isoprene) or poly(styrene)-b-poly(butadiene)

[48,50–52]. The low T_g phase, poly(isoprene) or poly(butadiene), creates a good contact with the parallel plates and also gives the polymer some mobility when shearing at high rates. The mechanical properties of the PEEMA-b-PDMAEMA block copolymer were not amenable to this type of mechanical testing, being too glassy and brittle while also temperature sensitive. In future studies, if LAOS is the mechanical testing method of choice, then block copolymers designed must include a low T_g mobile phase to facilitate large amplitude shearing.

5.3.7 Summary

Poly (1-ethoxyethyl methacrylate) (PEEMA) was synthesized by RAFT polymerization and investigated as protected poly(acid) alternative to PTBA because of its ability to deprotect at lower temperatures (80°C). The EEMA monomer, polymer, and block copolymer with PDMAEMA was successfully synthesized with relatively high molecular weights and in good yields, allowing for polymerization of a few grams of polymer, required for solid state mechanical testing. The thermal deprotection of PEEMA at 160°C in a few hours was confirmed using TGA. Deprotection at 90°C was confirmed using ^1H NMR and FTIR. When the heating was carried out in N_2 inert atmosphere, the thermal cleavage was not successful. It seems that the deprotection of PEEMA is slightly “acid catalyzed” and requires a small amount of moisture from the air to convert to PMAA.

When the PEEMA-b-PDMAEMA block copolymer was deprotected at 160°C the expected mass loss was observed. FTIR of deprotection at 90°C for 24 h, a lower temperature to prevent the crosslinking of PDMAEMA, did not show the expected broad OH stretch band associated with the deprotection to PMAA. It is hypothesized that the deprotection is occurring, but the lack of phase separation results in an immediate reaction with the PMAA, accounting for the missing OH band in the FTIR spectra.

In addition to the challenges faced with a lack of microdomain formation, the block copolymer was unable to be mechanically tested by large amplitude oscillatory shear (LAOS). The final block copolymer is glassy, resulting in very poor contact with the parallel plates used for shearing. This resulted in the plates slipping past the polymer sample during shearing. Finally, as the sample is annealed, large void formation due to deprotection and release of the hemiacetal ester moiety prevents accurate rheology measurements from being collected.

5.4 Conclusions

This chapter set out to investigate the use of a block copolymer made of a protected poly((meth)acrylic acid) (P(M)AA) and poly(dimethylamino-ethyl methacrylate) (PDMAEMA) for contact mechanochemistry. The objectives were to use the inherent phase separation due to thermodynamics of block copolymers, to isolate the two reactive polymer phases, and then utilize large amplitude oscillatory shearing to break up the phases and induce a reaction or complex between PAA and PDMAEMA. The studies conducted and here reported conclude that there are a number of fundamental obstacles hindering the use of this polymer system for block copolymer mechanochemistry.

First, the phases of the block copolymer synthesized were miscible, and did not phase separate. This made the block copolymer system fundamentally unsuitable for contact mechanochemistry. The second obstacle was in the thermal deprotection of the protected group. Major challenges in this area involved deprotection temperatures which were too high, causing crosslinking of the PDMAEMA phase. In addition, the use of thermal deprotection involved the release of either the isobutylene or hemiacetal ester moiety as a gas, for PTBA and PEEMA, respectively, causing significant volume change. While volume change of the material should not affect the end goal of contact mechanochemistry, it did change the molded sample geometry required for LAOS.

For future designs one should either not use thermal deprotection schemes if LAOS is the chosen mechanical testing method, or explore other mechanical testing options, in which accurate mechanical data collected is insensitive to changing physical nature of the material. In the next chapter, a new chemistry involving a protected or “masked” thiol used to ring open an epoxide functionality will be investigated as a possible chemistry for contact mechanochemistry.

REFERENCES

- [1] F.S. Bates, G.H. Fredrickson, Block Copolymers—Designer Soft Materials, *Physics Today*. 52 (1999) 32.
- [2] T.P. Lodge, Block Copolymers: Past Successes and Future Challenges, *Macromolecular Chemistry and Physics*. 204 (2003) 265–273.
- [3] L. Leibler, Theory of Microphase Separation in Block Copolymers, *Macromolecules*. 13 (1980) 1602–1617.
- [4] E. Helfand, Block Copolymer Theory. III. Statistical Mechanics of the Microdomain Structure, *Macromolecules*. 8 (1975) 552–556.
- [5] T.L. Lebedeva, G.A. Shandryuk, T.I. Sycheva, V.S. Bezborodov, R.V. Talroze, N.A. Platé, Structure of β -N-dimethylamino-4-dodecyloxypropionophenone complexes with di- and polycarboxylic acids, *Journal of Molecular Structure*. 354 (1995) 89–96.
- [6] R.V. Tal’roze, S.A. Kuptsov, T.I. Sycheva, V.S. Bezborodov, N.A. Plate, Order and Liquid Crystalline Phase Behavior of Polyacid-Tertiary Amine Complexes, *Macromolecules*. 28 (1995) 8689–8691.
- [7] P.G.M. Wuts, *Greene’s protective groups in organic synthesis*, 4th ed, Wiley-Interscience, Hoboken, N.J., 2007.
- [8] K.A. Davis, K. Matyjaszewski, Atom Transfer Radical Polymerization of tert-Butyl Acrylate and Preparation of Block Copolymers, *Macromolecules*. 33 (2000) 4039–4047.
- [9] G. Wallraff, J. Hutchinson, W. Hinsberg, F. Houle, P. Seidel, R. Johnson, *et al.*, Thermal and acid-catalyzed deprotection kinetics in candidate deep ultraviolet resist materials, in: *AVS*, New Orleans, Louisiana (USA), 1994: pp. 3857–3862.
- [10] J. Duvigneau, H. Schönherr, G.J. Vancso, Atomic Force Microscopy Based Thermal Lithography of Poly(tert-butyl acrylate) Block Copolymer Films for Bioconjugation, *Langmuir*. 24 (2008) 10825–10832.
- [11] S.M. Kim, S.J. Ku, J.-B. Kim, SiO₂ nanodot arrays using functionalized block copolymer templates and selective silylation, *Nanotechnology*. 21 (2010) 235302.

- [12] Y.-H. La, E.W. Edwards, S.-M. Park, P.F. Nealey, Directed Assembly of Cylinder-Forming Block Copolymer Films and Thermochemically Induced Cylinder to Sphere Transition: A Hierarchical Route to Linear Arrays of Nanodots, *Nano Letters*. 5 (2005) 1379–1384.
- [13] O. Samsonova, C. Pfeiffer, M. Hellmund, O.M. Merkel, T. Kissel, Low Molecular Weight pDMAEMA-block-pHEMA Block-Copolymers Synthesized via RAFT-Polymerization: Potential Non-Viral Gene Delivery Agents?, *Polymers*. 3 (2011) 693–718.
- [14] P. van de Wetering, N.J. Zuidam, M.J. van Steenberg, O.A.G.J. van der Houwen, W.J.M. Underberg, W.E. Hennink, A Mechanistic Study of the Hydrolytic Stability of Poly(2-(dimethylamino)ethyl methacrylate), *Macromolecules*. 31 (1998) 8063–8068.
- [15] F.L. Baines, S. Dionisio, N.C. Billingham, S.P. Armes, Use of Block Copolymer Stabilizers for the Dispersion Polymerization of Styrene in Alcoholic Media, *Macromolecules*. 29 (1996) 3096–3102.
- [16] F.L. Baines, S.P. Armes, N.C. Billingham, Z. Tuzar, Micellization of Poly(2-(dimethylamino)ethyl methacrylate-block-methyl methacrylate) Copolymers in Aqueous Solution, *Macromolecules*. 29 (1996) 8151–8159.
- [17] P. Ni, M. Zhang, L. Ma, S. Fu, Poly(dimethylamino)ethyl Methacrylate for Use as a Surfactant in the Miniemulsion Polymerization of Styrene, *Langmuir*. 22 (2006) 6016–6023.
- [18] X. Wang, M.A. Winnik, I. Manners, Synthesis and Self-Assembly of Poly(ferrocenyldimethylsilane-b-dimethylaminoethyl methacrylate): Toward Water-Soluble Cylinders with an Organometallic Core, *Macromolecules*. 38 (2005) 1928–1935.
- [19] Amphiphilic block copolymers: self-assembly and applications, 1st ed, Elsevier, Amsterdam ; New York, 2000.
- [20] L.-H. Gan, P. Ravi, B.W. Mao, K.-C. Tam, Controlled/living polymerization of 2-(diethylamino)ethyl methacrylate and its block copolymer with tert-butyl methacrylate by atom transfer radical polymerization, *J. Polym. Sci. A Polym. Chem*. 41 (2003) 2688–2695.
- [21] X. Zhang, K. Matyjaszewski, Synthesis of Well-Defined Amphiphilic Block Copolymers with 2-(Dimethylamino)ethyl Methacrylate by Controlled Radical Polymerization, *Macromolecules*. 32 (1999) 1763–1766.
- [22] R. Hoogenboom, U.S. Schubert, W. Van Camp, F.E. Du Prez, RAFT Polymerization of 1-Ethoxyethyl Acrylate: A Novel Route toward Near-Monodisperse Poly(acrylic acid) and Derived Block Copolymer Structures, *Macromolecules*. 38 (2005) 7653–7659.
- [23] D.A. Shipp, J.-L. Wang, K. Matyjaszewski, Synthesis of Acrylate and Methacrylate Block Copolymers Using Atom Transfer Radical Polymerization, *Macromolecules*. 31 (1998) 8005–8008.
- [24] X. Zhang, J. Xia, K. Matyjaszewski, Controlled/“Living” Radical Polymerization of 2-(Dimethylamino)ethyl Methacrylate, *Macromolecules*. 31 (1998) 5167–5169.
- [25] S. Creutz, P. Teyssié, R. Jérôme, Living Anionic Homopolymerization and Block Copolymerization of (Dimethylamino)ethyl Methacrylate, *Macromolecules*. 30 (1997) 6–9.

- [26] F.L. Baines, N.C. Billingham, S.P. Armes, Synthesis and Solution Properties of Water-Soluble Hydrophilic–Hydrophobic Block Copolymers, *Macromolecules*. 29 (1996) 3416–3420.
- [27] A. B. Lowe, N. C. Billingham, S. P. Armes, Synthesis and aqueous solution properties of novel zwitterionic block copolymers, *Chem. Commun.* (1997) 1035–1036.
- [28] S. Krause, J.J. Gormley, N. Roman, J.A. Shetter, W.H. Watanabe, Glass temperatures of some acrylic polymers, *Journal of Polymer Science Part A: General Papers*. 3 (1965) 3573–3586.
- [29] S.K. Varshney, C. Jacobs, J.P. Hautekeer, P. Bayard, R. Jerome, R. Fayt, *et al.*, Anionic polymerization of acrylic monomers. 6. Synthesis, characterization, and modification of poly(methyl methacrylate)-poly(tert-butyl acrylate) di- and triblock copolymers, *Macromolecules*. 24 (1991) 4997–5000.
- [30] L. Toman, M. Janata, J. Spěvák, J. Brus, A. Sikora, P. Látalová, *et al.*, Amphiphilic conetworks. II. Novel two-step synthesis of poly[2-(dimethylamino)ethyl methacrylate]–polyisobutylene, poly(N-isopropylacrylamide)–polyisobutylene, and poly(N,N-dimethylacrylamide)–polyisobutylene hydrogels, *J. Polym. Sci. A Polym. Chem.* 44 (2006) 6378–6384.
- [31] G. Socrates, *Infrared and Raman characteristic group frequencies: tables and charts*, 3rd ed, Wiley, Chichester ; New York, 2001.
- [32] H.S. Shin, Y.M. Jung, J. Lee, T. Chang, Y. Ozaki, S.B. Kim, Structural Comparison of Langmuir–Blodgett and Spin-Coated Films of Poly(tert-butyl methacrylate) by External Reflection FTIR Spectroscopy and Two-Dimensional Correlation Analysis, *Langmuir*. 18 (2002) 5523–5528.
- [33] H. Inata, S. Matsumura, Chain extenders for polyesters. I. Addition-type chain extenders reactive with carboxyl end groups of polyesters, *Journal of Applied Polymer Science*. 30 (1985) 3325–3337.
- [34] H. Inata, S. Matsumura, Chain extenders for polyester. II. Reactivities of carboxyl-addition-type chain extenders; bis cyclic-imino-ethers, *Journal of Applied Polymer Science*. 32 (1986) 5193–5202.
- [35] M. Ooka, H. Ozawa, Recent developments in crosslinking technology for coating resins, *Progress in Organic Coatings*. 23 (1994) 325–338.
- [36] J. Mykytiuk, S.P. Armes, N.C. Billingham, Group-transfer polymerization of benzyl methacrylate: A convenient method for synthesis of near-monodisperse poly(methacrylic acids), *Polymer Bulletin*. 29 (1992) 139–145.
- [37] S.P. Rannard, N.C. Billingham, S.P. Armes, J. Mykytiuk, Synthesis of monodisperse block copolymers containing methacrylic acid segments by group-transfer polymerization: choice of protecting group and catalyst, *European Polymer Journal*. 29 (1993) 407–414.
- [38] C.S. Patrickios, W.R. Hertler, N.L. Abbott, T.A. Hatton, Diblock, ABC triblock, and random methacrylic polyampholytes: synthesis by group transfer polymerization and solution behavior, *Macromolecules*. 27 (1994) 930–937.

- [39] V. Bütün, M. Vamvakaki, N.C. Billingham, S.P. Armes, Synthesis and aqueous solution properties of novel neutral/acidic block copolymers, *Polymer*. 41 (2000) 3173–3182.
- [40] Y. Nakane, M. Ishidoya, T. Endo, Synthesis and thermal dissociation of polymers having hemiacetal ester moieties, *J. Polym. Sci. A Polym. Chem.* 37 (1999) 609–614.
- [41] S. Perrier, P. Takolpuckdee, C.A. Mars, Reversible Addition–Fragmentation Chain Transfer Polymerization: End Group Modification for Functionalized Polymers and Chain Transfer Agent Recovery, *Macromolecules*. 38 (2005) 2033–2036.
- [42] W. Van Camp, F.E. Du Prez, S.A.F. Bon, Atom Transfer Radical Polymerization of 1-Ethoxyethyl (Meth)acrylate: Facile Route toward Near-Monodisperse Poly((meth)acrylic acid), *Macromolecules*. 37 (2004) 6673–6675.
- [43] B. Dervaux, W. Van Camp, L. Van Renterghem, F.E. Du Prez, Synthesis of poly(isobornyl acrylate) containing copolymers by atom transfer radical polymerization, *J. Polym. Sci. A Polym. Chem.* 46 (2008) 1649–1661.
- [44] D. Wouters, W. Van Camp, B. Dervaux, F.E. Du Prez, U.S. Schubert, Morphological transition during the thermal deprotection of poly(isobornyl acrylate)-b-poly(1-ethoxyethyl acrylate), *Soft Matter*. 3 (2007) 1537–1541.
- [45] M. Sahnoun, M.-T. Charreyre, L. Veron, T. Delair, F. D’Agosto, Synthetic and characterization aspects of dimethylaminoethyl methacrylate reversible addition fragmentation chain transfer (RAFT) polymerization, *J. Polym. Sci. A Polym. Chem.* 43 (2005) 3551–3565.
- [46] R.M. Silverstein, *Spectrometric identification of organic compounds*, 7th ed, John Wiley & Sons, Hoboken, NJ, 2005.
- [47] K.M. Wiggins, J.N. Brantley, C.W. Bielawski, *Methods for activating and characterizing mechanically responsive polymers*, Chemical Society Reviews. (2013).
- [48] Z.-R. Chen, A.M. Issaian, J.A. Kornfield, S.D. Smith, J.T. Grothaus, M.M. Satkowski, Dynamics of Shear-Induced Alignment of a Lamellar Diblock: A Rheo-optical, Electron Microscopy, and X-ray Scattering Study, *Macromolecules*. 30 (1997) 7096–7114.
- [49] F.A. Morrison, H.H. Winter, W. Gronski, J.D. Barnes, Effect of unidirectional shear on the structure of triblock copolymers. 2. Polystyrene-polyisoprene-polystyrene, *Macromolecules*. 23 (1990) 4200–4205.
- [50] U. Wiesner, Lamellar diblock copolymers under large amplitude oscillatory shear flow: Order and dynamics, *Macromol. Chem. Phys.* 198 (1997) 3319–3352.
- [51] D.B. Scott, A.J. Waddon, Y.G. Lin, F.E. Karasz, H.H. Winter, Shear-induced orientation transitions in triblock copolymer styrene-butadiene-styrene with cylindrical domain morphology, *Macromolecules*. 25 (1992) 4175–4181.
- [52] B.S. Pinheiro, K.I. Winey, Mixed Parallel–Perpendicular Morphologies in Diblock Copolymer Systems Correlated to the Linear Viscoelastic Properties of the Parallel and Perpendicular Morphologies, *Macromolecules*. 31 (1998) 4447–4456.

CHAPTER 6

CONTACT MECHANOCHEMISTRY: POLY(DISULFIDES) AND POLY(GLYCIDYL METHACRYLATE)

6.1 Introduction

Block copolymers and polymer blends undergo phase separation due to the incompatibility and the large thermodynamic cost to mix [1,2]. The concept of contact mechanochemistry is to exploit this thermodynamic phenomenon, in the design of a material that produces a chemical reaction when the phase separated domains come in contact or are mixed, by mechanical force. The properties of polymer blends and block copolymers can be varied by different microphase separation morphologies [3–5]. Morphology changes can also be force induced, and have been well studied [6–10]. The concept of contact mechanochemistry goes beyond harnessing force to manipulate the phase separated morphology, which result in polymer properties that lie between the bounds of polymer A or polymer B. Rather, the use of force to bring in contact isolated (phase separated) reactive domains holds much potential in the design of polymers which can undergo drastic changes in polymer properties, beyond the innate properties of the starting combination polymers (polymer A and polymer B).

The results reported in Chapter 5 demonstrated that, while choosing reactive chemistry seems like a simple question with various possible answers, choosing a chemistry which meets all the criteria for solid state contact mechanochemistry is not trivial. Through the study in Chapter 5, a number of design parameters required for contact mechanochemistry were discussed as major research challenges arose. For example, the thermal deprotection scheme proposed required high deprotection temperatures causing chemical changes in the second polymer phase, and also large

volume changes, not suitable for the proposed mechanical testing method. In addition, the chemistry and polymers chosen were miscible, and therefore not phase separated. In this chapter the exploration of a nucleophilic thiol epoxide ring opening chemistry for contact mechanochemistry will be explored.

Epoxides are very reactive, due to their strained ringed structure [11]. They are common throughout industry as low molecular weight pre-polymers used to form thermosetting polymers. The high reactivity of the epoxide functionality and its ability to undergo ring opening with the most common nucleophiles such as alcohols, thiols, or amines, motivates its selection as one of the reactive functionalities for contact mechanochemistry [12–14]. As a complimentary phase, a polymer with disulfides side-chains will be explored. The disulfide, can mask the reactive thiol nucleophile, and can easily be reduced by common reducing agents [15,16], resulting in the active functionality. Thiols, also known as mercaptans, are known to react very readily with the epoxide group, even at ambient temperatures, making them suitable candidates for ring opening of the epoxy functionality [17,18]. In this chapter, poly(glycidyl methacrylate) (PGMA) (Figure 1a), commonly used in epoxy resins, will be synthesized as one reactive phase, and a recently reported on [19] disulfide methacrylate polymer (Figure 1b), will be synthesized as the protected or masked second phase.

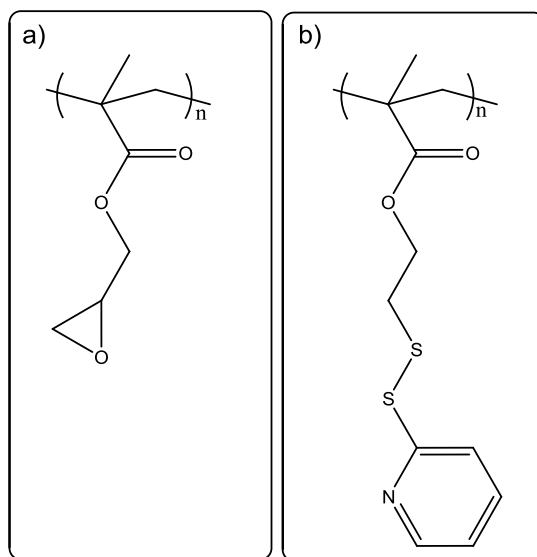


Figure 6.1 – Chemical structures of a) poly(glycidyl methacrylate) (PGMA) and b) poly disulfide polymer, poly(2-(pyridine-2-yl)disulfanyl) ethyl methacrylate (PPDSEMA).

The first step in the development of contact mechanochemistry using the ring opening of epoxides with thiols is to create a polymer blend of the PGMA and poly disulfide polymer. When the two polymers are blended, they should separate into isolated domains due to the thermodynamic cost of mixing long chain polymers. A reducing agent can then be used to swell the blend and cut the disulfide bond, exposing the thiol nucleophile, isolated from the epoxide side chain of the PGMA due to phase separation. Then, using mechanical force to break up the phase separation or mix the phases, the now exposed thiol can come in contact with the epoxide group, inducing a ring opening reaction, causing the formation of covalent bonds between the two polymers, fundamentally changing the properties of the polymer blend.

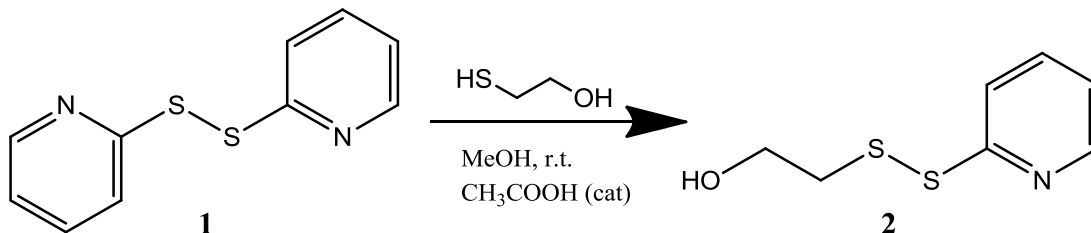
6.2 Experimental Methods

6.2.1 Synthesis

Materials: Glycidyl methacrylate (GMA), was filtered through basic alumina to remove the inhibitor. Toluene was sparged with N₂ for 10-15 minutes before use. All other reagents were used as received, unless otherwise mentioned.

For a typical GMA polymerization [20]: A Schlenk flask equipped with a Teflon stir bar was purged with N₂ for 10-15 minutes followed by the addition of GMA monomer (5.35g, 36.9mmol), CuBr (26.4mg, 0.184mmol), *N,N,N',N'',N'''*-pentamethyldiethylenetriamine (PMDETA) ligand (31.9mg, 0.184mmol), and 10mL of toluene. The flask was immediately sealed and three freeze-pump-thaw cycles were applied to remove dissolved oxygen. The flask was backfilled with N₂, and ethyl 2-bromoisobutyrate (EBIB) initiator (35.9mg, 0.184mmol) was then added. Finally, the flask was placed in an oil bath thermostated at 50°C for 2 h. The polymerization was opened to air, chloroform was added and the polymer was filtered through a silica plug to remove the CuBr. After most of the solvent was removed *in vacuo*, the polymer was precipitated by drop wise addition to stirring hexane. The resulting white powder was collected by vacuum filtration and dried under vacuum at room temperature. Addition of the white solid to solvents results in a cloudy mixture, suggesting that there is some crosslinked PGMA within this polymer product. For GPC, NMR, and all other analysis, PGMA was first dissolved, then filtered with a syringe filter (to removed crosslinked material), and then used for analysis (see Appendix A for PGMA NMR spectra).

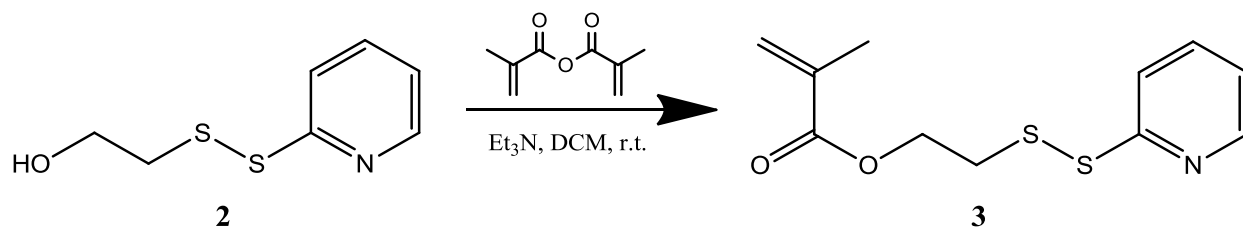
Synthesis of 2-(pyridine-2-yl)disulfanyl ethyl methacrylate (PDSEMA):



DSEMA is prepared in 2 steps using a modified procedure from that reported by Ghosh *et al.* [19].

Synthesis of 2: Aldrithiol-2, **1** (15g, 0.068mol) was dissolved in 75 mL of methanol and 1 mL of glacial acetic acid was added to it. To this mixture, a solution of mercaptoethanol (2.65g, 33.97mmol) in 15 mL methanol was added drop-wise at room temperature with continuous stirring. Once the addition was over, the reaction mixture was stirred at room temperature for additional 3 h. The stirring was stopped, solvent was evaporated to get the crude product as a yellow oil. The crude product is redissolved in dichloromethane (DCM), and silica is added. The solvent was evaporated and the remaining silica was dry-loaded into a column on extra silica. The silica was first eluted using 30% ethyl acetate/hexane mixture until all the excess aldrithiol was removed. After the removal of aldrithiol confirmed by thin layer chromatography (TLC), the polarity of the eluent was increased to 40% ethyl acetate/hexane, giving pure **2** as a yellow oil after evaporation.

^1H NMR: (500 MHz, CDCl_3), δ (ppm): 8.5 (d, 1H, aromatic proton *ortho*-N), 7.58 (m, 1H, aromatic proton *meta*-N), 7.40 (m, 1H, aromatic proton *para*-N), 7.15 (m, 1H, aromatic proton, *ortho*-disulfide linkage), 3.8 (t, 2H, -S-S- $\text{CH}_2\text{CH}_2\text{OH}$), 2.95 (t, 2H, -SS- $\text{CH}_2\text{CH}_2\text{OH}$) (see ^1H NMR spectra in Appendix A)



Synthesis of monomer 3: To a solution of compound **2** (4.62g, 24.7mmol) in 20 mL of dry DCM was added 3g (29.7mmol) of triethylamine (Et_3N) and the mixture was cooled in an ice-bath. To this cold mixture, a solution of methacrylic anhydride (3.7g, 24.0mmol) in 10 mL DCM was added drop-wise with continuous stirring. After the addition was over, the reaction mixture was stirred at room temperature for 6 h before 10mL of methanol was added to react with any excess methacrylic anhydride. The stirring was stopped and the reaction mixture washed with 3x30 mL distilled water and then with 30 mL of brine. The organic layer was collected, dried over anhydrous Mg_2SO_4 overnight, filtered and concentrated to provide pure product as a yellow oil.

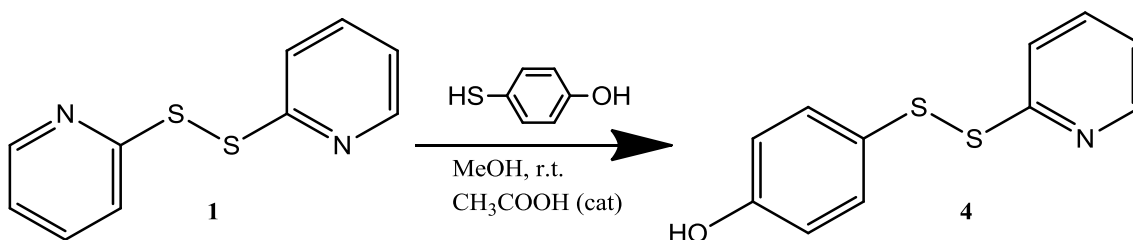
^1H NMR: (500 MHz, CDCl_3), δ (ppm): 8.46 (m, 1H, aromatic proton *ortho*-N), 7.61-7.70 (m, 2H, aromatic proton *meta*-N and *para*-N), 7.09 (m, 1H, aromatic proton, orthodisulfide linkage), 6.12 (d, 1H, vinylic proton, *cis*-ester), 5.58 (d, 1H, vinylic proton, *trans*-ester) 4.3 (t, 2H, -S-S- $\text{CH}_2\text{CH}_2\text{O-}$), 3.08 (t, 2H, -S-S- $\text{CH}_2\text{CH}_2\text{O-}$), 1.93(s, 3H, methyl proton of the methacryloyl group). (see ^1H NMR spectra in Appendix A)

Typical Polymerization Procedure for 2-(pyridine-2-yl)disulfanyl ethyl methacrylate (PDSEMA): 500mg of PDSEMA monomer **3** was dissolved in 1mL of anisole and degassed using N_2 for 15 minutes. AIBN (4.0mg, 0.024mmol) was then added to the solution, and the solution was heated to 80°C for 5 h. The reaction was open to air, and the polymer precipitated in

hexane. The product was collected by vacuum filtration, and dried under vacuum at room temperature. NMR spectra of the PPDSEMA polymer can be found in the Appendix A.

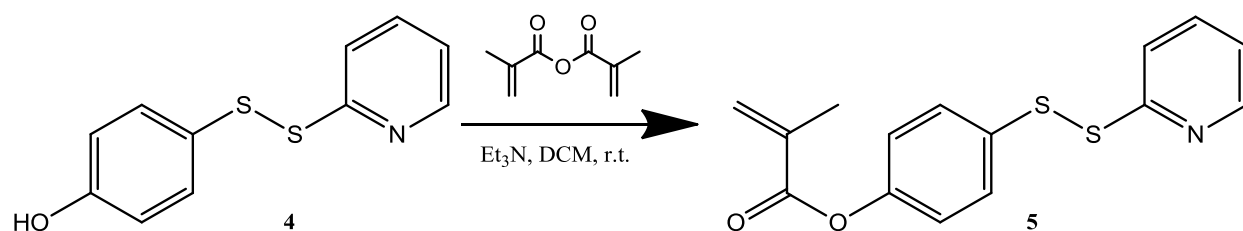
^1H NMR: (500 MHz, CDCl_3), δ (ppm): 8.44 (1H, aromatic proton *ortho*-N), 7.66 (2H, aromatic proton *meta*-N and *para*-N), 7.09 (1H, aromatic proton, orthodisulfide linkage), 4.21 (2H, -S-S-CH₂CH₂O-), 3.01 (2H, -S-S-CH₂CH₂O-)

Synthesis of 4-(pyridine-2-ylidisulfanyl) phenyl methacrylate (PPDSPMA):



Synthesis of 4: Aldrithiol-2, **1** (20.0g, 90.8mmol) was dissolved in 100 mL of methanol and 1.5mL of glacial acetic acid was added. To this mixture, a solution of 4-mercaptophenol (5.0g, 39.6mmol) in 20 mL methanol was added drop-wise at room temperature with continuous stirring. Once the addition was over, the reaction mixture was stirred at room temperature for additional 3 h. The stirring was stopped, and the solvent evaporated to give the crude product as yellow solid powder. ^1H NMR confirmed that the crude product was a mixture of **4** and **1**. This mixture was used without further purification.

4: ^1H NMR: (500 MHz, CDCl_3), δ (ppm): 8.47 (d, 1H, aromatic proton *ortho*-N), 7.77 (m, 1H, aromatic proton *para*-N), 7.68 (dt, 1H, aromatic proton, *ortho*-disulfide linkage), 7.34 (d, 1H, aromatic proton *meta*-N), 7.41 (dt, 2H, aromatic proton, *ortho*-disulfide linkage), 6.75 (dt, 2H, aromatic proton, *ortho*-OH) (see ^1H NMR spectra in Appendix A)



Synthesis of monomer 5: To a solution of compound **4** (including residual of **1**) (10g) in 20 mL of dry DCM was added 5mL (35.9mmol) of triethylamine (Et_3N) and the mixture was cooled in an ice-bath. To this mixture, a solution of methacrylic anhydride (3.7g, 24.0mmol) in 10 mL DCM was added drop-wise with continuous stirring. The reaction mixture was stirred at room temperature for 6 h before 10mL of methanol was added to react with excess methacrylic anhydride. The stirring was stopped and the reaction mixture washed with 3x30 mL distilled water and then with 30 mL of brine. The organic layer was collected, dried over anhydrous Mg_2SO_4 and concentrated to get the crude product as yellowish brown oil. The crude product was loaded onto a 600mL fritted filtration funnel with silica. The silica was first eluted using 10% ethyl acetate/hexane mixture until all the excess aldrithiol was removed (confirmed by TLC). After this, the polarity of the eluent was increased to 30% ethyl acetate/hexane, giving pure **5** as a pale yellow waxy solid after evaporation.

^1H NMR: (500 MHz, CDCl_3), δ (ppm): 8.47 (m, 1H, aromatic proton *ortho*-N), 7.66-7.61 (m, 2H, aromatic proton *meta*-N and *para*-N), 7.12-7.09 (m, 1H, aromatic proton, *para*-disulfide linkage), 7.55 (dt, 2H, aromatic proton, *ortho* disulfide linkage), 7.07 (dt, 2H aromatic proton, *ortho* ester bond), 6.32 (1H, vinylic proton, *cis*-ester), 5.75 (1H, vinylic proton, *trans*-ester), 2.04 (s, 3H, methyl proton of the methacryloyl group). (see ^1H NMR spectra in Appendix A)

^{13}C NMR (126 MHz, CDCl_3) δ (ppm) 165.85, 159.62, 150.57, 149.86, 137.55, 135.85, 133.49, 129.72, 129.04, 127.81, 122.66, 122.63, 121.23, 119.90, 77.51, 77.46, 77.25, 77.00, 53.66, 18.59. (see ^{13}C NMR spectra in Appendix A)

Typical Polymerization Procedure for 4-(pyridine-2-yl)disulfanyl phenyl methacrylate (PDSPMA): PDSPMA (900mg, 2.97mmol) was dissolved in 2mL toluene and 2mL of chloroform, and degassed using N_2 for 15 minutes. AIBN (3mg, 0.018mmol) was then added to the solution, and was heated to 70°C and left to polymerize overnight. The reaction was open to air, and the polymer precipitated in hexane, resulting in a white precipitate. The polymer was collected by vacuum filtration. In order to increase the yield, the cloudy filtrate was centrifuged at 4500rpm for 5 min. Polymer was collected at the bottom of the centrifuge tube. (see ^1H NMR spectra in Appendix A)

6.2.2 Characterization Methods

Nuclear Magnetic Resonance: ^1H and ^{13}C NMR spectra were obtained using a Varian 500 MHz spectrometer in the VOICE NMR laboratory at the University of Illinois; the residual solvent protons were used to reference the chemical shift [21]. Coupling constants (J) are reported in Hertz (Hz), and splitting patterns are designated as s (singlet), d (doublet), t (triplet), q (quartet), dd (double doublet), dt (double triplet), m (multiplet), and br (broad).

Raman Spectroscopy: Confocal Raman spectroscopy was done using a high-resolution research-grade Horiba Lab RAM using a 633 nm laser for irradiation.

6.3 Poly(2-(pyridine-2-yl)disulfanyl) ethyl methacrylate (PPDSEMA)

6.3.1 Polymerization of PPDSEMA

PPDSEMA was first polymerized by ATRP, following the procedure reported by Ghosh *et al.* [19], but little to no polymer was recovered. Solvent from the polymerization solution was removed, and the remaining compound was confirmed to be monomer. Due to the low quantity of available monomer, further attempts to polymerize PPDSEMA by ATRP were abandoned, and free radical polymerization in solution by AIBN was attempted instead. Free radical polymerization of AIBN still resulted in fairly low yields, but solid polymer was collected, and ^1H NMR confirmed that the polymer was indeed PPDSEMA.

6.3.2 Reducing Agents for PPDSEMA

Dithiothreitol (DTT) is a strong reducing agent, due to its ability to form a stable six-membered ring with an internal disulfide bond after it has been oxidized [22]. To test the efficiency of DTT as a reducing agent in this system, compound **2** was reacted with DTT (5 times excess) in solution. ^1H NMR collected an hour later (Figure 6.2) shows clear cleavage of the disulfide bond by disappearance of the pyridine protons.

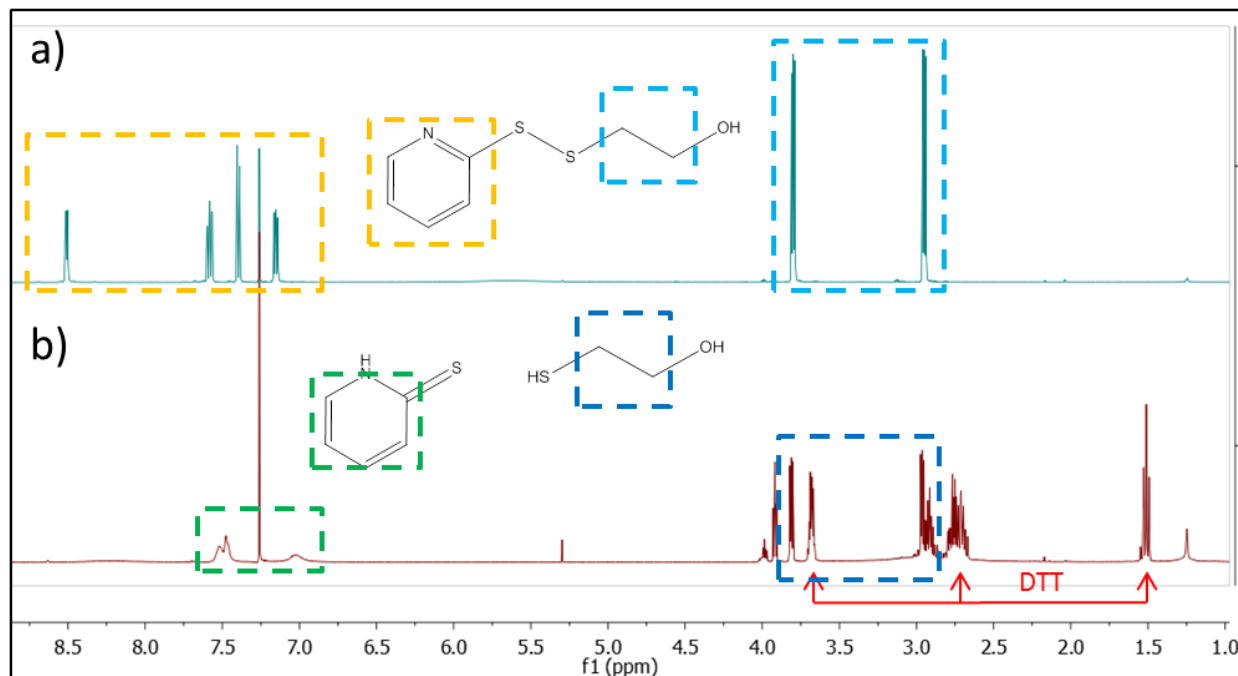


Figure 6.2 – ^1H NMR in CDCl_3 of a) compound **2** and b) compound **2** after reduction with DTT reducing agent.

6.3.3 Catalyzed Ring Opening of PGMA

GMA monomer or PGMA was combined with mercaptoethanol (ME) in an NMR tube to test the reaction between an aliphatic thiol (similar to the one produced after disulfide reduction) and epoxide side chain. ^1H NMR in CDCl_3 after mixing showed no changes for the GMA or PGMA, indicating no chemical reaction. The mixture was heated at 40°C for 2 h and then overnight, and also at 60°C for 2 h, and still no evidence for ring opening was observed. The neat mixture left for over 1 week still showed no significant change, which indicated that a catalyst may be required for this reaction.

Throughout literature, tertiary amines are common catalyst in the ring opening of epoxides [23,12]. The PGMA polymer was mixed with catalytic quantities of triethylamine (TEA), dimethylaniline (DMA), or 1,4-diazabicyclo[2.2.2]octane (DABCO), and each was combined with ME in NMR tubes. ^1H NMR indicated no reaction in these cases at room temperature. The

NMR tubes were then heated at 60°C for a few hours, and still ^1H NMR spectra showed no reaction between the thiol and epoxide side chain, even after left to react for over 1 week, no significant ring opening was observed. As an alternative to the tertiary amines, (bromodimethyl)sulfonium bromide (BDSB), reported as a mild, rapid and highly regioselective catalyst for epoxide ring opening by mercaptans was investigated [24]. The addition of the BDSB catalyst to GMA monomer and ME did show evidence of reactivity and ring opening of the epoxide group. In Figure 6.3 the appearance of new peaks suggest that the BDSB is able to catalyze the ring opening of the epoxy side chain by the aliphatic thiol.

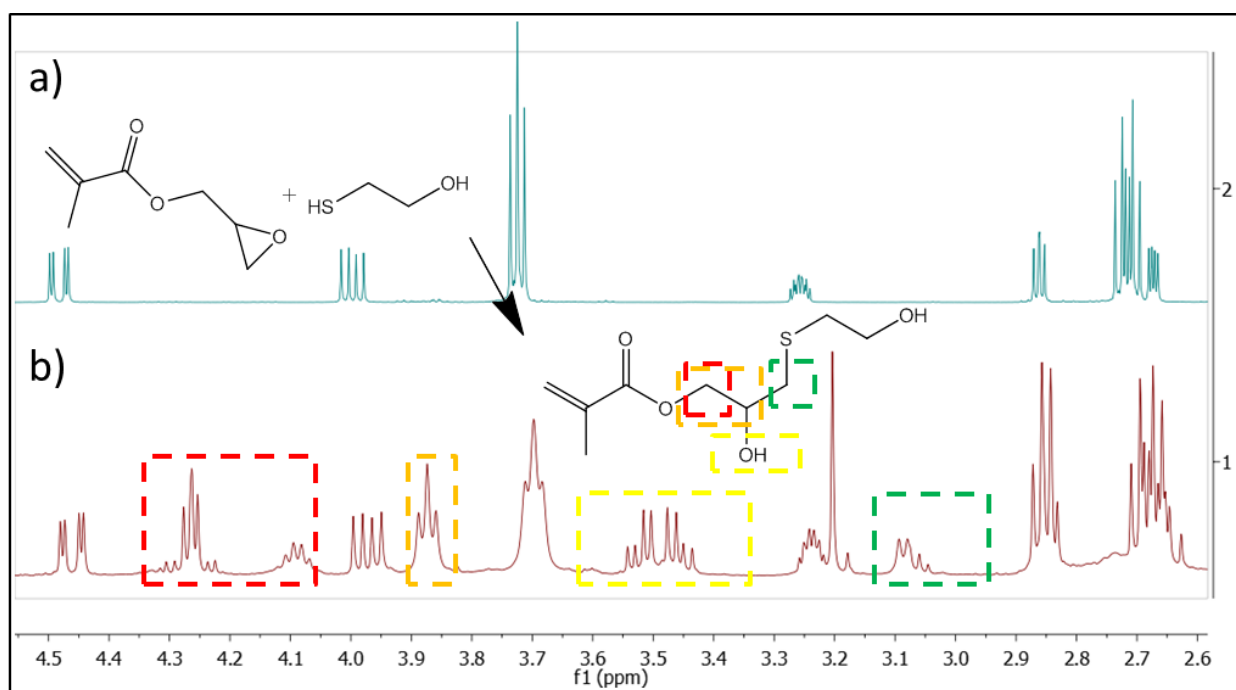


Figure 6.3 – ^1H NMR in CDCl_3 of a) GMA monomer and ME and b) GMA monomer and ME with BDSB catalysts, appearance of new peaks at δ 4.25, 3.88, 3.5, and 3.1 ppm suggest successful ring opening of epoxide side chain of GMA monomer.

Next, PGMA was mixed with BDSB catalyst and ME in solution of CDCl_3 . Immediately after mixing, a white solid precipitated. ^1H NMR of the solution including the white precipitate

showed no PGMA peaks, suggesting that the white precipitate is crosslinked PGMA. ME is a monofunctional thiol, and should not cause PGMA crosslinking, suggesting that BDSB is acting as a Lewis acid and catalyzing the self-crosslinking reactions of epoxides with neighboring epoxide side chains. Therefore, while the BDSB is a better catalyst for ring opening compared to basic catalyst like tertiary amines, it causes crosslinking side reactions and cannot be used for this study. In the next section, the use of an aromatic thiol will be explored as a more reactive alternative to the aliphatic mercaptan, and less reactive tertiary amine catalysts will again be screened as possible catalysts.

6.3.4 Tertiary Amine Catalyst and Thiophenol

The lack of reactivity between the ME and PGMA in the presence of tertiary amine catalysts was unexpected, since tertiary amines have been commonly reported as catalyst for ring opening epoxides. To further investigate the lack of reactivity, thiophenol was mixed with the PGMA, since aromatic thiols are known to be more reactive. Thiophenol with catalytic quantities of TEA, DMA, and DABCO were combined with PGMA in CDCl_3 and reacted in a NMR tube. In Figure 6.4, the ^1H NMRs of the three catalysts mixed with thiophenol (TP) and PGMA, as well as the NMR of PGMA for comparison (Figure 6.4d) are presented. From the ^1H NMR spectra we can see that after 1 day at room temperature, DABCO proved to be the most active catalyst (Figure 6.4a), showing complete disappearance of PGMA peaks at δ 4.30, 3.81, 3.23, 2.84, and 2.64 ppm. The DMA catalyst (Figure 6.4c), shows partial conversion to the ring opened product; and finally for the TEA catalyst no ring opening of the epoxide group is observed, and all five PGMA peaks are still present. This study demonstrates that thiophenol is indeed capable of ring opening reactions with epoxides, and that DABCO is an efficient amine catalyst for this reaction.

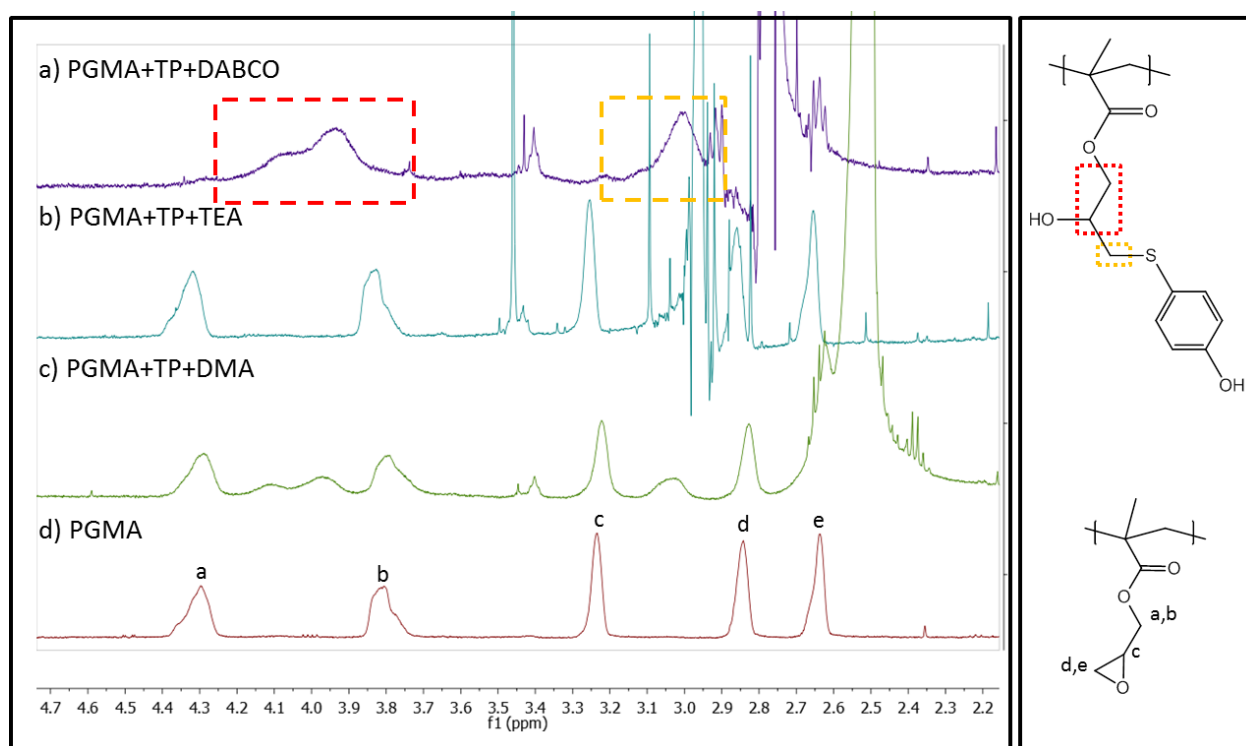


Figure 6.4 – ¹H NMR in CDCl₃ of PGMA polymer mixed with thiolphenol (TP) and amine catalyst a) 1,4-diazabicyclo[2.2.2]octane (DABCO) b) triethylamine (TEA) and c) dimethylaniline (DMA) after 1 day at room temperature. d) ¹H NMR in CDCl₃ of PGMA homopolymer.

6.4 Poly(4-(pyridine-2-yl)disulfanyl) phenyl methacrylate) (PPDSPMA)

6.4.1 Reduction of PPDSPMA with DTT

Data from *section 6.3.3* demonstrated that thiophenol in the presence of an amine catalyst like DABCO can ring open and react with the epoxide side chain of PGMA. This inspired the design and synthesis of a new disulfide monomer which can be reduced to unmask an aromatic thiol side chain (Figure 6.5).

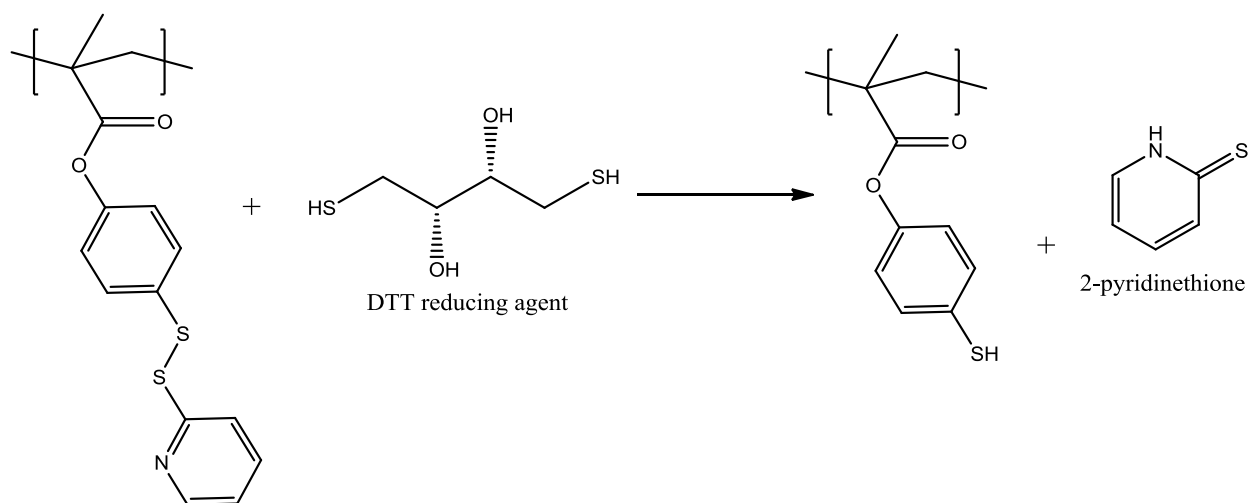


Figure 6.5 – Chemical structure of poly(4-(pyridine-2-yl)disulfanyl) phenyl methacrylate (PPDSPMA) and the proposed reduction by DTT to form the poly(thiophenol) (PTP) side chained polymer and 2-pyridinethione byproduct.

Polymerization of the PDSPMA monomer was first attempted using single-electron-transfer living-radical polymerization (SET-LRP), but similar to the unsuccessful attempts using ATRP, only monomer was recovered at the end of the reaction. Therefore, polymerization of PDSPMA was initiated using AIBN, in solution. The reaction yield was still low (yield < 10%).

PPDSPMA polymer was dissolved in CDCl_3 and mixed with DTT reducing agent to confirm that the disulfide bond could be reduced, producing aromatic thiols side chains and 2-pyridinethione. When mixed, the solution immediately turned yellow, as typically observed from the release of 2-pyridinethione which has an absorbance (λ_{max}) at 375 nm [19]. After 10-15 minutes, white insoluble solid precipitated from the solution, as seen in Figure 6.6. When the ^1H NMR of this mixture was taken, it was clear that the disulfide bond had been reduced, confirmed by the disappearance of the peaks at δ 8.47, 7.61, and 7.10 ppm from the pyridine side chain functionality (Figure 6.7b). However, the peaks for protons of the thiol functionality had also disappeared. In addition, the proton peaks at δ 1.0-2.5 ppm corresponding to the acrylate polymer backbone were also not present. This suggests that the exposed thiols may be

immediately oxidized, forming disulfide crosslinks with neighboring thiols and forming the white precipitate observed.

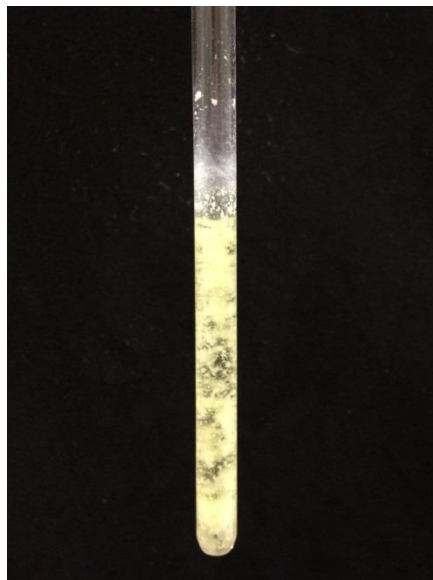


Figure 6.6 – NMR tube containing PPDSPMA mixed with DTT reducing agent in CDCl_3 displaying yellow coloration from disulfide reduction, release of 2-pyridinethione, and white precipitate.

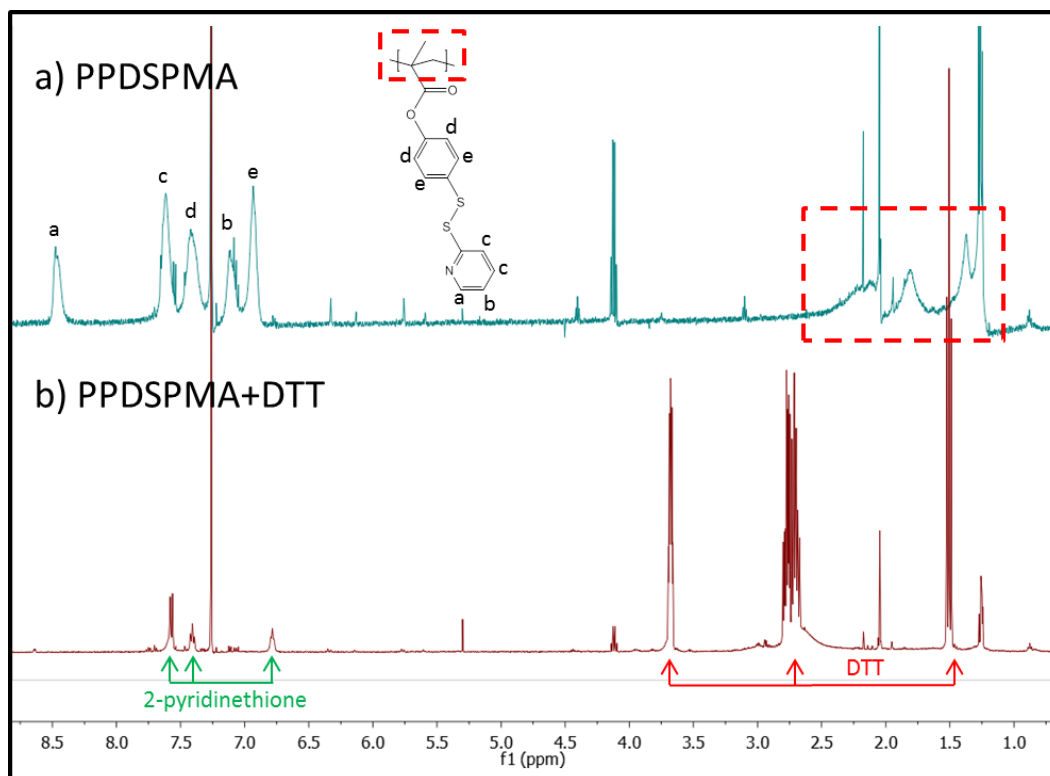


Figure 6.7 – a) ^1H NMR spectra of PPDSPMA b) PPDSPMA reacted with DTT reducing agent showing disappearance of pyridine peak from δ 7.10-8.47 ppm, but also the disappearance of the polymer backbone protons from δ 1.25-2.5 ppm.

6.4.2 Reduction of PPDSPMA with DTT in a Glove Box

To test the hypothesis that the white precipitate was reduced PPDSPMA which had been crosslinked due to immediate oxidation, and to demonstrate that this disulfide to thiol and PGMA chemistry is feasible for contact mechanochemistry, several reactions were conducted in an oxygen free environment. First, PPDSPMA was dissolved in both CD_2Cl_2 and deuterated tetrahydrofuran (THF), and DTT reducing agent was added at five times excess. Within 5 minutes the two solutions turned yellow, but in the CD_2Cl_2 solution a white solid precipitated, just as it had done previously in experiments conducted in air (Figure 6.8a). In the THF, no precipitate was observed, but there was a very small fraction of insoluble polymer, which can be seen at the bottom of the NMR tube (Figure 6.8b). The precipitation from the CD_2Cl_2 solution

implies that oxidation was not have been the cause of precipitation, since the reaction was now carried out in an oxygen free environment and the precipitation still occurs. An alternative explanation is that the PPDSPMA polymer is soluble in chlorinated solvents, such as chloroform and DCM, but after the disulfide reduction, the formed poly(thiophenol) (PTP) is insoluble and therefore precipitates out. We observed that PPDSPMA is mostly insoluble in THF, but after addition of the reducing DTT, the insoluble polymer, now reduced, is soluble, suggesting this theory to be correct. This THF solution will therefore be used for further experiments.

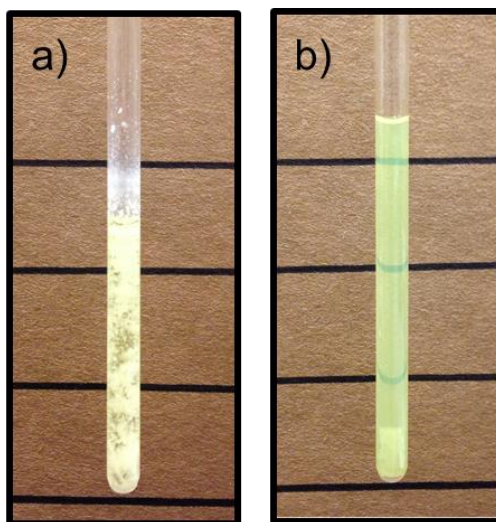


Figure 6.8 – PPDSPMA and DTT reducing agent in a) CD_2Cl_2 displaying white precipitate after about 5 minutes of mixing and b) in deuterated THF displaying solubility after reduction of the disulfide group.

^1H NMR was collected for both the disulfide reduction reaction in CD_2Cl_2 and THF (Figure 6.9b and 6.9d). Similar to the conclusions drawn in *section 6.4.1* (Figure 6.7), it appears that the white precipitate is the thiophenol polymer product (PTP), which is not soluble in CD_2Cl_2 . This is confirmed by the observation of only 2-pyridinethione byproduct peaks in the aromatic region (Figure 6.9a and 6.9b). The spectra for the reduced PPDSPMA in THF seen in Figure 6.9d shows broad peaks, suggesting that the polymer product is soluble, and in addition the peaks are

different than the PPDSPMA peaks (Figure 6.9c) demonstrating the reduction to PTP. The broad peaks centered around δ 7.6 and 7.1 ppm are likely from the aromatic thiol protons, confirming the disulfide reduction of the PPDSPMA by DTT reducing agent.

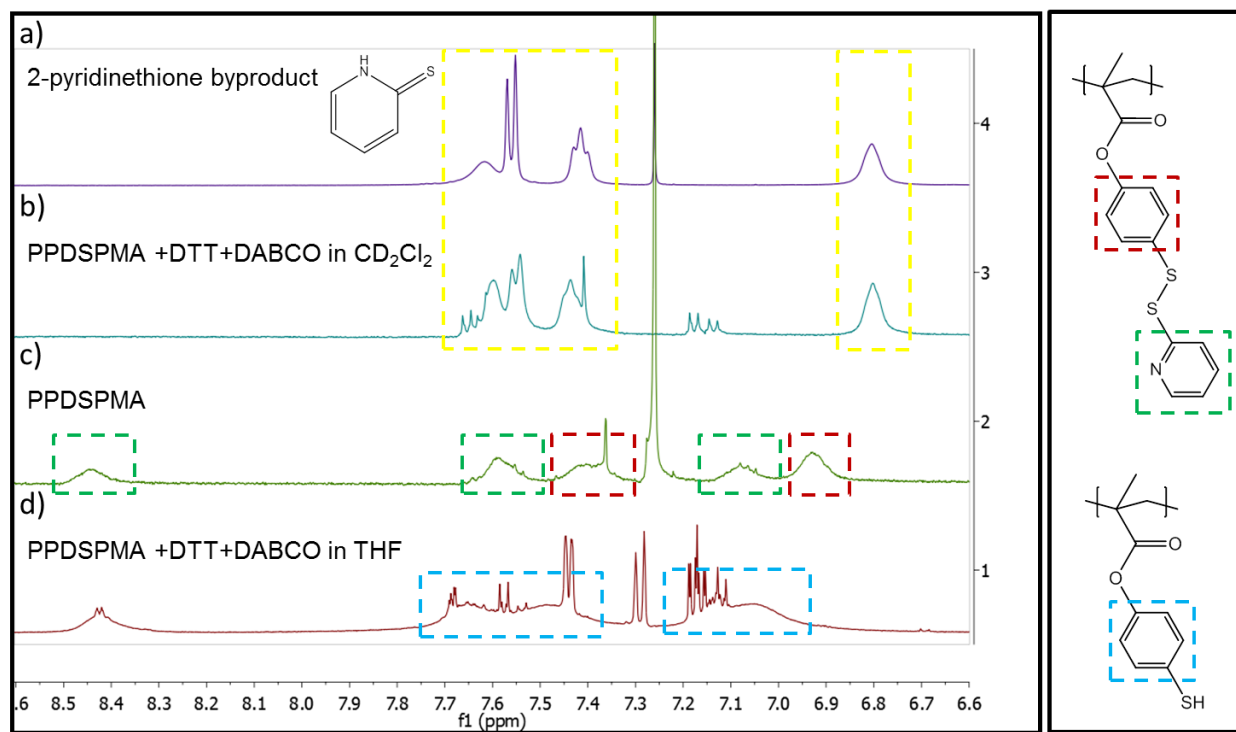


Figure 6.9 – ^1H NMR spectra of a) 2-pyridinethione byproduct b) PPDSPMA reacted with DTT and DABCO in CD_2Cl_2 , displaying 2-pyridinethione byproduct peaks, but no polymer peaks c) spectra of PPDSPMA d) PPDSPMA reacted with DTT and DABCO in THF, displaying broad polymer peaks at δ 7.4-7.7 ppm, and δ 6.9-7.2 ppm attributed to the aromatic peaks of the PTP product.

6.4.3 Ring Opening of PGMA Epoxide by Reduced PPDSPMA

After confirmation that the disulfide in PPDSPMA could be reduced by DTT, the actual reactivity of the two polymers (PPDSPMA and PGMA) was investigated. In a glove box, PPDSPMA (25mg) with DTT (50mg) and DABCO (7mg) were dissolved in THF (1mL). Initially, the solution was not soluble, but as the disulfide was reduced (5-10 minutes), the solution became a yellow clear solution. This solution was filtered and then mixed with a

solution of filtered PGMA (25mg) in THF (1mL). When mixed together, the polymer solution remained clear, but after 24 hours at room temperature the polymer solution had gelled, indicating the formation of a crosslinked polymer, which could be the result of the epoxy side chain of the PGMA undergoing ring opening reactions with the thiol side chains of the reduced PPDSPMA. (Figure 6.10)

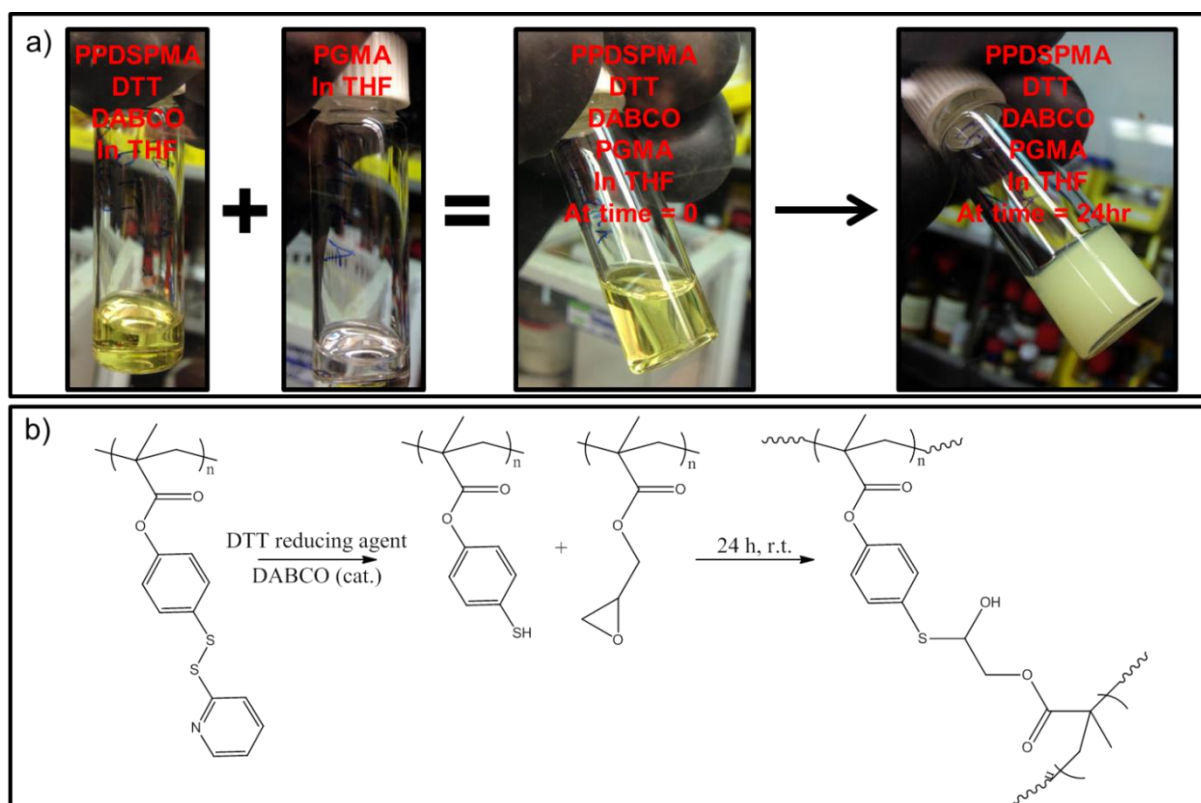


Figure 6.10 – a) Images of the reaction of PPDSPMA and PGMA with DTT reducing agent and DABCO base catalyst in THF solvent. When first mixed, the mixture is a clear yellow solution, after 24 hours in the glove box the solution transforms to a solidified gel. b) Chemical schematic of the reduction of PPDSPMA and the reaction of PTP and PGMA, resulting in the gelled solid.

Two control experiments were conducted to confirm that the gelled polymer was a reaction between PPDSPMA and PGMA rather than just a crosslinking reaction with one of the individual polymers. In Control 1, 2,2'-dipyridyldisulfide (12mg) was mixed with DTT (50mg), DABCO (7mg), and PGMA (25mg) in 1mL of THF to confirm that the gelling seen in Figure

6.10 was not due to self-crosslinking of the PGMA. The 2,2'-dipyridyldisulfide was added to produce similar amounts of the 2-pyridinethione byproduct. This was added to ensure that the byproduct is inert and not a source of reactivity. In Control 2, PPDSPMA (12mg) was mixed with DTT (25mg), DABCO (3.5mg) in 0.5mL of THF, to confirm that gelling did not occur from the self-crosslinking of the reduced PPDSPMA. Control 2 was conducted in the glove box, to accurately mimic the conditions used for the PPDSPMA-PGMA reaction. As seen in Figure 6.11, both controls were still polymer solutions after 24 h. There was a small quantity of solid at the bottom of Control 1 (PGMA), but the amount was small when compared to the complete gelation of PPDSPMA and PGMA solution, and is probably due to minor thermal self-crosslinking of the PGMA.

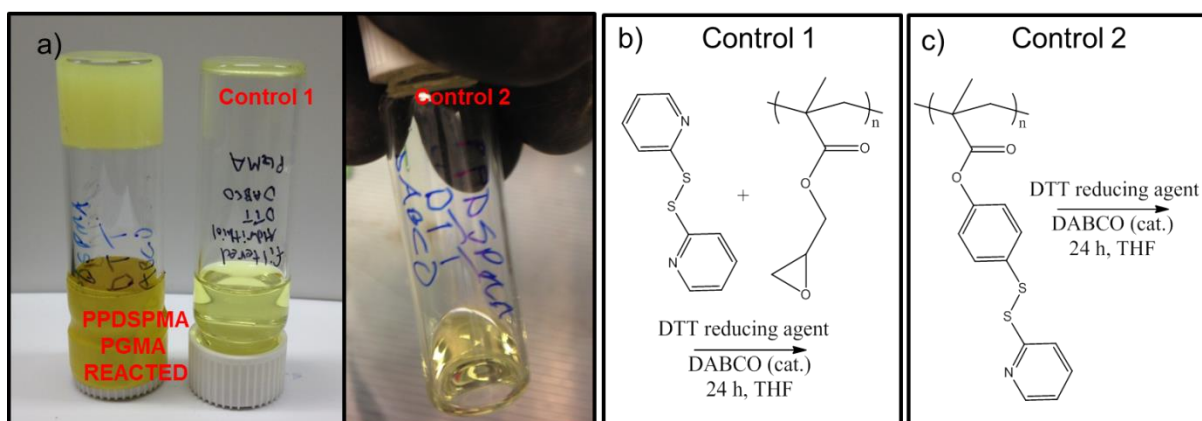


Figure 6.11 – a) Images of Control 1 (2,2'-dipyridyldisulfide, DDT, DABCO and PGMA in THF) and Control 2 (PPDSPMA, DDT, and DABCO in THF), still a polymer solution after 24 h, compared to the PPDSPMA and PGMA gelled reacted mixture. b) Chemical schematic of Control 1 c) Chemical schematic of Control 2.

Raman spectroscopy was conducted to confirm the reduction of the PPDSPMA and the ring opening of PGMA. First, the reacted PPDSPMA+PGMA gel was washed and filtered with DCM to remove excess DTT and DABCO and the 2-pyridinethione byproduct. The initially yellow gel

after rinsing became a white gel. The swollen white gel was then dried under vacuum until all the solvent had been removed resulting in a yellowish brown solid (≈ 30 mg).

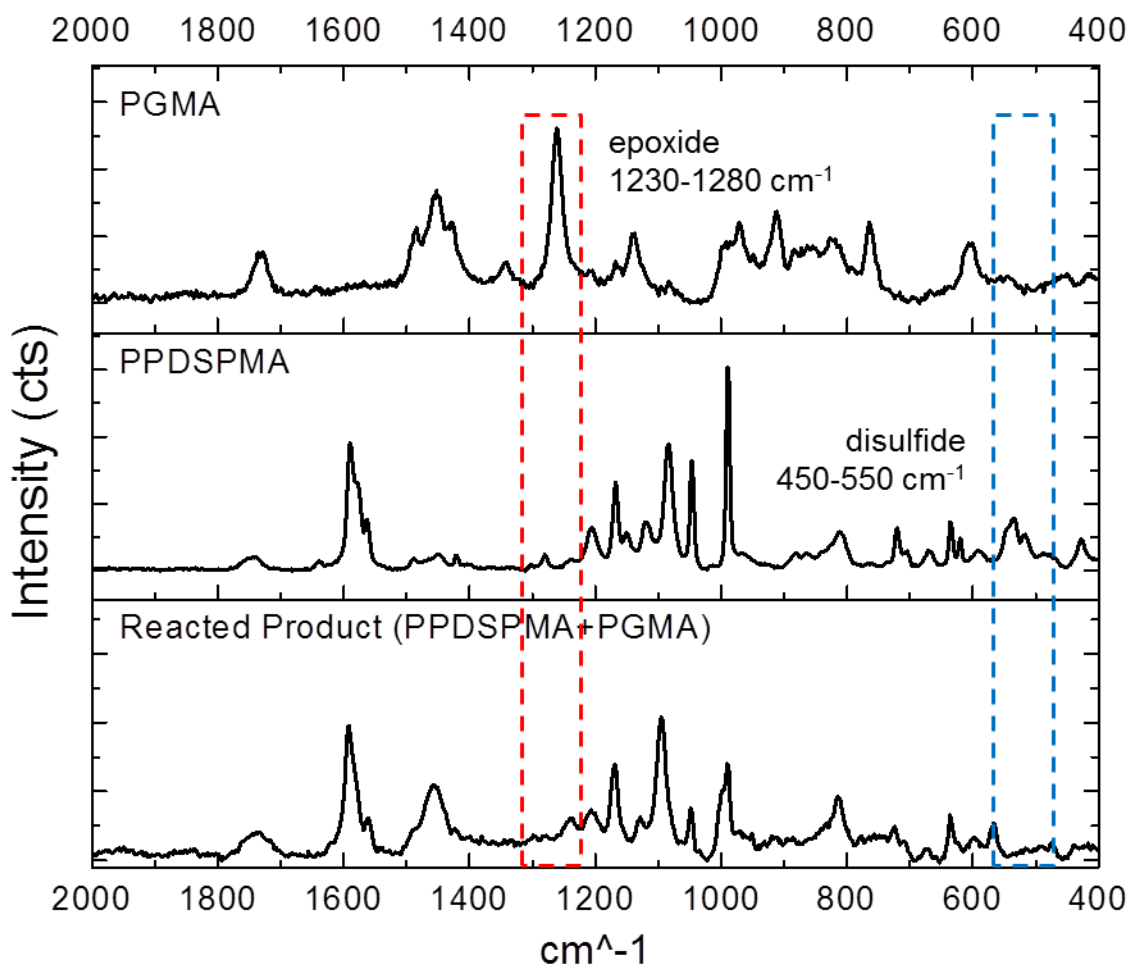


Figure 6.12 – Raman spectra of PGMA, PPDSPMA, and the Reacted Product (PPDSPMA+PGMA) demonstrating the disappearance of the epoxide peak (≈ 1260 cm^{-1}) from PGMA and the disulfide peak ($450\text{--}550$ cm^{-1}) from PPDSPMA, both not present in the Reacted Product spectra.

Raman spectroscopy was collected for PPDSPMA, PGMA, and the “Reacted Product” (Figure 6.12). Raman bands for the epoxide vibration range from $1230\text{--}1280$ cm^{-1} [25], which match well with the strong peak in the PGMA Raman spectra seen at 1260 cm^{-1} . There are no clear

characteristic peaks in this range for the PPDSPMA, therefore the disappearance of the epoxide peak in the “Reacted Product” of PPDSPMA+PGMA is evidence that the epoxide ring was opened. The disulfide vibration normally ranges from 450-550 cm^{-1} [26]. In the PPDSPMA spectra, there are peaks in this range, likely attributed to the disulfide bond. When compared to the “Reacted Products” spectra, peaks in the 450-550 cm^{-1} are no longer present, demonstrating that the disulfide bond was indeed reduced by the DTT, and also providing further evidence that the thiol functionality, a product of the disulfide reduction in PPDSPMA, was present and likely reacted with the PGMA epoxide side chain, resulting in the gelled polymer. In addition, the “Reacted Products” spectra contain peaks from both polymers, providing further evidence that the cause of gelation was not crosslinking from an individual polymer’s side chain, but rather from a reaction between the PGMA and the PPDSPMA after disulfide reduction.

6.5 Phase Separation of PPDSPMA and PGMA Polymer Blends

The key to the contact block copolymer mechanochemistry is the innate phase separation of block copolymers and polymer blends. For this particular chemistry to work in the solid state phase separation of PPDSPMA and PGMA is required in order to isolate the two different functionalities of the thiol and epoxide. To test this, a 50:50 wt% solution of PPDSPMA and PGMA was prepared in DCM, and solution casted onto a glass slide. The glass slide was covered with a petri dish, to ensure even evaporation of the solvent. Once the solvent had evaporated there was a hazy film where the polymer had been casted. When the solvent casted film was viewed at 10x magnification, a clear phase separated pattern was observed (Figure 6.13a). A second polymer film was solvent casted from a 25:75 wt% solution of PPDSPMA to PGMA in DCM as seen in Figure 6.13b. The image was taken at 50x magnification, and the darker

domains are on the order of 2-5 μm , much smaller than the 10-50 μm domains seen in the 50:50 polymer blend.

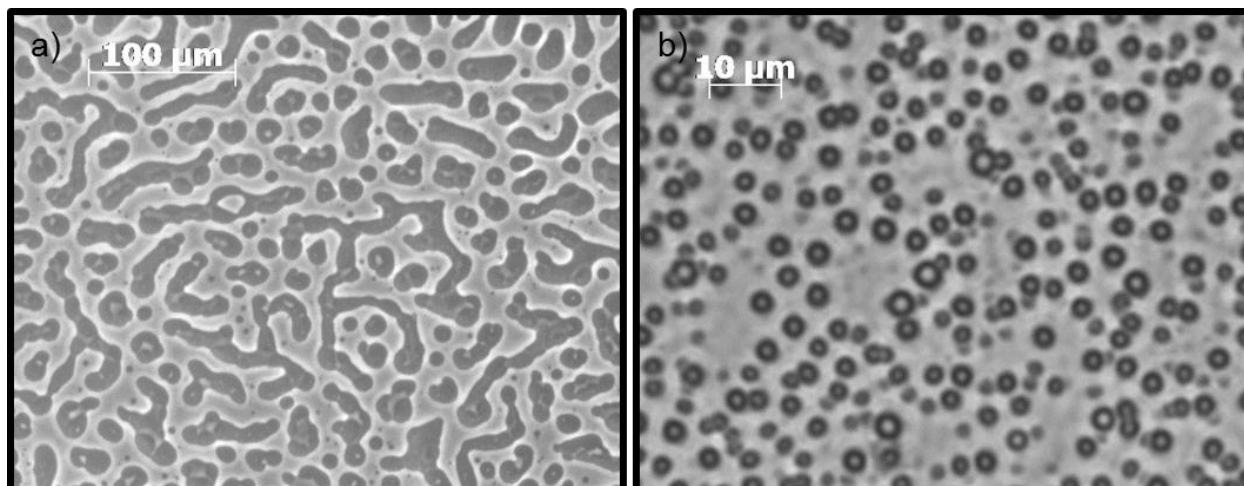


Figure 6.13 – Optical images of solvent (DCM) casted films of a) 50:50 PPDSPMA to PGMA polymer blend at 10x magnification and b) 25:75 PPDSPMA to PGMA polymer blend taken at 50x magnification.

Using Image J analysis software, the darker domains were calculated to be 0.52 area fraction for Figure 6.13a and 0.34 area fraction for Figure 6.13b, matching well with the actual ratio of the polymer blends. Comparing the two ratios of polymer blends, it can be concluded that the darker regions correspond to the PPDSPMA and the lighter regions to the PGMA.

6.6 Future Work

The work laid out in this chapter has demonstrated that the reaction between PGMA and PPDSPMA is indeed feasible. This now allows for the engineering of this chemistry into a solid state polymer system. The next steps will be to demonstrate these chemical reactions in the solid state. As a solid state mechanochemical system there are a number of challenges that must be addressed. First, the ring opening reaction requires a catalyst, how will the catalyst be

incorporated into the polymer blend? One proposed solution is to create the polymer blend in solution. The PGMA and PPDSPMA could be dissolved in a solvent along with the DABCO catalyst. When the solvent is removed or polymer is solvent casted, the resulting phase separated polymer blend would have DABCO catalyst distributed within the entire blend, available to catalyze the epoxide ring opening reaction.

The next challenge lies in the reduction and unmasking of the thiol, while preserving the phase separation of the polymer blend. One proposed method is to reduce the disulfide phase by swelling the polymer blend in a solvent which does not dissolve either polymer, but does dissolve DTT. From preliminary experiments, the reduction of disulfides using DTT, is very effective even in the solid state. In Figure 6.14, 2,2'-dipyridyldisulfide, DABCO catalyst, and DTT reducing agent, all initially white solids were placed into a vile. Almost immediately, the 2,2'-dipyridyldisulfide turned yellow, representing the reduction of the disulfide into colored 2-pyridinethione. This result, suggest that the swollen polymer blend, in contact with dissolved DTT should easily reduce the PPDSPMA domains. After reduction with DTT, the solvent can be removed, likely also removing the 2-pyridinethione byproduct and excess DTT, leaving behind a phase separate polymer blend of PGMA and PTP.

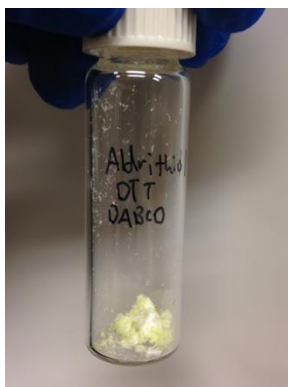


Figure 6.14 – 2,2'-dipyridyldisulfide, DABCO catalyst, and DTT reducing agent, initially all white solids, shows immediate yellowing when combined in a vile, representing the reduction of the 2,2'-dipyridyldisulfide to colored 2-pyridinethione even in the solid state.

A number of mechanical testing techniques are available to induce the mechanical mixing as well as characterize the mechanical properties of polymer systems. As a proof of concept, the grinding of the polymer blend by mortar and pestle may be an effective method to break the phase separation and bring in contact the PGMA and PTP. The polymer solution experiment described in *section 6.4.3* demonstrated that confocal Raman spectroscopy of the polymer powders was an effective method of characterization for this mechanochemical system. Therefore, Raman spectra of the polymer blend before and after grinding could be compared, and the disappearance of characteristic peaks, such as the epoxide peak, 1230-1280 cm^{-1} [25], and disulfide peak, 450-550 cm^{-1} [26], could be used to confirm the crosslinking of the polymer blend. Control experiments, involving the grinding of the polymer blend with no disulfide reduction and with no grinding should also be conducted as well.

6.7 Conclusions

In this chapter the ring opening of epoxides with thiols was investigated as a potential chemistry for contact mechanochemistry. The epoxide functionality was present as a side chain in poly(glycidyl methacrylate) (PGMA), selected as one of the reactive phases for the polymer blend. The second phase was a methacrylate polymer with a disulfide side chain. 2-(pyridine-2-yl)disulfanyl ethyl methacrylate (PDSEMA) monomer, was successfully synthesized, and polymerized to PPDSEMA. Moreover, it was confirmed that the disulfide bond could be readily reduced by the common reducing agent DTT, but the ring opening of the PGMA by mixing mercaptoethanol (ME) (to mimic the reduced thiol from PPDSEMA) with PGMA showed no reactivity. The mixtures of ME and PGMA were heated, left to react for up to a week, and also mixed with a number of common tertiary amine catalyst, but no evidence of the ring opening of the epoxide side chain of PGMA was observed. It was concluded that the reactivity of the

aliphatic thiol was not high enough, and therefore the ring opening of the epoxy side chain with thiophenol was explored. Thiophenol was mixed with PGMA in the presence of catalytic quantities of DABCO, and ring opening of the epoxide side chain was confirmed using ^1H NMR. This inspired the design of a new monomer, which exposes a more reactive aromatic thiol when reduced. The new monomer, 4-(pyridine-2-ylidisulfanyl) phenyl methacrylate (PDSPMA), was successfully synthesized and polymerized to PPDSPMA. It was confirmed that PPDSPMA could also be reduced by DTT to produce poly(thiophenol) (PTP), but when reduced in chlorinated solvents such as chloroform or DCM resulted in precipitation of the poly(thiophenol) (PTP), due to its insolubility in these solvents, and not due to oxidation.

A polymer solution experiment demonstrating the reduction of the disulfide polymer and the reactivity of the unmasked thiol with PGMA was conducted. A solution of PPDSPMA, DTT, and DABCO catalyst, were mixed in THF, resulting in the PTP polymer. The PTP polymer solution was then mixed with polymer solution of PGMA in THF, and after 24 h solidified into a gel. Control experiments confirmed that the gelation was not due to self-crosslinking reaction of either homopolymer. Raman spectroscopy revealed the disappearance of the epoxide and the disulfide peaks in the final gel, providing further evidence of the ring opening of the PGMA epoxide side chain by PTP. In addition, solution casted films of PPDSPMA-PGMA polymer blends confirmed that the blend was indeed phase separated, making this system yet a stronger candidate for contact mechanochemistry.

The feasibility of this thiol – epoxy chemistry presented in this chapter has laid out a foundation for the demonstration of contact mechanochemistry using a PGMA and PPDSPMA polymer blend system. The next steps in this research will be to confirm the solid state reactivity of this chemistry, and then to engineer this chemistry into a polymer mechanochemical system,

which reacts to force, by the mixing of reactive polymer phase in the solid state. The force induced phase break up will bring in contact the isolated (phase separated) PGMA and PTP reactive domains, resulting in the crosslinking of the polymer blend phases, leaving a final material, with fundamentally different properties from PGMA or PTP, demonstrating the ability to drastically alter the polymer properties of a polymer blend by force.

REFERENCES

- [1] F.S. Bates, G.H. Fredrickson, Block Copolymers—Designer Soft Materials, *Phys. Today*. 52 (1999) 32.
- [2] L.M. Robeson, Polymer blends: a comprehensive review, Hanser [u.a.], Munich, 2007.
- [3] J.F. Beecher, L. Marker, R.D. Bradford, S.L. Aggarwal, Morphology and mechanical behavior of block polymers, *J. Polym. Sci. Part C Polym. Symp.* 26 (2007) 117–134.
- [4] B.S. Pinheiro, K.I. Winey, Mixed Parallel–Perpendicular Morphologies in Diblock Copolymer Systems Correlated to the Linear Viscoelastic Properties of the Parallel and Perpendicular Morphologies, *Macromolecules*. 31 (1998) 4447–4456.
- [5] D. Wang, K. Nakajima, S. Fujinami, Y. Shibasaki, J.-Q. Wang, T. Nishi, Characterization of morphology and mechanical properties of block copolymers using atomic force microscopy: Effects of processing conditions, *Polymer*. 53 (2012) 1960–1965.
- [6] Z.-R. Chen, A.M. Issaian, J.A. Kornfield, S.D. Smith, J.T. Grothaus, M.M. Satkowski, Dynamics of Shear-Induced Alignment of a Lamellar Diblock: A Rheo-optical, Electron Microscopy, and X-ray Scattering Study, *Macromolecules*. 30 (1997) 7096–7114.
- [7] F.A. Morrison, H.H. Winter, W. Gronski, J.D. Barnes, Effect of unidirectional shear on the structure of triblock copolymers. 2. Polystyrene-polyisoprene-polystyrene, *Macromolecules*. 23 (1990) 4200–4205.
- [8] D.B. Scott, A.J. Waddon, Y.G. Lin, F.E. Karasz, H.H. Winter, Shear-induced orientation transitions in triblock copolymer styrene-butadiene-styrene with cylindrical domain morphology, *Macromolecules*. 25 (1992) 4175–4181.
- [9] K. Shimizu, H. Saito, Orientation of cylindrical microdomains of triblock copolymers by *in situ* stress-strain- birefringence measurements, *J. Polym. Sci. Part B Polym. Phys.* 47 (2009) 715–723.
- [10] U. Wiesner, Lamellar diblock copolymers under large amplitude oscillatory shear flow: Order and dynamics, *Macromol. Chem. Phys.* 198 (1997) 3319–3352.
- [11] K. Hodd, Epoxy Resins, in: *Compr. Polym. Sci. Suppl.*, Elsevier, (1989) 667–699.

- [12] J. Wu, H.-G. Xia, Tertiary amines as highly efficient catalysts in the ring-opening reactions of epoxides with amines or thiols in H₂O: expeditious approach to β -amino alcohols and β -aminothioethers, *Green Chem.* 7 (2005) 708.
- [13] B. Sreedhar, P. Radhika, B. Neelima, N. Hebalkar, Regioselective ring opening of epoxides with amines using monodispersed silica nanoparticles in water, *J. Mol. Catal. Chem.* 272 (2007) 159–163.
- [14] J.C. Mullis, W.P. Weber, Regiospecificity of reactions of epoxides and oxetanes with trimethylsilyl cyanide, *J. Org. Chem.* 47 (1982) 2873–2875.
- [15] J.T. Ayers, S.R. Anderson, A Preparative Scale Reduction of Alkyl Disulfides with Tributyl Phosphine and Water, *Synth. Commun.* 29 (1999) 351–358.
- [16] W.W. Cleland, Dithiothreitol, a New Protective Reagent for SH Groups, *Biochemistry (Mosc.)*. 3 (1964) 480–482.
- [17] H. Adams, R. Bell, Y.-Y. Cheung, D.N. Jones, N.C.O. Tomkinson, The cleavage of meso-epoxides with homochiral thiols: synthesis of (+)- and (–)-trans-1-mercaptocyclohexan-2-ol, *Tetrahedron Asymmetry*. 10 (1999) 4129–4142.
- [18] N. Devan, P.R. Sridhar, K.R. Prabhu, S. Chandrasekaran, Tetrathiomolybdate Assisted Epoxide Ring Opening with Masked Thiolates and Selenoates: Multistep Reactions in One Pot, *J. Org. Chem.* 67 (2002) 9417–9420.
- [19] S. Ghosh, S. Basu, S. Thayumanavan, Simultaneous and Reversible Functionalization of Copolymers for Biological Applications, *Macromolecules*. 39 (2006) 5595–5597.
- [20] P.F. Cañamero, J.L. de la Fuente, E.L. Madruga, M. Fernández-García, Atom Transfer Radical Polymerization of Glycidyl Methacrylate: A Functional Monomer, *Macromol. Chem. Phys.* 205 (2004) 2221–2228.
- [21] H.E. Gottlieb, V. Kotlyar, A. Nudelman, NMR Chemical Shifts of Common Laboratory Solvents as Trace Impurities, *J. Org. Chem.* 62 (1997) 7512–7515.
- [22] U.T. Rüegg, J. Rudinger, [10] Reductive cleavage of cystine disulfides with tributylphosphine, in: *Methods Enzymol.*, Elsevier, (1977) 111–116.
- [23] Comprehensive asymmetric catalysis, Springer, Berlin ; New York, 2004.
- [24] M. Shailaja, A. Manjula, B. Vittal Rao, (Bromodimethyl)sulfonium Bromide–Mediated Thiolytic of Epoxides: An Easy Access to β -Hydroxy Sulfides and Benzoxathiepinones in Solvent-Free Conditions, *Synth. Commun.* 40 (2010) 3629–3639.
- [25] G. Socrates, Infrared and Raman characteristic group frequencies: tables and charts, 3rd ed, Wiley, Chichester ; New York, 2001.
- [26] H.E. Van Wart, A. Lewis, H.A. Scheraga, F.D. Saeva, Disulfide Bond Dihedral Angles from Raman Spectroscopy, *Proc. Natl. Acad. Sci.* 70 (1973) 2619–2623.

CHAPTER 7

CONCLUSIONS AND FUTURE DIRECTIONS

7.1 Summary of Thesis Research

In the first half (Chapters 2-4) of this dissertation the spiropyran (SP) mechanophore was studied in different polymeric systems. The SP was first incorporated into polyurethane (PU) via step growth polymerization, and demonstrated to be mechanochromic. In addition, the inherent balance of mechanical toughness and elasticity of the PU enabled the effects of mechanical force on the SP-MC equilibrium to be studied. Experimental results demonstrated that when held at constant strain, the mechanically induced colored merocyanine (MC) form of the mechanophore did not revert back to its thermodynamically preferred (under no load) SP form, indicating a strain-induced change in the energy landscape of the SP mechanophore system.

Taking advantage of the phase separation in segmented polyurethane (SPU) and the ability to control the location of the SP mechanophore via step growth polymerization, the SP mechanophore was incorporated into either the soft or the hard segment of SPU. Exploiting the ability of the SP to be force activated, the mechanophore was used as a molecular probe of force and orientation. When the SP was incorporated into either the soft segment (SPSS) or the hard segment (SPHS) in a 22 wt% (low) hard segment SPU, the same levels of orientation (determined via an order parameter) and activation were observed, suggesting a lack of phase segregation. In the 40 wt% (high) hard segment SPU, phase segregation was evident and the SPSS and SPHS resulted in different average order parameters. The higher level of orientation observed for the SPSS in 40 wt% material compared to the SPHS suggested that the force felt by

the mechanophore in each phase was different. Additional studies showed that the SPHS mechanically activated at lower levels of alignment, suggesting that it mechanically activates by a different mechanism than the SPSS. The different mechanism by which force is transferred to the mechanophore in each phase provided insight into force distribution at the molecular level in each local environment (soft or hard domain).

The SP mechanophore was also incorporated as a crosslinker to study forces in swelled crosslinked PMMA. It was demonstrated that the force on the SP crosslinks during polymer swelling in several mid-polarity solvents were sufficient to activate the electrocyclic ring-opening of the SP mechanophore. Using gravimetric analysis and fluorescence imaging, it was demonstrated that in most cases, swelling and activation were directly correlated, providing evidence that the forces due to polymer swelling were causing the mechanical activation of the SP mechanophore. A study on the solvent interaction with the SP mechanophore was also conducted and concluded that in most cases (except in THF) the solvent-mechanophore interactions were not influencing the SP-MC equilibrium. Finally, the effect of crosslink density was investigated demonstrating that higher crosslink density polymers tend to swell slower and less. However, by comparing the amount of swelling to the total fluorescence, it was demonstrated that the samples with higher crosslink densities accumulate greater force at the crosslinks.

In the second half of this dissertation (Chapters 5-6), a new concept in mechanochemistry termed, contact mechanochemistry was explored. The concept utilizes the inherent phase separation of block copolymer or polymer blends to mask complimentary functionalities from coming into contact. Then, by use of mechanical force or shear, break up those phase separated domains in order to induce a chemical reaction, changing the innate properties of the starting

polymer. Initially, a poly(acid) and poly(amine) block copolymer was synthesized and tested as a potential polymer system to demonstrate contact mechanochemistry, but ultimately a lack of phase separation, and a number of other fundamental challenges ruled out this system as viable for contact mechanochemistry. Next, a ring-opening epoxide chemistry by a thiol, initially masked as a disulfide side chain, was explored. Poly(glycidyl methacrylates) (PGMA) and poly(4-(pyridin-2-yl)disulfanyl) phenyl methacrylate) (PPDSPMA) were synthesized, and experiments mixing polymer solutions of PGMA and PPDSPMA with Dithiothreitol (DTT) reducing agent and a base catalyst resulted in gelation of the polymer. Control experiments and Raman spectroscopy confirmed that the final gelled product was a crosslinking reaction between the polymer blend, demonstrating that the PGMA-PPDSPMA polymer blend is a strong candidate for contact mechanochemistry.

7.2 Future Directions

The SP mechanophore has been extensively studied in different polymers environments, architectures, and loading conditions, adding to the understanding of how macroscopic force is transferred at the molecular level [1–4]. While the focus on the activation characteristics of SP have largely been due to ease of incorporation and detectability, there exist a growing library of mechanophores with many different functionality [5], which have only been demonstrated to be mechanically triggered by solution sonication experiments. Drawing upon the knowledge gained from the successful solid state activation of the SP mechanophore, future directions in the field of mechanophores will be their incorporation into bulk polymeric materials, and their mechanical activation in the solid state, resulting in the development of mechanoresponsive materials, which can self-strengthen or self-heal.

The concept of contact mechanochemistry is new, and holds much potential for the design and development of polymers which can undergo drastic changes in polymer properties, beyond the innate properties of the starting combination of polymers. In this dissertation a PGMA-PPDSPMA polymer blend was introduced as a polymer system to test the ideas of contact mechanochemistry. While the feasibility of this chemistry has been demonstrated (Chapter 6), future directions will involve engineering this chemistry into a solid state mechanochemical system. The PGMA-PPDSPMA polymer blend is promising, but there are in addition different solid state chemistry that could also be exploited for contact mechanochemistry, such as thiol-ene chemistries, acid-base chemistries, and click chemistries. The exploration of these different chemistries coupled with thermodynamic polymer phase separation and domain break up through mechanical force gives much potential for this new field in mechanochemistry.

REFERENCES

- [1] D.A. Davis, A. Hamilton, J. Yang, L.D. Cremer, D. Van Gough, S.L. Potisek, *et al.*, Force-induced activation of covalent bonds in mechanoresponsive polymeric materials, *Nature*. 459 (2009) 68–72.
- [2] C.M. Kingsbury, P.A. May, D.A. Davis, S.R. White, J.S. Moore, N.R. Sottos, Shear activation of mechanophore-crosslinked polymers, *J Mater Chem*. (2011).
- [3] B.A. Beiermann, D.A. Davis, S.L.B. Kramer, J.S. Moore, N.R. Sottos, S.R. White, Environmental effects on mechanochemical activation of spiropyran in linear PMMA, *J Mater Chem*. (2011).
- [4] G. O'Bryan, B.M. Wong, J.R. McElhanon, Stress Sensing in Polycaprolactone Films via an Embedded Photochromic Compound, *Acs Appl. Mater. Interfaces*. (2010).
- [5] J.N. Brantley, K.M. Wiggins, C.W. Bielawski, Polymer mechanochemistry: the design and study of mechanophores, *Polym. Int.* 62 (2013) 2–12.

APPENDIX A

NMR SPECTRA

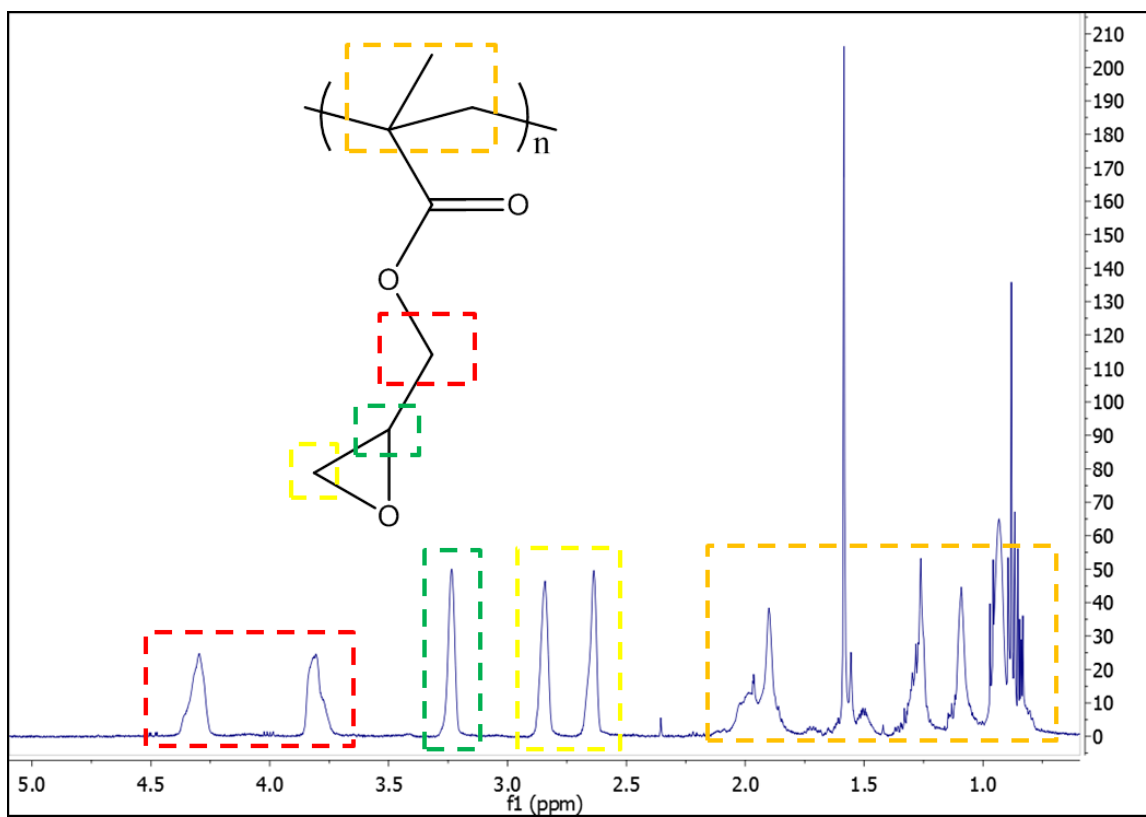


Figure A.1 – ^1H NMR spectra of poly(glycidyl methacrylates) PGMA in CDCl_3 .

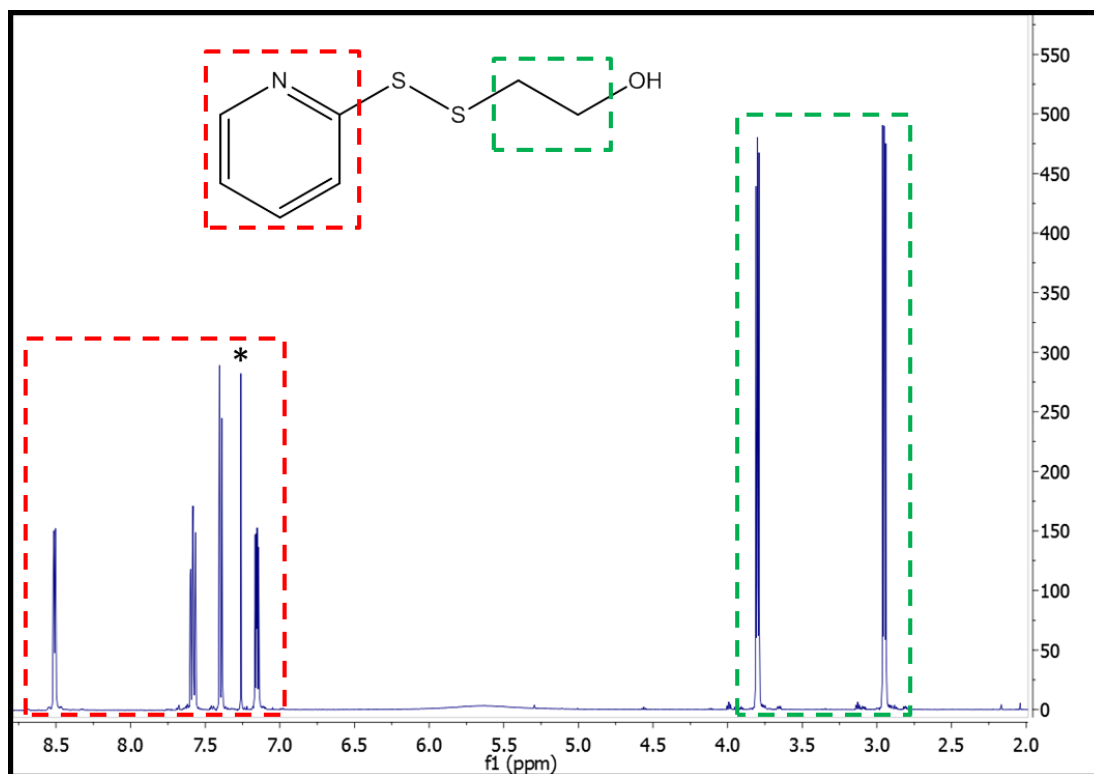


Figure A.2 – ¹H NMR spectra of 2-(pyridin-2-yl)disulfanylethanol in *CDCl₃.

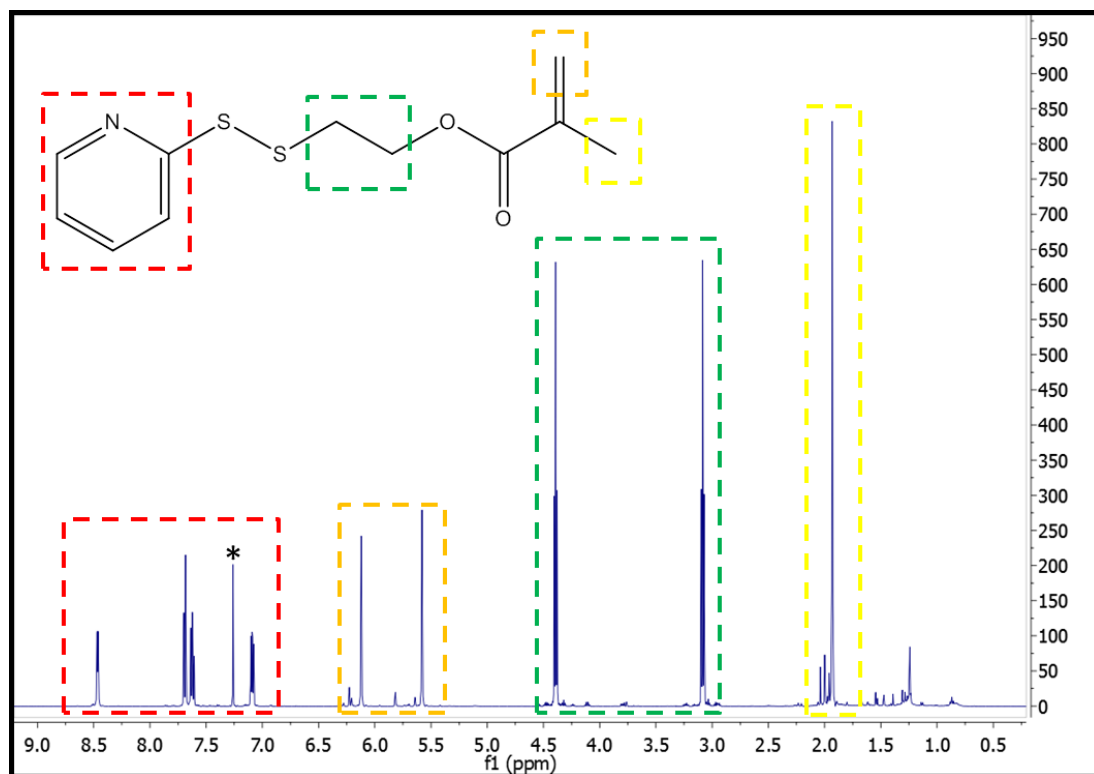


Figure A.3 – ¹H NMR spectra of 2-(pyridin-2-yl)disulfanylethyl methacrylate in *CDCl₃.

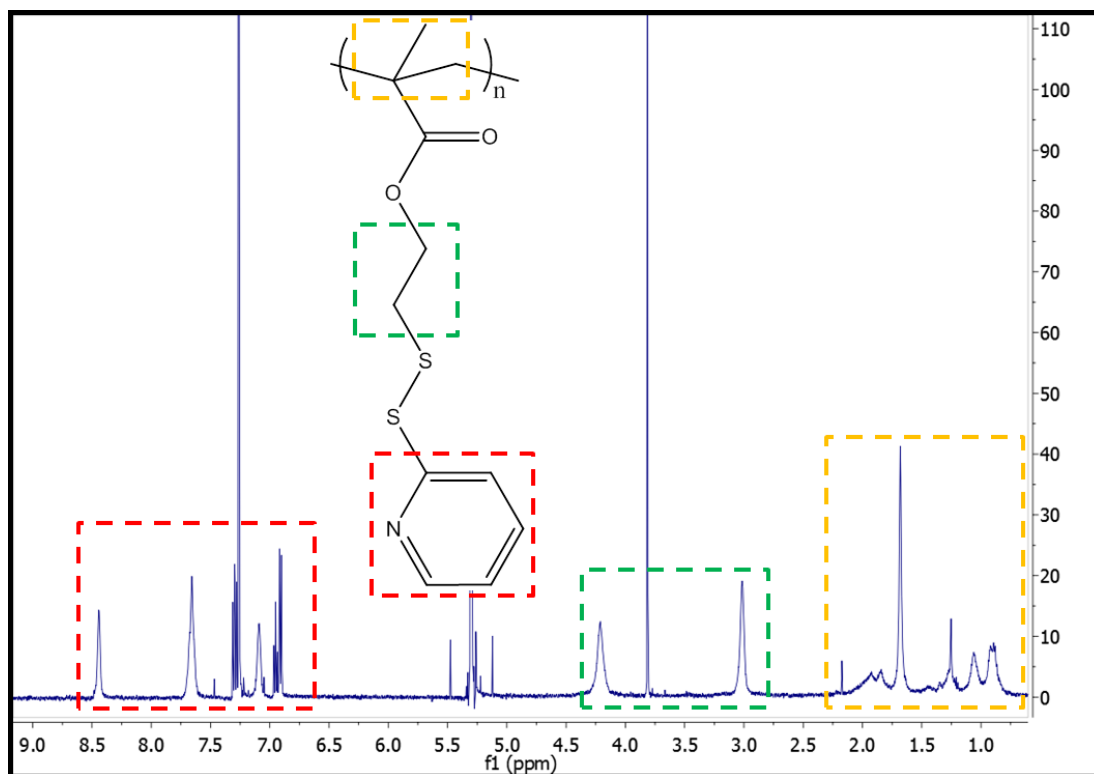


Figure A.4 – ¹H NMR spectra of poly(2-(pyridin-2-yl)disulfanyl)ethyl methacrylate) in CDCl₃.

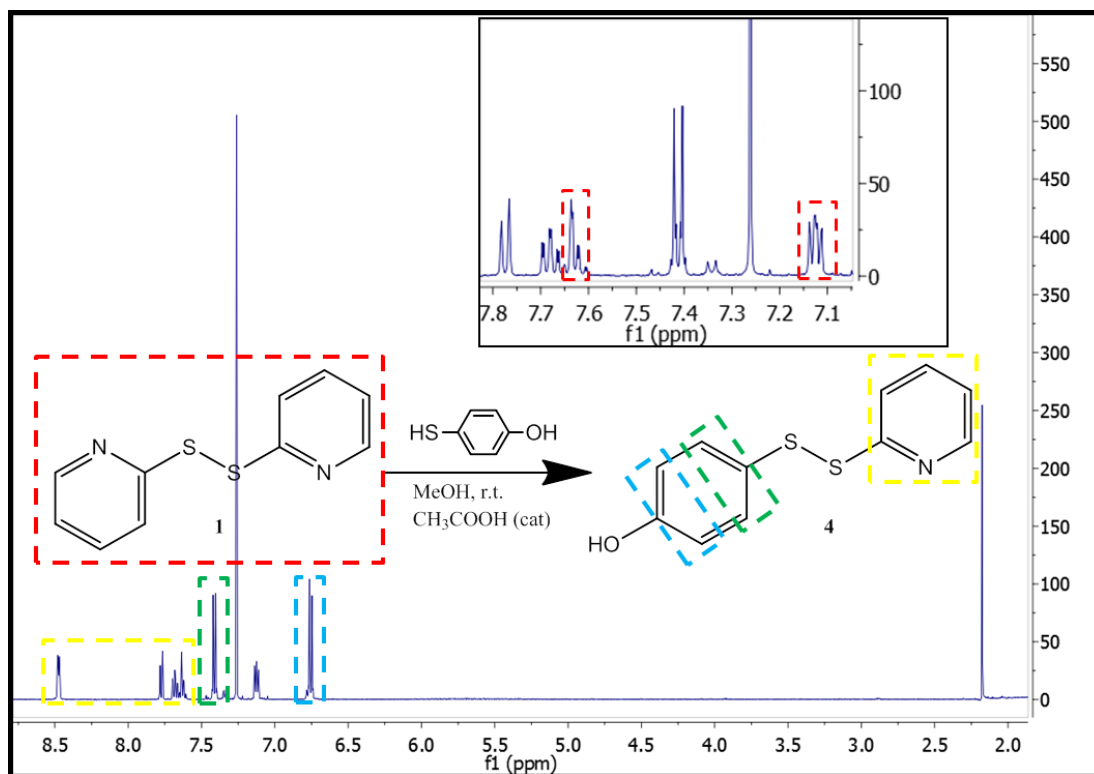


Figure A.5 – ¹H NMR spectra of compound **4** with residual **1** in CDCl₃.

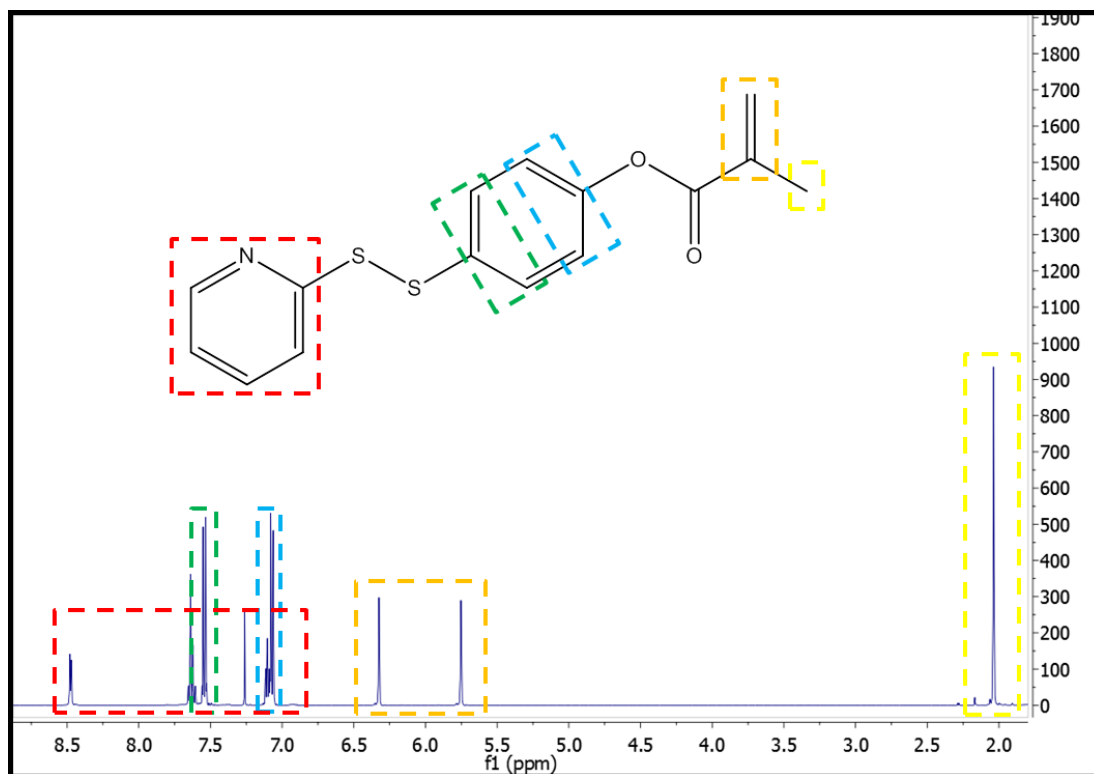


Figure A.6 – ^1H NMR spectra of PDSPMA monomer in CDCl_3 .

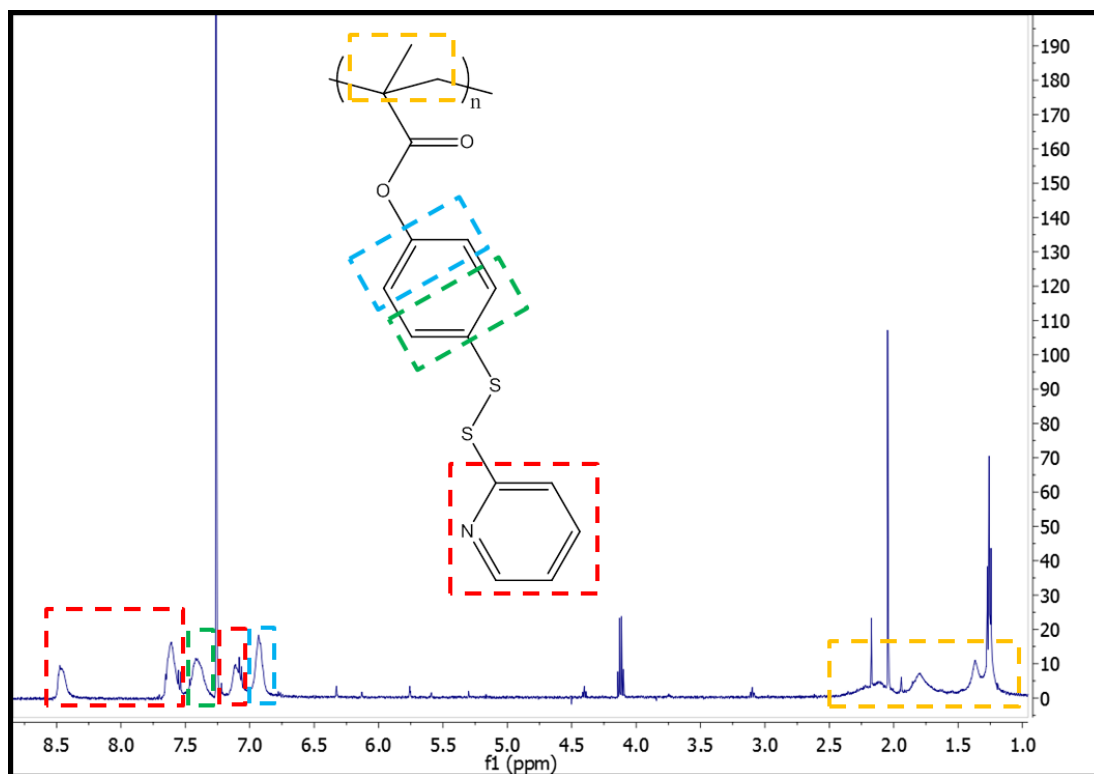


Figure A.7 – ^1H NMR spectra of PPDSPMA monomer in CDCl_3 .